NUREG/CR–4219
ORNL/TM–9593/V11&N1
Vol. 11, No. 1

Heavy-Section Steel Technology Program

Semiannual Progress Report for October 1993 – March 1994

Prepared by:
W. E. Pennell

Oak Ridge National Laboratory

Prepared for
U.S. Nuclear Regulatory Commission

D602 01

AVAILABILITY NOTICE

Availability of Reference Materials Cited in NRC Publications

Most documents cited in NRC publications will be available from one of the following sources:

1. The NRC Public Document Room, 2120 L Street, NW., Lower Level, Washington, DC 20555-0001

2. The Superintendent of Documents, U.S. Government Printing Office, P. O. Box 37082, Washington, DC 20402-9328

3. The National Technical Information Service, Springfield, VA 22161-0002

Although the listing that follows represents the majority of documents cited in NRC publications, it is not intended to be exhaustive.

Referenced documents available for inspection and copying for a fee from the NRC Public Document Room include NRC correspondence and internal NRC memoranda; NRC bulletins, circulars, information notices, inspection and investigation notices; licensee event reports; vendor reports and correspondence; Commission papers; and applicant and licensee documents and correspondence.

The following documents in the NUREG series are available for purchase from the Government Printing Office: formal NRC staff and contractor reports, NRC-sponsored conference proceedings, international agreement reports, grantee reports, and NRC booklets and brochures. Also available are regulatory guides, NRC regulations in the *Code of Federal Regulations*, and *Nuclear Regulatory Commission Issuances*.

Documents available from the National Technical Information Service include NUREG-series reports and technical reports prepared by other Federal agencies and reports prepared by the Atomic Energy Commission, forerunner agency to the Nuclear Regulatory Commission.

Documents available from public and special technical libraries include all open literature items, such as books, journal articles, and transactions. *Federal Register* notices, Federal and State legislation, and congressional reports can usually be obtained from these libraries.

Documents such as theses, dissertations, foreign reports and translations, and non-NRC conference proceedings are available for purchase from the organization sponsoring the publication cited.

Single copies of NRC draft reports are available free, to the extent of supply, upon written request to the Office of Administration, Distribution and Mail Services Section, U.S. Nuclear Regulatory Commission, Washington, DC 20555-0001.

Copies of industry codes and standards used in a substantive manner in the NRC regulatory process are maintained at the NRC Library, Two White Flint North, 11545 Rockville Pike, Rockville, MD 20852-2738, for use by the public. Codes and standards are usually copyrighted and may be purchased from the originating organization or, if they are American National Standards, from the American National Standards Institute, 1430 Broadway, New York, NY 10018-3308.

NUREG/CR-4219
ORNL/TM-9593/V11&N1
Vol. 11, No. 1

Heavy-Section Steel Technology Program

Semiannual Progress Report for October 1993 – March 1994

Manuscript Completed: April 1995
Date Published: November 1995

Prepared by
W. E. Pennell

Oak Ridge National Laboratory
Managed by Martin Marietta Energy Systems, Inc.

Oak Ridge National Laboratory
Oak Ridge, TN 37831-6285

S. N. Malik, NRC Project Manager

Prepared for
Division of Engineering Technology
Office of Nuclear Regulatory Research
U.S. Nuclear Regulatory Commission
Washington, DC 20555-0001
NRC Job Code B0119

Abstract

The Heavy-Section Steel Technology (HSST) Program is conducted for the U.S. Nuclear Regulatory Commission (NRC) by Oak Ridge National Laboratory (ORNL). The program focus is on the development and validation of technology for the assessment of fracture-prevention margins in commercial nuclear reactor pressure vessels. The HSST Program is organized in seven tasks: (1) program management, (2) constraint effects analytical development and validation, (3) evaluation of cladding effects, (4) ductile to cleavage fracture mode conversion, (5) fracture analysis methods development and applications, (6) material property data and test methods, and (7) integration of results into a state-of-the-art methodology. The program tasks have been structured to place emphasis on the resolution fracture issues with near-term licensing significance. Resources to execute the research tasks are drawn from ORNL with subcontract support from universities and other research laboratories. Close contact is maintained with the sister Heavy-Section Steel Irradiation Program at ORNL and with related research programs both in the United States and abroad. This report provides an overview of principal developments in each of the seven program tasks from October 1993–March 1994.

Contents

List of Figures

List of Tables

Preface

The Heavy-Section Steel Technology (HSST) Program, which is sponsored by the Nuclear Regulatory Commission, is an engineering research activity devoted to extending and developing the technology for assessing the margin of safety against fracture of the thick-walled steel pressure vessels used in light-water-cooled nuclear power reactors. The program is being carried out in close cooperation with the nuclear power industry. This report covers HSST work performed in October 1993–March 1994. The work performed by the Oak Ridge National Laboratory (ORNL) and by subcontractors is managed by the Engineering Technology Division (ETD) of ORNL. Major tasks at ORNL are carried out by the ETD and the Metals and Ceramics Division. The following is a list of previous progress reports on this program:

ORNL-4176
ORNL-4315
ORNL-4377
ORNL-4463
ORNL-4512
ORNL-4590
ORNL-4653
ORNL-4681
ORNL-4764
ORNL-4816
ORNL-4855
ORNL-4918
ORNL-4971
ORNL/TM-4655 (Vol. II)
ORNL/TM-4729 (Vol. II)
ORNL/TM-4805 (Vol. II)
ORNL/TM-4914 (Vol. II)
ORNL/TM-5021 (Vol. II)
ORNL/TM-5170
ORNL/NUREG/TM-3
ORNL/NUREG/TM-28
ORNL/NUREG/TM-49
ORNL/NUREG/TM-64
ORNL/NUREG/TM-94
ORNL/NUREG/TM-120
ORNL/NUREG/TM-147
ORNL/NUREG/TM-166
ORNL/NUREG/TM-194
ORNL/NUREG/TM-209
ORNL/NUREG/TM-239
NUREG/CR-0476 (ORNL/NUREG/TM-275)
NUREG/CR-0656 (ORNL/NUREG/TM-298)
NUREG/CR-0818 (ORNL/NUREG/TM-324)
NUREG/CR-0980 (ORNL/NUREG/TM-347)
NUREG/CR-1197 (ORNL/NUREG/TM-370)
NUREG/CR-1305 (ORNL/NUREG/TM-380)
NUREG/CR-1477 (ORNL/NUREG/TM-393)
NUREG/CR-1627 (ORNL/NUREG/TM-401)
NUREG/CR-1806 (ORNL/NUREG/TM-419)
NUREG/CR-1941 (ORNL/NUREG/TM-437)
NUREG/CR-2141, Vol. 1 (ORNL/TM-7822)
NUREG/CR-2141, Vol. 2 (ORNL/TM-7955)
NUREG/CR-2141, Vol. 3 (ORNL/TM-8145)
NUREG/CR-2141, Vol. 4 (ORNL/TM-8252)
NUREG/CR-2751, Vol. 1 (ORNL/TM-8369/V1)
NUREG/CR-2751, Vol. 2 (ORNL/TM-8369/V2)
NUREG/CR-2751, Vol. 3 (ORNL/TM-8369/V3)
NUREG/CR-2751, Vol. 4 (ORNL/TM-8369/V4)
NUREG/CR-3334, Vol. 1 (ORNL/TM-8787/V1)
NUREG/CR-3334, Vol. 2 (ORNL/TM-8787/V2)
NUREG/CR-3334, Vol. 3 (ORNL/TM-8787/V3)
NUREG/CR-3744, Vol. 1 (ORNL/TM-9154/V1)
NUREG/CR-3744, Vol. 2 (ORNL/TM-9154/V2)
NUREG/CR-4219, Vol. 1 (ORNL/TM-9593/V1)
NUREG/CR-4219, Vol. 2 (ORNL/TM-9593/V2)
NUREG/CR-4219, Vol. 3, No. 1 (ORNL/TM-9593/V3&N1)
NUREG/CR-4219, Vol. 3, No. 2 (ORNL/TM-9593/V3&N2)
NUREG/CR-4219, Vol. 4, No. 1 (ORNL/TM-9593/V4&N1)
NUREG/CR-4219, Vol. 4, No. 2 (ORNL/TM-9593/V4&N2)
NUREG/CR-4219, Vol. 5, No. 1 (ORNL/TM-9593/V5&N1)
NUREG/CR-4219, Vol. 5, No. 2 (ORNL/TM-9593/V5&N2)
NUREG/CR-4219, Vol. 6, No. 1 (ORNL/TM-9593/V6&N1)
NUREG/CR-4219, Vol. 6, No. 2 (ORNL/TM-9593/V6&N2)
NUREG/CR-4219, Vol. 7, No. 1 (ORNL/TM-9593/V7&N1)
NUREG/CR-4219, Vol. 7, No. 2 (ORNL/TM-9593/V7&N2)
NUREG/CR-4219, Vol. 8, No. 1 (ORNL/TM-9593/V8&N1)
NUREG/CR-4219, Vol. 8, No. 2 (ORNL/TM-9593/V8&N2)
NUREG/CR-4219, Vol. 9, No. 1 (ORNL/TM-9593/V9&N1)
NUREG/CR-4219, Vol. 9, No. 2 (ORNL/TM-9593/V9&N2)
NUREG/CR-4219, Vol. 10, No. 1 (ORNL/TM-9593/V10&N1)
NUREG/CR-4219, Vol. 10, No. 2 (ORNL/TM-9593/V10&N2)

Executive Summary

W. E. Pennell

The Heavy-Section Steel Technology (HSST) Program is conducted for the U.S. Nuclear Regulatory Commission (NRC) by Oak Ridge National Laboratory (ORNL). The program focus is on the development, validation, and application of technology for the assessment of fracture-prevention margins in commercial nuclear reactor pressure vessels (RPVs). The scope of the project includes development and experimental validation of analysis methods, development of testing techniques and generation of materials property data, integration of analysis methods and materials data into a comprehensive RPV integrity assessment methodology, technology transfer through participation in national and international codes and standards activities, and support to NRC in the area of RPV integrity assessment. Program activities are structured to provide support to NRC for the resolution of specific RPV licensing issues. Licensing issues directly influenced by this technology include the definition of RPV pressure-temperature curves and low-temperature overpressure protection relief valve set points, evaluation of RPV integrity under pressurized-thermal-shock (PTS) transient loading, safety evaluations of RPVs containing material with low-upper-shelf Charpy energy, and data transfer from small-scale surveillance specimens for application in RPV structural integrity assessments.

1 Program Management

In this reporting period, the work-breakdown structure for the HSST Program was revised to focus on six RPV structural integrity issues of current concern to the NRC. These issues are crack-tip constraint effects on fracture toughness of RPV materials, effects of stainless steel cladding on the initiation and propagation of shallow surface cracks, ductile to cleavage fracture mode conversion; fracture analysis methods development, materials property data and test methods development, and integration of results from the research programs into a state-of-the-art methodology for RPV structural integrity assessments.

Two papers were produced in response to NRC direction. The papers provided a review of recent results from the HSST research program and were presented at the NRC 21st Water Reactor Safety Meeting at the Bethesda Marriott Hotel on October 25, 1993, and at the British Nuclear Energy Society Conference on Thermal Reactor Safety Assessment, in Manchester, England, in May 1994.

Subcontracts are either in place or planned for full-scale fracture testing of shallow-flaw beam specimens, development of computational procedures for the prediction of ductile tearing in advance of cleavage fracture, dynamic fracture toughness testing, and consulting support. Progress reviews and work-scope negotiations were held with the subcontractors. One result of these reviews was a decision to move fabrication responsibility for two full-scale test specimens from the test vendor to ORNL. This change was made to circumvent fabrication problems encountered by the test vendor and to avoid costs for repairs and replacements resulting from damage incurred to the test equipment in the second full-scale test.

The first of the full-scale, shallow-flaw fracture toughness tests resulted in a measured fracture toughness much lower than had been anticipated. The available shallow-flaw fracture toughness data were collected into a data base and evaluated using both the nil-ductility-transition temperature (NDT) and the reference temperature for nil-ductility-transition (RT_{NDT}) as normalizing parameters. Results from this evaluation showed that further testing of full-scale, shallow-flaw specimens would be of particular value in helping to define the lower-transition-zone, shallow-flaw, fracture toughness behavior of pressure vessel steels. A recommendation to extend the scope of the full-scale, shallow-flaw, fracture toughness testing program was made by ORNL and accepted by NRC.

Interactions with foreign fracture technology research organizations continued during this reporting period. Dr. Klingbeil of Bundesanstalt für Materialforschung und-prüfung (BAM), Berlin, Germany, and Professor Brocks of the Fraunhofer Institute, Freiburg, Germany, visited ORNL on Nov. 19, 1993, for discussions on constraint effects analysis and testing. Dr. Ing. Ludwig Stumpfrock of Staatliche Materialprufüngsanstalt Universitat Stuttgart, Germany, visited ORNL on February 15–16, 1994, for an exchange of information from ongoing fracture technology research programs. HSST Program thermal-shock test data were provided to Dr. M. Bethmont of the Department Etude Des Materiaux of Electricité de France (EdF) in response to his request.

Active participation was maintained in the work of the American Society of Mechanical Engineers Task Group on Operability and the Working Group on Operating Plant

Criteria. During the current reporting period, HSST Program personnel published two NUREG/CR reports, one letter report, and two papers in technical society publications; they gave 12 presentations at national and international meetings sponsored by technical societies and NRC.

2 Constraint Effects Analytical Development and Validation

The focus of this task is on the development and validation of dual-parameter stress-based correlations to reflect the effect of crack-tip constraint on the fracture toughness of pressure vessel steels. Crack-tip constraint conditions of particular concern in RPV structural integrity evaluations are those associated with shallow flaws and biaxial loading.

Several HSST test programs require the use of material with yield-stress (σ_y) and 68-J (50-ft·lb) Charpy-energy transition-temperature (T_{cv}) properties similar to those of RPV material that has been irradiated to a neutron fluence of 1.5×10^{19} neutrons/cm^2 (E > 1 MeV). Development of a heat-treatment cycle to produce the required properties in A 533 B material was continued in this reporting period. Room-temperature target values were defined for σ_y and T_{cv}. A number of heat-treatment cycles were evaluated. Normalizing at 1010°C followed by air cooling produced acceptable mechanical properties when applied to both as-received and quenched material.

Direction was received from NRC for the fabrication and testing of an additional four cruciform specimens. These specimens are required to complete the 1:1 biaxial-loading portion of the initial test matrix for the Combustion Engineering (CE) material.

In an attempt to reduce the specimen fabrication costs, a commercial vendor was used to perform the electron-beam (EB) welding required to join the loading arms to the test section of the specimen. The welds produced by the vendor were found to have a number of lack-of-fusion defects. In addition, discoloration of the specimens indicated that they may have been heated to a high temperature during the welding process and remained at high temperature at the time they were removed from the welding chamber. These defects raised concerns that the specimens were not suitable for their intended purpose. One of the specimens was tested, and failure occurred in both the test section and the attachment welds. The failure load was compatible with the test section having been overheated during the welding process. It was decided, therefore, to scrap the remaining specimens and fabricate replacements from the CE plate material available at ORNL. Material size limitations, which dictated the location of the EB welds in the previous specimens, are not present in the CE plate material. The design of the replacement specimens was, therefore, modified to move the EB weld to a more favorable location. EB welding of the loading arms to the test sections for these specimens will be performed at ORNL, where the earlier successful specimens were welded.

Development continued on an unclad cruciform specimen with a finite-length surface flaw. This development supports the Task 3 investigation of the effect of cladding on crack initiation from finite-length surface flaws. The investigation of flaw sharpening techniques was completed, and the previously reported conclusion that fatigue presharpening gave the most reliable results remained unchanged. A development series of three test specimens was fabricated. The reference 1.52-cm-deep by 3.31-cm-long (0.6-in. by 1.5-in.) surface flaw was introduced into the specimen by electrodischarge machining and was fatigue presharpened. The configuration of the load-diffusion-control slots (LDCSs) in these specimens was changed from that used in the through-flaw specimens such that the finite-length flaw was not aligned with any LDCS. One specimen was fatigue precracked and tested to evaluate the fatigue-induced flaw growth behavior.

The fatigue-induced crack growth was found to be relatively uniform around the crack front, confirming one element of the analytical predictions. The amount of flaw growth, however, was less than had been predicted, and the measured fracture toughness from this initial specimen is considered suspect. A repeat test with a deeper flaw gave similar results, leading to the conclusion that the low yield stress of the material used for these development specimens had a major influence on the test results. Analysis of the test results did, however, provide the information required to adjust and finalize the flaw geometry. The modified flaw geometry was incorporated into the design of the remaining four development specimens, which are currently being machined. The analysis results also indicated that a fracture-toughness/yield-stress (K_{Ic}/σ_y) ratio approaching unity is required for these tests. The available material characterization data indicate that the required K_{Ic}/σ_y ratio can be achieved at a test temperature of approximately –60°C.

3 Evaluation of Cladding Effects

Stainless-steel cladding can act to inhibit the initiation and propagation of cracks from finite-length surface flaws. This property is not reflected in existing RPV structural integrity analysis methods. Objectives for this task are to (1) experimentally determine the influence of cladding on

crack initiation from finite-length surface flaws in a prototypical RPV biaxial stress field and (2) develop and validate the technology required for incorporation of those effects into RPV structural-integrity assessment methods.

Fracture toughness tests were performed on three full-scale [232-mm-deep by 229-mm-wide (9.125-in.-deep by 9.0-in.-wide)] beams cut from the shell of an RPV from a cancelled nuclear plant. Constant-depth flaws were cut on the inside of the shell material, extending through the stainless steel cladding and into the structural weld joining two plate sections of the RPV shell segment. Two of the beams had shallow flaws (a/W = 0.05 and 0.1), and the third beam had a deep flaw (a/W = 0.5). The shell segments were fabricated from A 533 B plate material joined by matching weld material. The tips of the fatigue-sharpened shallow-flaw cracks were located in weld material that had experienced the metallurgical effects produced by the cladding and heat-treatment RPV production processes. The crack tip in the deep-flaw specimen was located in weld material that would not have been influenced by the cladding process. Tests on these beams provided a means to determine the effect of prototypical metallurgical gradients produced by the cladding process on the shallow-flaw fracture toughness of RPV weld material.

Extensive characterization tests were performed on the shell-segment weld material before performing the fracture toughness tests. Data from these tests showed the RT_{NDT} for this material to be –23°C (–9°F). This temperature was selected as the test temperature to produce data in the lower-transition portion of the fracture toughness curve. A finding of particular interest from the tensile characterization tests was that the room-temperature yield stress for the weld material (σ_{yw}) was 565 MPa (82 ksi). The as-fabricated shell segments had substantially overmatched welds with a σ_{yw}/σ_{yp} ratio of 1.36 at the selected test temperature.

Fracture toughness testing of the shallow- and deep-flaw beams was performed by the National Institute for Standards and Technology using their 53.4-MN (12-M lb) test machine. Development testing was performed to validate the temperature control systems and the fatigue pre-sharpening procedure. Fracture toughness (K_{Jc}) values for the deep flaw (a/W = 0.5) and the two shallow flaws (a/W = 0.05 and 0.10) were obtained as 173.5, 225.4, and 393.3 MPa$\sqrt{m}$ (157.9, 205.1, and 357.9 ksi$\sqrt{in.}$), respectively. The relative magnitude of the shallow-flaw fracture toughness values obtained at a/W ratios of 0.05 and 0.10 is not what would have been anticipated from a consideration of shallow-flaw crack-tip constraint effects alone and may indicate an influence of metallurgical gradient effects from the cladding process. Superposition of these data on the existing shallow-flaw fracture toughness data revealed that the NDT may be a better normalizing temperature than the RT_{NDT} for shallow-flaw fracture toughness data. Additional full-scale, shallow-flaw, fracture toughness tests are planned for both weld and plate materials.

Stainless steel cladding has a yield stress lower than that of the low-alloy steels used for RPV construction. Thermal stresses generated in the cladding by strain-controlled loading conditions, such as thermal-shock transient loading, are limited by yielding of the cladding material. This effect is not currently included in the linear-elastic-fracture-mechanics (LEFM) analysis methodology used to evaluate RPV integrity under PTS loading. Work was initiated on the development and validation of a clad yielding model that can be incorporated into a LEFM fracture analysis model. Preservation of the LEFM analysis approach is necessary because the probabilistic analysis procedures in use for the evaluation of RPV integrity under PTS loading require that a very large number of analyses be performed. Direct incorporation of nonlinear analysis into the PTS evaluation would, therefore, be impractical. An empirical approach using a matrix of clad vessel analysis results is, therefore, being used to develop a practical clad-yielding-effects methodology. Elastic and elastic-plastic analyses are being used to isolate the effect of clad yielding on the magnitude and distribution of stress-intensity factors (SIFs) around the periphery of a finite-length shallow surface flaw. Initial results show that SIFs in the near-surface region of the crack front drop significantly from the elastic analysis values when elastic-plastic analysis is used.

Investigation of surrogate stainless steel cladding materials continued with the objective of developing a cladding material that has the tearing toughness properties required for the clad/base-material tests. Low temperature is used to simulate the effects of neutron-radiation embrittlement in fracture toughness testing of RPV base materials. The cleavage fracture toughness and the tearing toughness of low-alloy RPV steel and the tearing toughness of cladding material respond differently to changes in test temperature. The ratio of clad-tearing toughness to base-material cleavage toughness will become higher than the value expected in an irradiated RPV if prototypical RPV material is simply cooled to a suitable base-material test temperature. A number of surrogate cladding materials were evaluated, but none of them had properties that were completely satisfactory for use in the clad/base-material test specimens. In a parallel action, analyses were initiated to determine if the clad-tearing toughness requirements could be relaxed without compromising the data to be obtained from the clad/base-material tests.

Participation in the international project for the fracture analysis of large-scale reference experiments (FALSiRE) is used as a means of validating fracture analysis methods. Analyses of clad-beam experiments performed by EdF were completed. The clad beams tested by EdF had subclad cracks and were tested at –170°C (–274°F). The test objective was to determine the influence of cladding on cleavage fracture initiation in the A508-forging base material. The elastic-plastic small-strain finite-element analysis predicted maximum crack-tip-opening displacements (CTODs) at the location on the crack front where cracking initiated in the tests. Evaluation of these analysis results is continuing.

4 Ductile to Cleavage Fracture Mode Conversion

This task investigates the effect of prior ductile tearing on cleavage-fracture-initiation toughness. Ductile tearing before cleavage fracture initiation is frequently observed in tests performed at temperatures corresponding with the lower-transition region of the fracture toughness curve. Evidence exists that ductile tearing may act to increase crack-tip constraint and thereby influence fracture toughness.

Plans were made for the metallurgical examination of fracture surfaces from a number of tests in which limited ductile tearing occurred before cleavage fracture initiation. These examinations will provide information on metallurgical and mechanical features that must be included in a tearing-cleavage mode-conversion model. Discussions were held with the personnel from the University of California–Santa Barbara and the University of Maryland to gain access to the special expertise required for this phase of the work. Planning for the development of a fracture-mode-conversion analysis model was also initiated. Discussions were held with researchers from FRAMATOME in France and AEA Technology in England concerning their experience with a "local-approach" model for predicting ductile tearing in RPV steels. The local-approach model uses a stress-state-dependent void growth and coalescence model to simulate tearing-induced crack extension.

5 Fracture Analysis Methods Development and Application

Development of the Fracture Analysis of Vessels, Oak Ridge (FAVOR) computer program continued. FAVOR is an advanced program for the analysis of RPV failure rates under PTS transient loading. The program is being developed in a manner that will make an executable version of FAVOR available to users without making the source deck available to them. This feature makes possible configuration control of the program.

Stress-intensity factor influence coefficients (SIFICs) were generated for finite-length axial and circumferential flaws located in the inner surface of a clad cylinder with an internal radius to thickness ratio (R_i/t) of 10. These geometric parameters are relevant to many of the pressurized-water-reactor (PWR) vessels currently in service in the United States. The ABAQUS computer program was used to perform the finite-element analysis required for generation of the SIFICs. ABAQUS is a nuclear-quality-assured (NQA-1) computer program. Generation of additional SIFICs is planned for RPVs with R_i/t ratios of 15 and 20. This development will extend the library of SIFICs to cover the geometry of boiling-water-reactor (BWR) pressure vessels. SIFICs for infinite-length surface flaws have been generated previously in this task. The SIFIC library will be incorporated into the FAVOR computer program together with interpolation routines. This development of the FAVOR computer program will make possible the rapid and accurate structural integrity assessment of any PWR or BWR vessel in service in the United States.

A user manual for the initial version of the FAVOR computer program was completed, and the program was distributed to organizations active in the field of RPV structural integrity evaluation. This initial-release version of FAVOR has a SIFIC library for infinite-length surface flaws. The program can perform the RPV structural integrity analysis defined in Regulatory Guide (RG) 1.154. The library of SIFICs for finite-length suface flaws was installed in a development version of the FAVOR program. In the development version of the program the K_I/K_{Ic} ratio is calculated at 10° intervals around the crack front at each time step in the PTS transient. Crack initiation is predicted when $K_I/K_{Ic} \geq 1.0$ at any location around the crack front. Parametric studies performed using the development version of the FAVOR program showed that the location of the critical K_I/K_{Ic} ratio along the crack-front of a semielliptical ($l/a = 6.0$) surface flaw moves a number of times during the course of a PTS transient event.

The FAVOR program employs a static equilibrium analysis to determine if a propagating crack will arrest. Some researchers have suggested that inclusion of dynamic effects in crack-arrest analysis would significantly increase the predicted probability of stable crack arrest. Analyses were performed to determine the potential impact of incorporating dynamic crack-arrest features in PTS analyses. Inclusion of a dynamic crack arrest feature in the analysis was found to have a beneficial effect only for those PTS transients that included a reheat phase. A survey of PTS

transients revealed that only a very small percentage of them included a reheat phase. It was concluded, therefore, that the static equilibrium crack-arrest model in the FAVOR program should remain unchanged at this time.

Assistance was provided to NRC in developing a definition of the work required to develop an update of RG 1.154, which incorporates fracture-mechanics advances made since the original version of the RG was issued.

6 Material Property Data and Test Methods

This task provides support to the other fracture technology development tasks and performs evaluations of specific RPV materials issues. A prior investigator had reported anomalous ductile tearing behavior in A 302 B RPV steel. A program of ductile tearing tests on a number of heats of A 302 B material was initiated to investigate this issue. The test matrix included 233 compact test specimens ranging in size from 1/2T to 4T. All except five of the 4T specimens had been tested at the close of the current reporting period. A preliminary finding from this investigation is that, with one exception, all of the heats of A 302 B material tested met the minimum upper-shelf energy requirements of the Code of Federal Regulations, Sect. 10, Part 50 (10CFR50).

A study of metallurgical gradients in RPV shell plates and welds was completed. It was found that significant metallurgical gradients can exist between the near-surface material and material near the mid-thickness of the vessel shell. These metallurgical gradients can influence the fracture toughness of the material. A letter report, summarizing and interpreting results from this study, is in preparation.

Material characterization requirements were defined for the specification of dynamic fracture toughness testing of RPV materials. The balance of the specification was produced in task 2. The specification will define the technical requirements for a dynamic fracture toughness testing subcontract, which will be placed by the HSST Program in the next reporting period. Data from this subcontract will be used in dynamic crack-arrest studies to assess the stability of arrested cracks.

7 Integration of Results Into a State-of-the-Art Methodology

The primary objective for this task is to extract and interpret fracture technology advances generated in the HSST Program research tasks, and in the Heavy-Section Steel Irradiation Program and other fracture technology research programs, and assemble them into a validated state-of-the-art methodology for assessing the structural integrity of irradiation-embrittled RPVs containing flaws. In addition, this task is responsible for the rapid transfer of fracture technology advances to national consensus codes and standards. Task 7 also provides special technical assistance to NRC for the evaluation and resolution of RPV structural integrity issues.

Elastic-plastic finite element analyses of the biaxial fracture toughness specimen have produced an underestimate of the measured CTOD when the material stress-strain curve derived from characterization tests is used directly in the analysis. In addition, analysis predicts that the ratio of crack-mouth-opening-displacement (CMOD) to load-line displacement (LLD) decreases as the ratio of transverse load (P_T) to longitudinal load (P_L) increases from 0.0 (uniaxial loading) to 0.6; the opposite trend was observed in the test results. An investigation was undertaken to determine if the material yield function used in the analysis was responsible for these discrepancies. The von Mises yield criterion was used in the finite element analyses of the biaxial specimens. A literature search revealed that, in the case of materials with an upper and lower yield stress and pronounced Lüders straining, the Tresca yield criterion may be a more appropriate choice. A preliminary scoping analysis showed that substituting the Tresca yield criterion in place of the von Mises yield criterion could have the effect of modifying the trend of the predicted CMOD vs LLD curve to match the trend observed in the test data. Direct confirmation of this result with finite-element analyses was not possible because the ABAQUS computer program used in the HSST Program for elastic-plastic analysis of the test specimens does not have a Tresca yield criterion capability. Two-dimensional (2-D) analyses of the test specimen were, however, performed by adapting the smoothed Mohr-Coulomb yield surface representation in ABACUS to give an approximate representation of the Tresca yield surface. These analyses showed the CMOD/LLD ratio to remain approximately constant over the loading range studied. Effects of biaxial loading, however, could not be investigated in this 2-D analysis. Further investigation of the influence of the yield criterion on the analysis predictions for the biaxial specimens will be contingent upon results obtained when a planned improvement in the representation of the material stress-strain properties has been incorporated into the analyses.

Heavy-Section Steel Technology Program Semiannual Progress Report for October 1993–March 1994

1 Program Management

W. E. Pennell

The Heavy Section Steel Technology (HSST) Program is conducted for the Nuclear Regulatory Commission (NRC) by Oak Ridge National Laboratory (ORNL). The program focus is on development and validation of technology for the assessment of fracture-prevention margins in commercial nuclear reactor pressure vessels (RPVs).

RPV structural integrity issues of current concern to the NRC are defined in the FY 1994 Statement of Work (SOW) for the HSST Program. Six technical issues are identified in the SOW: (1) crack-tip constraint effects on fracture toughness of RPV materials, (2) effects of stainless steel cladding on the initiation and propagation of shallow surface cracks, (3) ductile-to-cleavage fracture-mode conversion, (4) fracture-analysis methods development, (5) materials property data and test methods development, and (6) integration of results from the research programs into a state-of-the-art methodology for RPV structural integrity assessments. The HSST Program is structured to provide the research results required for resolution of these issues. Management direction and control of the program are implemented using a seven-element Level 1 work-breakdown structure (WBS) and a linked cost-schedule performance monitoring system. The current HSST Program Level 1 WBS is shown in Fig. 1.1. Each element of the Level 1 WBS represents a separate research or management task with a designated task leader. Within each of the Level 1 WBS elements, a Level 2 WBS defines research subtasks, and a Level 3 WBS defines the individual milestones within a subtask.

Staffing for the research tasks is drawn from the Engineering Technology (ETD), Metals and Ceramics, and Computing Applications Divisions at ORNL. Subcontracts with consultants, universities, and other research laboratories are used to gain access to special expertise and capabilities required for certain research tasks. A summary of resources applied to the HSST research tasks during this report period is given in Fig. 1.2.

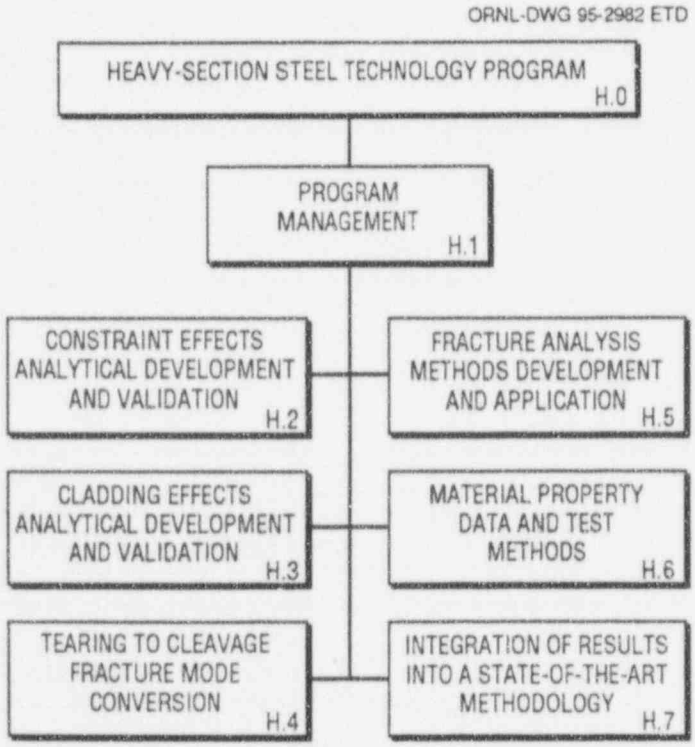

Figure 1.1 Level 1 breakdown structure for HSST Program

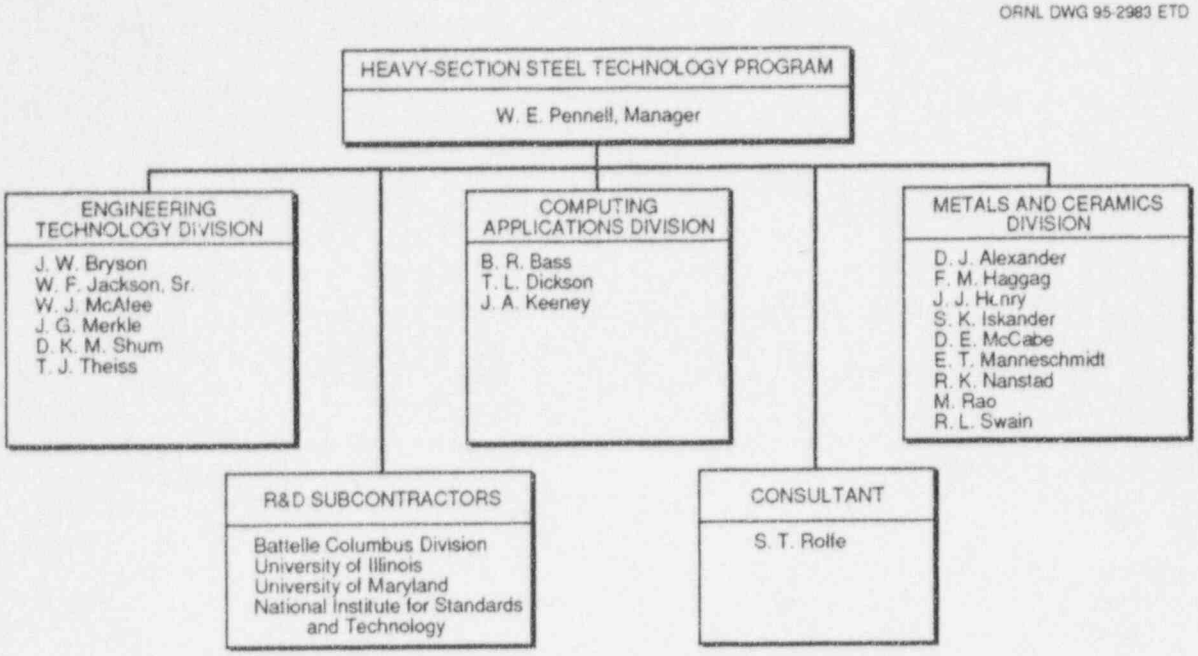

Figure 1.2 Resources applied to HSST Program R&D tasks

Two papers were produced in response to NRC direction during this reporting period. The first paper by W. E. Pennell, "Biaxial Loading and Shallow-Flaw Effects on Crack-Tip Constraint and Fracture-Toughness," and an associated viewgraph presentation, were prepared for presentation by the HSST program manager at the NRC 21st Water Reactor Safety Meeting at the Bethesda Marriott Hotel on October 25, 1993. The second paper by W. E. Pennell and W. R. Corwin, "Reactor Pressure Vessel Structural Integrity Research in the U.S. Nuclear Regulatory Commission HSST and HSSI Programs," was produced for presentation at the British Nuclear Energy Society Conference on Thermal Reactor Safety Assessment, in Manchester, England, in May 1994. The HSST program manager also prepared and gave two presentations outlining the objectives, technical approach, and current status of ongoing HSST Program research projects. "Overview of the HSST Program" was given to Drs. P. T. Kuo and J. W. Craig of NRC, and "HSST Program Research Into Constraint Effects in Fracture" was presented to Dr. H. L. Reynolds, Chairman of the ORNL Advisory Committee.

Discussions were held with the HSST Program subcontractors and consultants to review progress on existing subcontracts and define the subcontract work packages for FY 1995.

Progress on research topics defined in the SOW for the University of Maryland (UM) HSST Program subcontract for FY 1993 was reviewed in discussions with Prof. C. Schwartz and Prof. W. Fourney. It was determined that the reactor vessel dynamic analysis subtask could be completed on a schedule that would support the dynamic fracture toughness testing program schedule as defined in the HSST Program 189 for FY 1994.

A review of the status of the FY 1993 SOW items for the HSST subcontract with the National Institute for Standards and Technology (NIST) was conducted by telephone by the ORNL HSST program manager and the NIST subcontract manager, with input from the ORNL task managers. The focus of this status review was on the subcontract SOW items that had fallen behind schedule. It was agreed that NIST would assign additional resources to complete a letter report defining the large-scale biaxial-test fixture design, but completion would not be possible before the end date (March 31, 1994) for the existing interagency agreement (IAG). A no-cost extension to the IAG was, therefore, processed to move the completion date to June 30, 1994.

NIST also reported that its search for a vendor to perform electron beam welding of the reconstituted uniaxial large-scale clad-beam specimens had not been successful. It was, therefore, agreed that the HSST Program would fabricate specimens for the final two tests in the current test series from RPV shell segments available at ORNL. These test specimens were to be provided to NIST, eliminating any NIST costs for reconstituting the test specimens. In return, NIST absorbed the cost for repairs and replacements resulting from damage incurred in the second test. This arrangement produced the highest quality test results at a minimum cost to the program.

Telephone discussions were held with Prof. Bob Dodds of the University of Illinois (UI) to define the scope of work and deliverables for the UI subcontract for the FY 1994 performance period. This subcontract will focus on development of computational procedures for the prediction of ductile tearing in advance of cleavage fracture. The computational procedures incorporate the Gurson yield model and a node release algorithm to model crack growth.

Preliminary discussions on planned FY 1994 subcontracts and consulting agreements were also held with R. Link of the U.S. Naval Surface Warfare Center Research Laboratories (dynamic fracture-toughness testing) and Prof. S. Rolfe of the University of Kansas (consulting support). Preparation of documentation for the UM and UI subcontracts was completed.

The first of the full-scale, shallow-flaw, fracture-toughness tests performed by NIST resulted in a measured fracture toughness much lower than had been anticipated. Discussions were held between the HSST Program Manager and the NRC HSST Project Manager to determine the appropriate program response to this unanticipated result. It was agreed that additional large-scale, shallow-flaw, fracture toughness tests should be conducted in the FY 1994 performance period to further investigate the toughness of shallow flaws in full-thickness structural welds. The planned scope of the NIST IAG extension was to be modified to include these additional tests. Construction of the full-scale biaxial test facility at NIST was deferred until the FY 1995 performance period to accommodate this program change.

The available shallow-flaw, fracture-toughness data from tests conducted by ORNL, NIST, and the Carderock Division of the Naval Surface Warfare Center (CDNSWC) were collected into a data base. Material represented in the data base includes both A 533 B plate material and submerged-arc structural welds from a pressurized-water RPV. Test temperatures (T) spanning the lower shelf and the lower-transition range of the fracture-toughness curve were represented in the data base. The data were evaluated using both the nil-ductility transition temperature (NDT) and the reference temperature for nil-ductility transition (RT_{NDT}) as normalizing parameters. Results from this evaluation showed that lower-bound trends were similar for all three data sets when plotted as a function of $T - T_{NTD}$. When the data were plotted as a function of $T - RT_{NDT}$, however, they separated into two distinct families. Over a range of normalized test temperatures extending from $T - RT_{NDT} = -25°C$ to $+10°C$, the ORNL–NIST data exhibited pronounced transition range behavior, whereas the CDNSWC data did not. These results indicated that further testing of full-scale, shallow-flaw, fracture-toughness test specimens would be of particular value in helping to define the lower-transition-zone behavior of pressure vessel steels. Results from this evaluation provided support for the decision to extend the scope of the full-scale, shallow-flaw, fracture-toughness testing program at NIST.

A number of interactions with personnel from foreign fracture-technology research centers took place in this reporting period. Dr. Klingbeil of Bundesanstalt für Materialforschung und-prüfung (BAM), Berlin, Germany, and Prof. Brocks of the Fraunhofer Institute (IWM), Freiburg, Germany, visited ORNL on November 19, 1993 for discussions on constraint effects analysis and testing. Their crack-tip modeling development has proceeded to the point where they appear to be able to predict crack extension due to ductile tearing using a model based on void formation and coalescence. They expressed an interest in cooperating with the HSST Program in this area of fracture technology research. Their expression of interest was relayed to the NRC HSST project manager.

Dr. Ing. Ludwig Stumpfrock of Staatliche Materialprufungsanstalt Universitat Stuttgart (MPA) visited ORNL on February 15–16, 1994, for an exchange of information from ongoing fracture technology research programs. Dr. Stumpfrock presented results from the MPA dynamic fracture-toughness testing and constraint effects programs. Dynamic fracture-toughness tests were conducted for a number of materials using 10-mm-thick compact tension specimens. These tests showed no effect of loading rate on fracture toughness for loading rates spanning the range $1 < K_I < 2 \times 10^6$ MPa·$\sqrt{m}$ /s. The possible influence of loss of constraint in the 10-mm-thick specimens, on these results, was discussed but not resolved. Analysis and test results for notched round tensile specimens with varying notch root radii were also shown. The results showed that ductile tearing initiated at the point in the test specimen cross section where the ratio of the Von Mises equivalent stress to the hydrostatic stress (σ_E/σ_H) was a minimum.

A request for HSST Program data was received from Dr. M. Bethmont of the Department Etude Des Materiaux of Electricité de France. The request was for materials characterization data for the thermal shock experiments performed at ORNL. The data requested were compiled and forwarded to Dr. Bethmont, with the approval of the NRC HSST Project Manager.

The HSST Program manager is an active voting member of the American Society of Mechanical Engineers (ASME)

Program

Section XI Task Group on Operability and the ASME Section XI Working Group on Operating Plant Criteria. Two meetings of these groups were held in this reporting period.

The ASME Task Group on Operability is developing a proposed Code Case that is intended for use by a utility to determine the short-term operability of a nuclear power plant in which a nonconforming condition has been discovered during an operating cycle. The Working Group on Operating Plant Criteria has set priorities in the effort to develop an update proposal for Appendix G to Sect. XI of the code as (1) redefining the reference flaw geometry and (2) resolving the K_{Ic} vs K_{IR} issue. Proposals for redefinition of the reference flaw will reflect improvements in nondestructive examination technology that permits detection and sizing of flaws much smaller than the current reference 1/4t flaw. Fracture-toughness data produced by the HSST Program fracture-toughness tests of shallow-surface flaws will therefore be relevant to the item (1) initiative.

A listing of peer-reviewed research products generated by HSST Program personnel in FY 1993 was prepared and forwarded to the NRC HSST Program Monitor.

During the current reporting period, HSST Program personnel published 2 NUREG/CR reports,[1,2] 1 letter report,[3] 2 papers in technical society publications,[4,5] and they gave 12 presentations at technical society and NRC-sponsored national and international meetings.[6–17]

References

1. W. E. Pennell et al., Martin Marietta Energy Systems, Inc., Oak Ridge National Laboratory, "Heavy Section Steel Technology Program, Semiannual Progress Report for April–September 1992," USNRC Report NUREG/CR-4219 (ORNL/TM-9593/V9&N2) Vol. 9, No. 2, November 1993.*

2. B. R. Bass, J. W. Bryson, T. J. Theiss, and M. C. Rao, Martin Marietta Energy Systems, Inc., Oak Ridge National Laboratory, "Biaxial Loading and Shallow-Flaw Effects on Crack-Tip Constraint and Fracture Toughness," USNRC Report NUREG/CR-6132 (ORNL/TM-12498), January 1994.*

3. R. K. Nanstad, Martin Marietta Energy Systems, Inc., Oak Ridge National Laboratory, "Preliminary Review of Data Related to Inhomogenity of Steels for Reactor Pressure Vessels, ORNL/NRC/LTR-93/36, December 30, 1993.†

4. D. K M. Shum and J. G. Merkle, "Crack Initiation Under Generalized Plane-Strain Conditions," pp. 37–54 in *Fracture Mechanics: Twenty-Third Symposium*, ATSM STP 1189, Ravinder Chona, ed., American Society for Testing and Materials, Philadelphia, September 1993.‡

5. J. G. Merkle, "Near-Crack-Tip Transverse Strain Effects Estimated with a Large Strain Hollow Cylinder Analogy," pp. 95–114 in *Fracture Mechanics: Twenty-Third Symposium*, ASTM STP 1189, Ravinder Chona, ed., American Society for Testing and Materials, Philadelphia, September 1993.‡

6. R. K. Nanstad, J. A. Keeney, and D. E. McCabe, "Preliminary Review of the Bases for the K_{Ic} and K_{Ia} Curves in the ASME Code," presented to the ASME Section XI Working Group on Flaw Evaluation Meeting. Atlanta, Georgia, November 1993.

7. D. E. McCabe, "New Concepts in Transition Temperature Definition," presented at the Pressure Vessel Research Committee (PVRC) Workshop on K_{IR} Curves and RT_{NDTs}, New York, October 11, 1993.

8. R. K. Nanstad, J. A. Keeney, and D. E. McCabe, "Preliminary Review of the Bases for the K_{Ic} and K_{Ia} Curves in the ASME Code," presented at the PVRC Workshop on K_{IR} Curves and RT_{NDTs}, New York, October 11, 1993.

9. W. E. Pennell et al., "Biaxial Loading and Shallow-Flaw Effects on Crack-Tip Constraint and Fracture Toughness," presented at the 21st Water Reactor Safety Meeting, Bethesda, Maryland, October 1993.

10. T. J. Theiss, "Shallow-Flaw Biaxial Fracture Toughness Testing," presented at the JCCCNRS Working Group 3 Meeting in Rockville, Maryland, October 1993.

11. B. R. Bass, "Constraint Effects in Fracture," presented at the JCCCNRS Working Group 3 Meeting in Rockville, Maryland, October 1993.

12. W. E. Pennell, "Biaxial Loading and Shallow Flaw Effects on Crack-Tip Constraint and Fracture

Toughness," presented at the ASME Section XI Working Group on Operating Plant Criteria Meeting, Atlanta, Georgia, November 1993.

13. D. E. McCabe, Report to ASTM Task Group E08.03 on Ductile-to-Brittle Transition, presented at the ASTM Committee, Dallas, Texas, November 1993.

14. R. K. Nanstad, J. A. Keeney, and D. E. McCabe, "Preliminary Review of the Bases for K_{Ic} and K_{Ia} Curves in the ASME Code," presented at the ASME Section XI Working Group on Flaw Evaluation, ASME Meeting, Atlanta, Georgia, November 1993.

15. T. J. Theiss, B. R. Bass, and J. W. Bryson, Jr., "Experimental and Analytical Comparison of Constraint Effects Due to Biaxial Loading and Shallow Flaws," presented at the 2nd Constraint Effects in Fracture Symposium, Fort Worth, Texas, November 1993.

16. W. E. Pennell, "Overview of the HSST Program," presented to Dr. P. T. Kuo and J. W. Craig of the Division of Engineering, Office of Nuclear Regulatory Research, March 1994.

17. W. E. Pennell, "HSST Program Research into Constraint Effects in Fracture," presented to Dr. H. L. Reynolds, Chairman of the Oak Ridge National Laboratory/Engineering Technology Division Advisory Committee, March 1994.

18. T. L. Dickson, Martin Marietta Energy Systems, Inc., Oak Ridge National Laboratory, "FAVOR: Fracture Analysis Vessels: Oak Ridge," ORNL/NRC/LTR/94/1, February 1994.†

---

*Available from National Technical Information Service, Springfield, VA 22161.

†Available in NRC PDR for inspection and copying for a fee.

‡Available in public technical libraries.

2 Constraint Effects Analytical Development and Validation

W. J. McAfee

During this reporting period, the HSST Program was reorganized to consolidate related efforts into a more compact and efficient task structure. The effort in this Task 2 is then a composite of work that was formerly defined under Task 6, Cleavage Crack Initiation; Task 10, Fracture Evaluation Tests; and Task 12, Biaxial Loading Effects on Fracture Toughness. Currently, Task 2 is divided into three subtasks: 2.1 Biaxial Loading Effects Validation Testing (Verification Phase Testing and Analytical Support), 2.2 Constraint Effects Correlation, and 2.3 Unclad Finite-Length Flaw Development.

2.1 Development of Surrogate Irradiated Base Material

(S. K. Iskander, D. J. Alexander, R. K. Nanstad, G. M. Goodwin, J. F. King, J. J. Henry, Jr., and E. T. Manneschmidt)

Several of the HSST tasks require the use of materials with relevant properties that simulate "prototypical" irradiated RPV base metal properties. A desirable goal for the base metal is a temperature at the 68-J Charpy impact energy level ($T_{68\text{-}J}$) greater than 50°C (≈120°F) and a room temperature yield strength, YS_{RT}, in the range of 620 to 690 MPa (90 to 100 ksi). These are approximate values for a typical RPV steel irradiated to a fluence of 1.5×10^{19} neutrons/cm^2 (>1 MeV).

One approach used to simulate the irradiated properties is similar to that used in a previous task of the HSST Program:[1] the material is quenched in water and then tempered at a relatively low temperature. Two blocks of material were quenched. To one block, a thermal buffer ("a picture frame") was attached. The object of the buffer, which is removed after the quenching, is to limit the heat transfer during the quenching operation to the top and bottom surfaces of the plate only, thereby simulating quenching operations on a "large" plate. To allow for the removal of the decarburized surface layer, the dimensions of the second block were slightly larger than the final ones of the test section of the biaxial specimen. Two such blocks from HSST Plate 14 were first austenitized at 900°C (1650°F) for 5.5 h, followed by a water quench. These austenitizing and quenching operations were performed by a commercial vendor, and an ORNL representative attended the quenching operation and performed a quality assurance check.

Different tempering and normalizing treatments were then performed on ~13-mm-thick coupons machined from quenched material. Charpy V-notch (CVN) and tensile specimens were then machined and tested from material in the various heat-treated conditions, in many cases at several depths through the thickness, to determine whether properties varied through the thickness. A summary of the different heat treatments and tests performed is given in Table 2.1. Note that the YS_{RT} of the quench-only material exceeded 1200 MPa (175 ksi), the ultimate strength was >1500 MPa (>215 ksi), and the $T_{68\text{-}J}$ was ~100°C. A 510°C/5-h tempering decreased the YS_{RT} to 970 MPa (140 ksi), which is still considerably higher* than the target. Moreover, the shift of the Charpy energy curve at the 41-J energy level was 75°C toward lower temperatures, and the upper-shelf energy was ~70 J.

However, tests on a 13-mm coupon of the *quenched* material that was normalized [austenitized at 1010°C (1850°F) for 30 min and then air-cooled] were more promising. These tests have shown that the $T_{68\text{-}J}$ is ~90°C (193°F), and YS_{RT} is ~627 MPa (91 ksi). Metallographic and fractographic examinations on broken Charpy specimens have not revealed any atypical microstructure or fracture surface features. Because of these promising results, this normalization was applied to a block of HSST Plate 14 of the same size as that planned for use as the test sections of the biaxial beams, namely 115 mm thick, 150 m wide, and 150 mm long. The time-at-temperature was increased to 4 h to adjust for the greater thickness of the material. Tensile and CVN impact tests have been performed, and the results are given in the following paragraphs.

The CVN results of specimens machined in the T-L orientation and at various depths through the thickness are shown in Fig. 2.1. A hyperbolic tangent equation was fit through each set of data from a particular depth through the thickness. The resulting parameters and the temperature at various energy levels are given in Table 2.2. The temperature at the 27-J (20-ft-lb) level often correlates with the drop-weight NDT temperature. The $T_{68\text{-}J}$ could be used to estimate the RT_{NDT} temperature if the CVN criteria were dominant in the RT_{NDT} determination.

The results of room-temperature tensile tests of material from various depths through the thickness are shown in

*It is estimated that yield strengths higher than 690 MPa (100 ksi) may exceed the capacity of the machine to break the specimen.

Table. 2.1 Characterization performed on HSST Plate 14 in various heat-treated conditions

Code	Heat treatment	Charpy orientation and specimen numbers	Tensile orientation and specimen numbers	Miscellaneous[a]
1	As received	L-S 01401–01424		Fracture toughness K_J, L-S orientation with flaws prepared by: Fatigue precracking 014Nxx EDM 014Exx EB/H_2 charging 014Hxx ABI on 1/2 CVN 01408 X Drop-weight NDT
2	100-mm (4-in.) *unbuffered* block, quench-only, 900°C (1650°F)/water	T-L at 3 depths: Surface Q1401-12 Near surface Q1420-32 Midthickness Q1440-52	T through thickness Near surface Q1408 to Q1414 near mid-(t)	HRC on 1/2 CVNs: Surface Q1401 Midthickness Q1447 Top Layer Q1409 ABI on 1/2 CVN Q1408 ✓
3	13-mm slab from Code 2 + tempered 510°C (950°F)/5 h	T-L at 3 depths: Surface A1401-18 Near surface A1420-38 Midthickness A1440-58	T through thickness Near surface Q1401 to Q1406 near mid-(t)	Hardness RC on coupons "6B" and "1B" ABI on 1/2 CVN A1445 X
4	Quench-only, 100-mm (4-in.) *buffered* block	T-L, QB1401-12	T, QB141-2	Hardness RC on 1/2 CVN QB1414 ABI on 1/2 CVN QB1408 X
5	13-mm slab from Code 2 + tempered 676°C (1250°F)/91 h	T-L, A1401-9, A1410-12	T, A1401-2	Hardness RB on 1/2 CVN A1408 ABI on 1/2 CVN A1410 ✓
6	13-mm slab from Code 2 + normalized 1010°C (1850°F)/0.5 h	T-L, N1401-9, N1410-12	T, N1401-2	Hardness RB on 1/2 CVN N1410 ABI on 1/2 CVN A1402 X
7	As-received, 100-mm (4-in.) block normalized 1010°C (1850°F)/4 h	T-L, 4 layers, 14E01-48	T, 14E01-07	Hardness RB on 1/2 CVN 14E12, -28, -50, -67

[a] ✓ = indicates test is complete; X = indicates specimens were put in hot cell but testing not performed.

Fig. 2.2. The YS_{RT} is ~560 MPa (81 ksi) and varied less than ±10 MPa (±1.5 ksi) over the entire 115-mm thickness of the block. Although this yield strength is less than the target value, it may still be usable because material in this heat-treated condition appears to harden rapidly (Fig. 2.3). Detailed finite-element analyses (FEA) are necessary to evaluate its usability. Some judgment is required to determine a suitable yield strength as an input value to the FEA, because the conventional 0.2% yield strength does not correspond to any unique change in material behavior (see Fig. 2.3). This particular normalization heat treatment is still being evaluated with regard to its suitability to produce a surrogate irradiated material.

Note that both the YS_{RT} and $T_{68\text{-}J}$ values of the material normalized at 1010°C from the 115-mm block are lower than those from the 13-mm coupon. The thermal inertia due to the different sizes likely resulted in different cooling rates. Another difference may have been due to slightly different metallographic features (grain size) caused by the severe quenching undergone by the 13-mm coupon. The normalization on the 115-mm block was performed on the as-received condition of Plate 14, whereas that on the 13-mm coupon was carried out on a block of material from the same plate, but was water quenched.

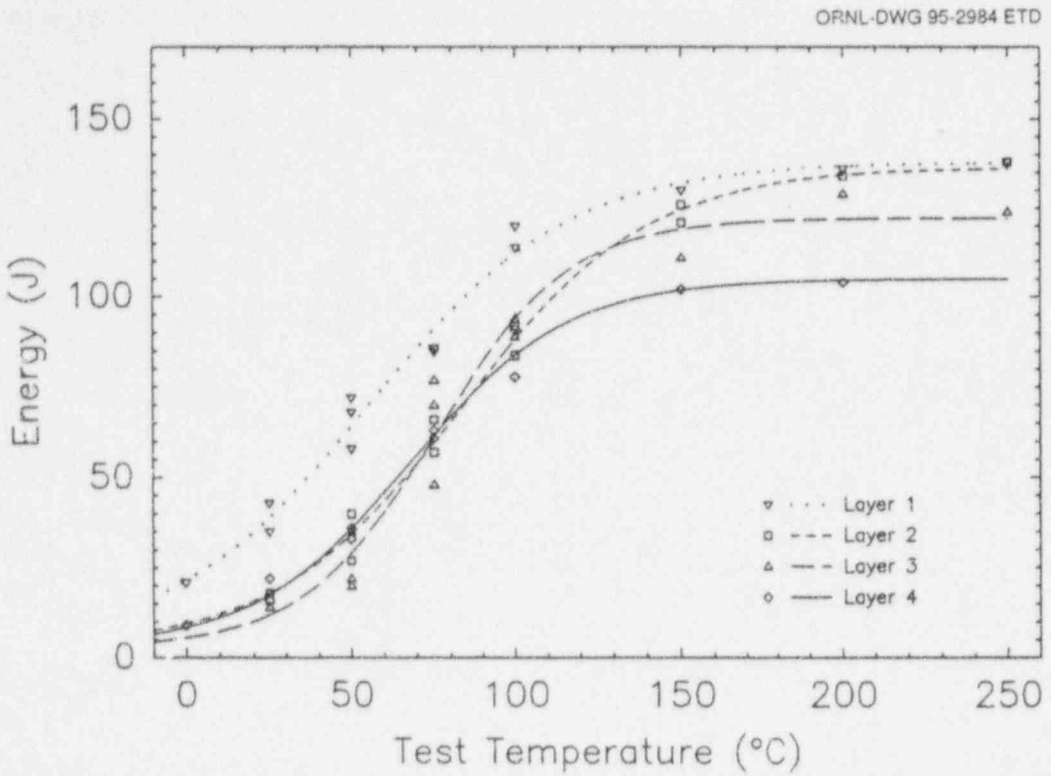

Figure 2.1 Results of testing CVN specimens in T-L orientation and at various depths through the thickness. Specimens were machined from a 115 × 150 × 150-mm-thick block from HSST Plate 14 that was normalized at 1010°C (1850°F) for 4 h and then air cooled

Table 2.2 Summary of CVN energy testing on specimens in the T-L orientation [machined from different depths of a 115-mm-thick × 150-mm-long × 150-mm-wide block from HSST Plate 14 normalized at 1010°C (1850°F) for 4 h and air cooled]

Layer[a]	Tanh fit parameters[b]			Temperature at three energy levels [°C(°F)]		
	USE [°C(°F)]	MTT [°C(°F)]	TZW [°C(°F)]	27 J (20 ft-lb)	41 J (30 ft-lb)	68 J (50 ft-lb)
1	137.9 (101.7)	55.5 (131.9)	121.9 (219.4)	9.42 (49.0)	27.2 (81.0)	53.4 (128.1)
2	136.5 (100.7)	83.5 (182.3)	114.3 (205.7)	40.7 (105.3)	57.4 (135.3)	82.1 (179.8)
3	122.3 (90.2)	75.8 (168.4)	82.0 (147.6)	47.9 (118.2)	60.4 (140.7)	79.6 (175.3)
4	105.0 (77.4)	67.5 (153.5)	95.9 (172.6)	39.7 (103.5)	55.2 (131.4)	81.1 (178.0)

[a]Layer 1 was about 2 mm below the mill-scale surface and was adjacent to a steel plate during heat treatment; layer 2 was just below the centerline of the 115-mm block; layers 3 and 4 were adjacent to each other, with layer 4 about 2 mm below the sawn surface.

[b]Equation used to fit data: (USE + 2.7)/2 + [(USE – 2.7)/2] Tanh (T – MTT)/TZW/2), where USE = upper-shelf energy, 2.7 = lower-shelf energy, MTT = midtransition temperature, and TZW = transition zone width. The 2.7 J is the lower-shelf energy and was determined experimentally from five tests conducted at liquid nitrogen temperature, –196°C, on SAW from the Midland RPV.

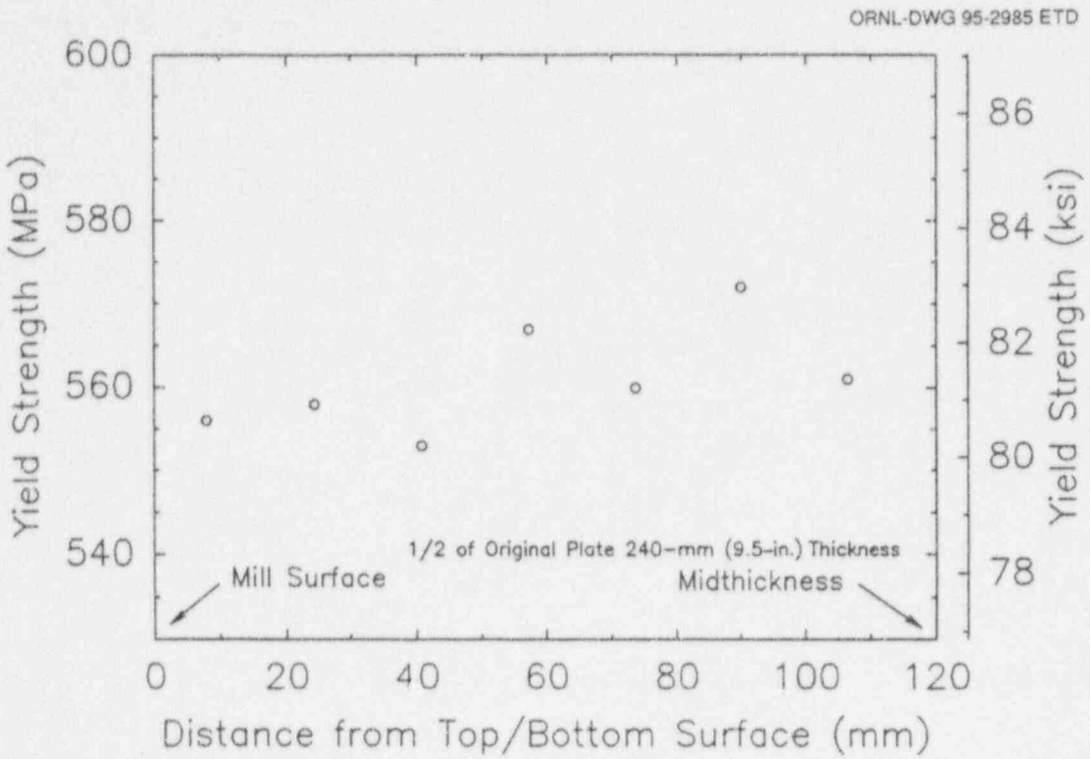

Figure 2.2 Results of room-temperature tensile test on specimens in T-orientation and at various depths through the thickness. Specimens were machined from a 115 × 150 × 150-mm-thick block from HSST Plate 14 that was normalized at 1010°C (1850°F) for 4 h and then air cooled

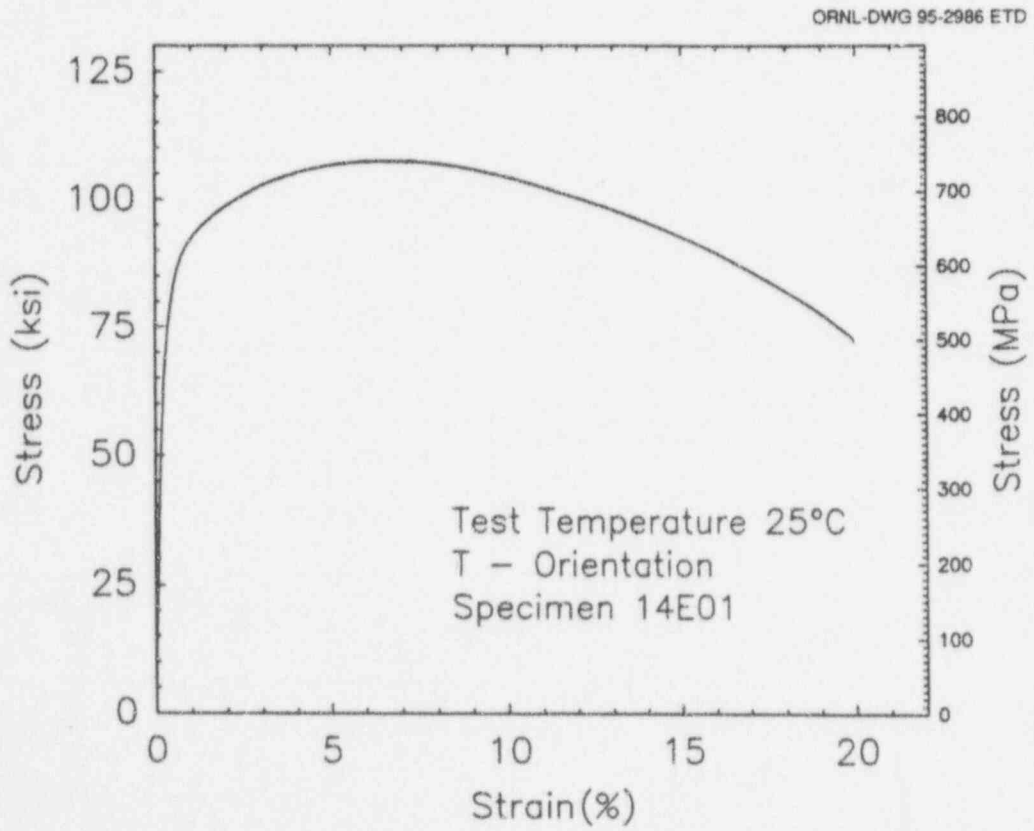

Figure 2.3 Room-temperature tensile stress-strain curve of transversely oriented specimen from HSST Plate 14 normalized at 1010°C (1850°F) for 4 h and then air cooled

2.2 Test and Analysis of Load-Ratio Matrix Cruciform Specimens

(W. J. McAfee, B. R. Bass, J. W. Bryson, and W. F. Jackson, Jr.)

Under direction of the sponsor, plans were initiated to fabricate and test an additional four cruciform beams to complete the load-ratio matrix. These specimens were of the same design and of the same material as the first five. The test matrix defined three specimens to be tested under 1:1 biaxial loading and one to be tested under to-be-determined (TBD) biaxial conditions. All other test variables were to be the same as for the previous set of five specimens.

All fabrication sequences were the same except for electron beam (EB) welding of the beam arms to the test section. In an attempt to develop an alternate supplier for EB welding, a contract was placed with an outside vendor to weld the beam arms onto these four specimens. When the specimens, in uniaxial configuration, were returned and machining to removed the EB weld run-off tabs and weld beads was completed, surface defects in the form of surface voids were observed in the EB welds. One beam, having what appeared to be the least amount of defects, was x-rayed to determine the extent of the voids, that is, were they surface or volumetric defects. It was found that the voids were indeed volumetric. In discussions with the vendor, it was concluded that this porosity might be removed by re-fusing (re-welding) the joints. The beams were thus returned, and the beam arm to test section weld joints were re-fused using the EB weld process. The beam that had been identified as having the least amount of initial porosity was next carried through the complete fabrication and test process. It was fatigue precracked, returned to the vendor for attachment of the transverse beams arms, final machined, instrumented, and tested to failure.

Because the integrity of the specimen was suspect due to the fabrication difficulties, the specimen was tested under 0.6:1 biaxial loading at –46°C (–50°F) to provide a benchmark against the previous data set. The test was not successful. One of the EB welded ligaments failed before failure of the test flaw as shown in Fig. 2.4. While the failure mode was predominantly cleavage and the initiation site was within the desired flaw-tip region (center two-thirds of flaw length), a meaningful value of fracture toughness could not be determined due to the redistribution of load on the test section after failure of the ligament. Also, during failure, the specimen underwent gross plasticity in the test section as can be seen in Fig. 2.5. When compared to previous biaxial tests, this specimen exhibited a 250% increase in measured load-line displacement (LLD) and crack-mouth-opening displacement (CMOD) with only an 8% increase in failure load. This plasticity increase is consistent with a softer material, and it was suspected that the

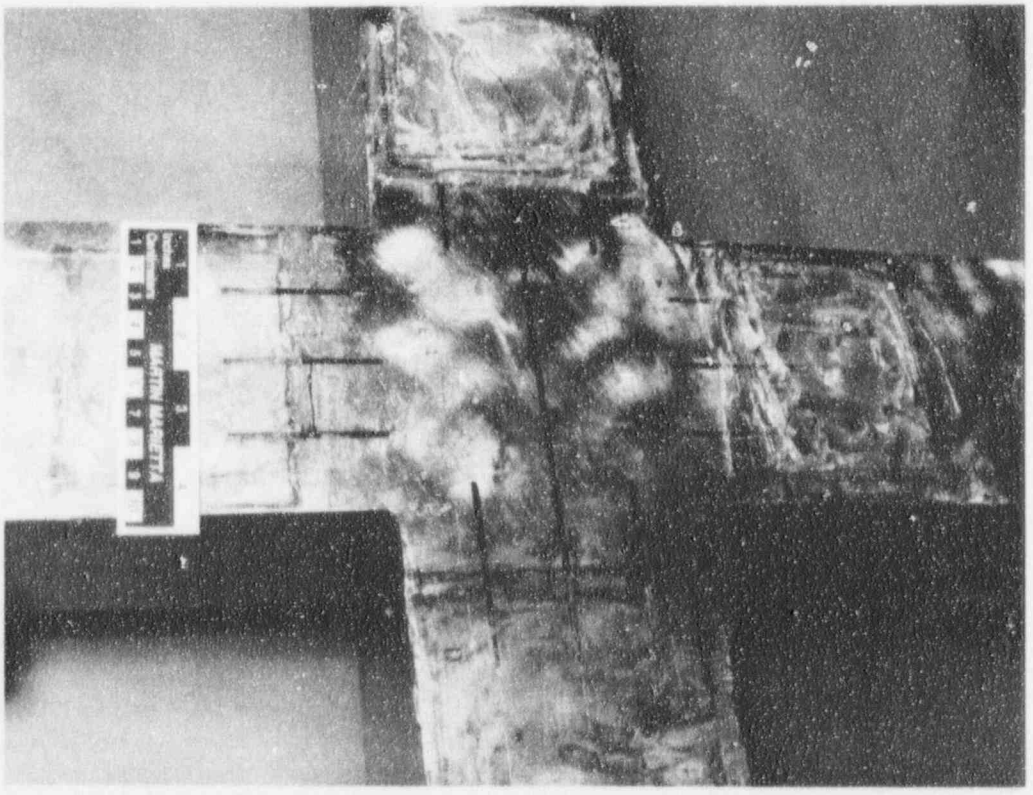

Figure 2.4 View of biaxial specimen BB-6 showing failed EB weld ligament

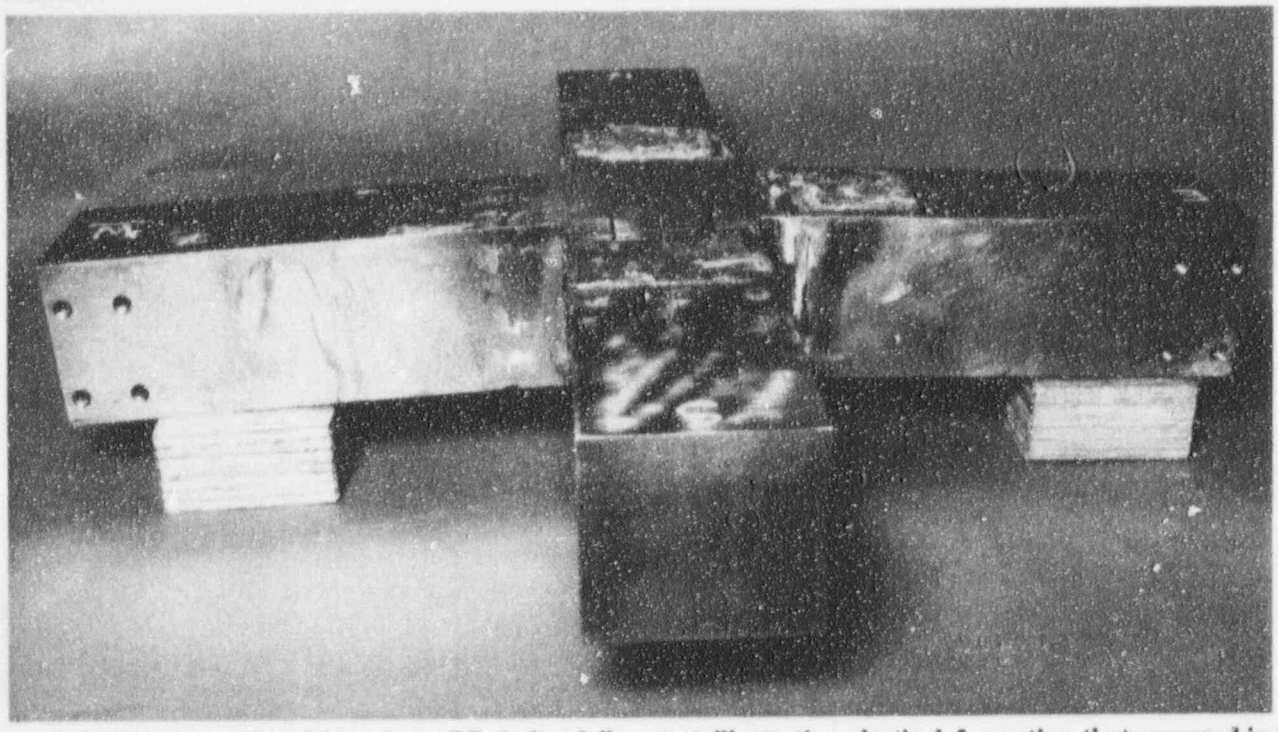

Figure 2.5 Side view of biaxial specimen BB-6 after failure test, illustrating plastic deformation that occurred in test section

properties of the test material may have been modified by inadvertent heat treatment during fabrication. This was substantiated by the appearance of the specimens. As returned from the EB weld vendor, all of the specimens appeared to be heat-tinted blue. Some blue tint is expected from the EB weld process and is associated with vaporization and surface deposition of material during welding. This is a common phenomenon and has been observed on other specimens but not to the extent seen here. When compared to a temper color chart,[2] the specimen may have been as hot as 350°C. Because EB welding is performed in a vacuum, this may represent the temperature of the specimen when it was removed from the chamber, that is, not the maximum temperature achieved. Discussions with the vendor could not establish conclusively the heat input and specimen temperature during the repair weld process.

As a further attempt to establish the possibility that the test material may have been slightly heat treated, hardness measurements were made on coupons from specimen BB-6 and material from the previous set of specimens. There was little difference in hardness, but it should be remembered that hardness correlates more with ultimate strength than with yield strength.

It was concluded that the data obtained from this particular batch of specimens would be suspect even if the EB weld ligaments remained intact. It was thus recommended to and accepted by NRC that the remaining three specimens not be tested. It has been further proposed that four new specimens be fabricated using additional Combustion Engineering (CE) plate material on hand. A modified design would be employed as is shown in Fig. 2.6. The legs of the test section have been extended such that the load diffusion control slots (LDCSs) can be contained completely within the leg proper. The EB weld joining the test section to the beam arm then joins homogeneous materials. In the previous design, the EB weld was made across the center length of the LDCS, which required use of a shim insert in each slot to fill what would otherwise be a void. It was hypothesized that this may have contributed to the porosity observed in welds. In fabricating these new specimens, the EB welding will be done in-house.

2.3 Test and Analysis of Unclad Finite-Length Flaw Cruciform Specimens

(W. J. McAfee, B. R. Bass, J. W. Bryson, and W. F. Jackson, Jr.)

The overall objective of these tests is to investigate the influence of finite-length flaw profiles, out-of-plane loading, and material condition on the effective fracture toughness of RPV plate material. The specific objectives for the subtask are to develop and qualify a viable test specimen, to develop appropriate fabrication procedures, to develop appropriate test procedures, and to generate a limited set of data to examine the influence of flaw geometry and biaxial loading on fracture toughness. An important consideration

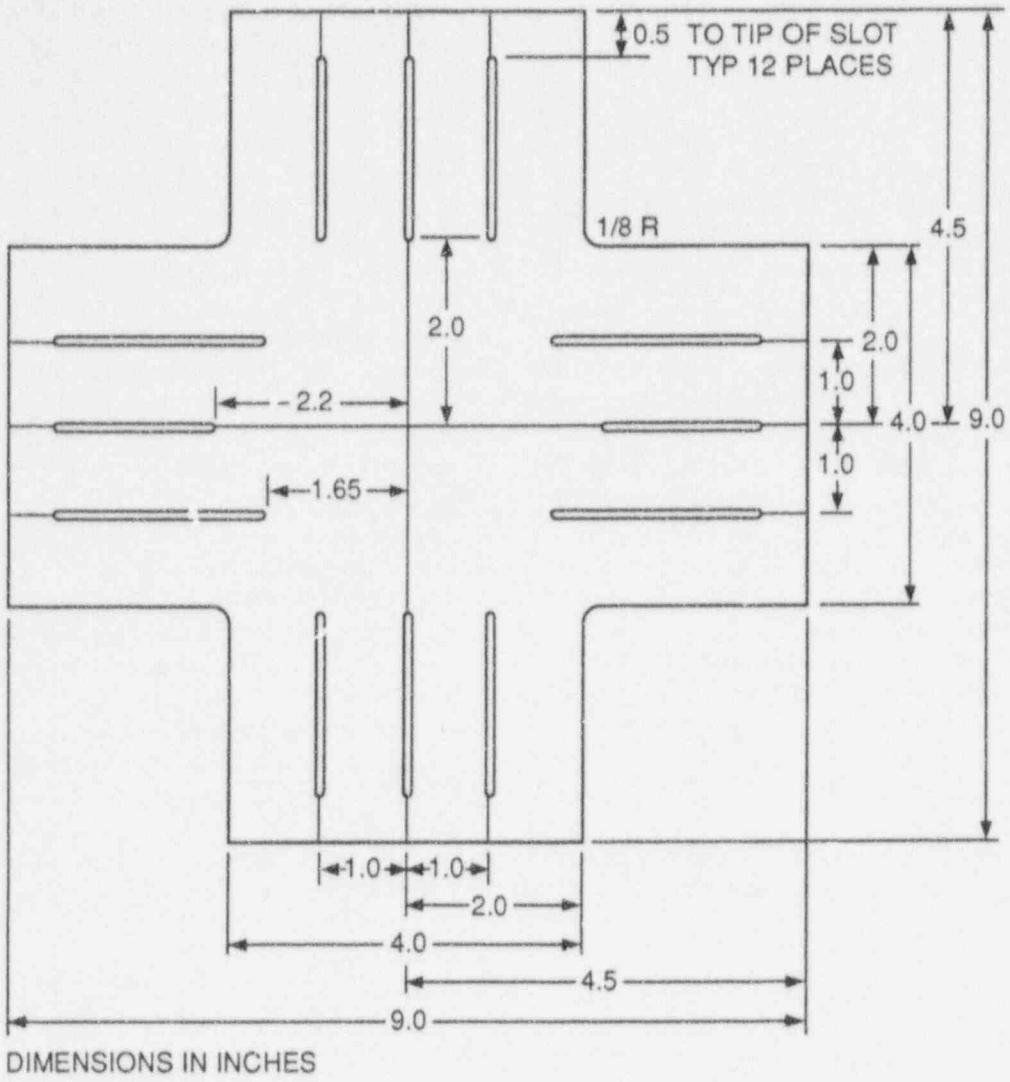

Figure 2.6 Schematic of modified test section for cruciform beam specimens

in the development of a test specimen and appropriate test procedures is establishing a specimen size that permits investigation of the desired range of test parameters yet does not exceed the test capacity of the biaxial fixture. The elements of this subtask are discussed below.

2.3.1 Investigation of Flawing Procedures

(W. J. McAfee, S. K. Iskander, R. K. Nanstad, J. J. Henry, W. F. Jackson, and E. T. Manneschmidt)

In fabrication of shallow-flaw beam specimens, the EDM process has been used successfully to machine the flaw. As with compact tension (CT) fracture specimens, fatigue precracking is then used to sharpen the flaw with the intent of achieving reduced scatter in the data. For the cruciform beam specimens, this requires multiple steps to machine the flaw, assemble the specimen into a uniaxial beam, fatigue precrack, complete assembly, and test to failure. Conventional fracture toughness data are generated using fatigue precracked CT specimens while previous thermal-shock cylinder tests incorporated flaws prepared using the EB weld–hydrogen charge technique. Utilization of these different flawing techniques in conjunction with concerns about control of flaw geometry for the finite-length flaws and the desire to make more efficient the overall cruciform beam fabrication process led to definition of an effort to investigate the fracture behavior of flaws developed using different techniques. The intent is to provide a basis for selection of a flawing technique for the finite-length flaw specimens. A matrix of 36 1TCT specimens was machined, 12 specimens in each of three configurations: (1) conventional chevron-grooved CT, (2) straight-through flaw with minimum achievable flaw-tip radius using the wire electrodischarge machining process (EDM), and (3) straight-through flaw sharpened using the EB weld–hydrogen

charge technique. The EDM flawing procedure with no fatigue precracking was considered because this represents a very simple, inexpensive, and highly controllable technique for flaw preparation.

Testing of this matrix of the 36 1TCT flaw development specimens has been completed. The flaw types were separated into two groups of six specimens each. Six was selected as being sufficient to yield a statistically significant set. The groups were tested at –62°C (–80°F) and –34°C (–30°F). The chevron-grooved fatigue precracked specimens gave very consistent results at both test temperatures as shown in Fig. 2.7. Also shown in Fig. 2.7 are the results for the EDM flaw (no fatigue precracking) specimens. The EDM flaw specimens yielded an artificially high value of toughness, which is probably due to the bluntness of the initial flaw. This process alone for generating a test flaw is then not considered to be a viable option for the finite-length flaw beam specimens. This observation is somewhat at variance with the work of Wilshaw et al., which indicated that there was a lower bound to crack-tip sharpness (~0.005 cm) below which indicated toughness would not change.[3] The results are consistent, however, with the recent work of Joyce and Link.[4]

It had been intended to test six of the EB weld–hydrogen charged specimens at –85°C and six at –30°C as with the other specimen types. The first six specimens tested at –30°C and gave inconsistent results as shown in Fig. 2.8. Three of these specimens underwent pop-ins at low-toughness values followed by failure at relatively high-toughness values (compared to the results for the fatigue precracked specimens). The remaining three specimens failed at toughness values less than those of the fatigue precracked specimens tested at the same temperature. One hypothesis for this behavior is that residual hydrogen at the crack tip caused embrittlement of the specimens exhibiting pop-ins. To investigate this, the last six EB weld–hydrogen charged specimens were baked at 140 to 150°C for 90 h to remove any residual hydrogen. The specimens were then tested at –30°C. The results are shown in Fig. 2.8. The K_{Jc} mean and standard deviation are 105 and 41 MPa$\sqrt{m}$, respectively, compared to 113 and 23 MPa$\sqrt{m}$ for the fatigue precracked specimens. For the six EB weld–hydrogen charged specimens that were not baked, the corresponding mean and standard deviation were 112 and 37 MPa$\sqrt{m}$. The role of residual hydrogen at the flaw tip would appear to be to lower the initiation toughness to a value below the arrest toughness for this material. However, this effect must be considered to be small when comparing the scatterbands for the unbaked and baked specimens. The mean and standard deviation for all EB weld–hydrogen charged specimens were 109 and 37 MPa$\sqrt{m}$, respectively. Thus, while the mean K_{Jc} for all EB weld–hydrogen charged specimens is only slightly less than that for fatigue precracked specimens, the scatter is

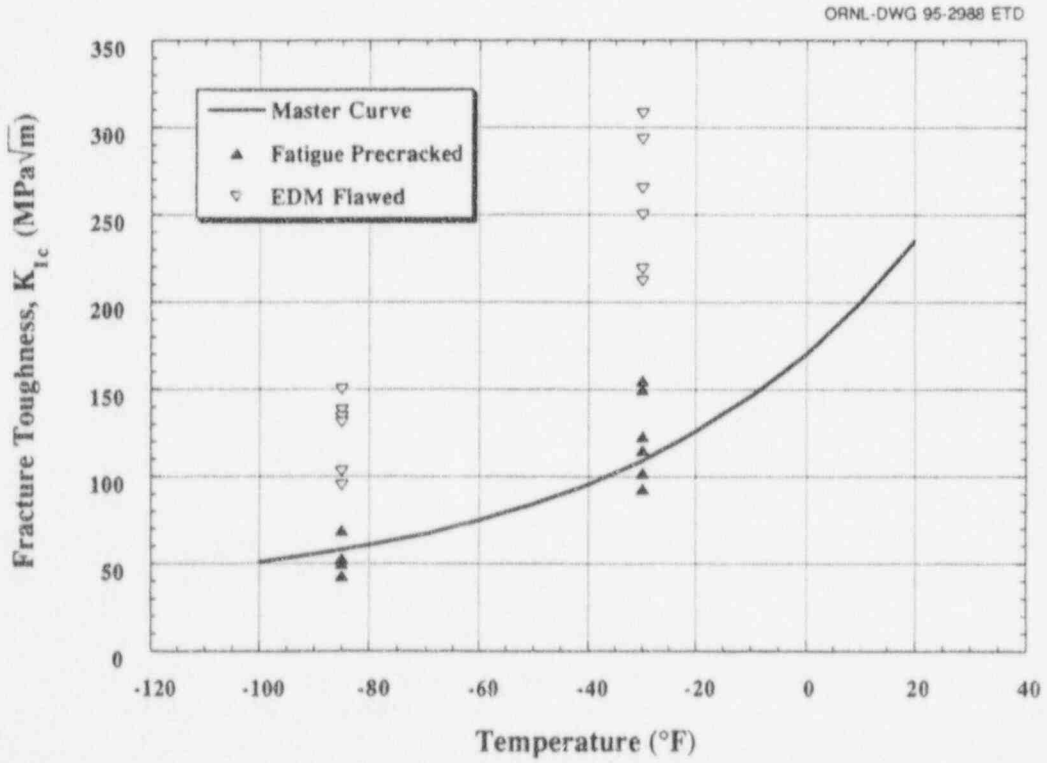

Figure 2.7 Comparison of toughness values determined from 1T CT specimens with either EDM sharpened flaw or chevron-grooved fatigue precracked flaw

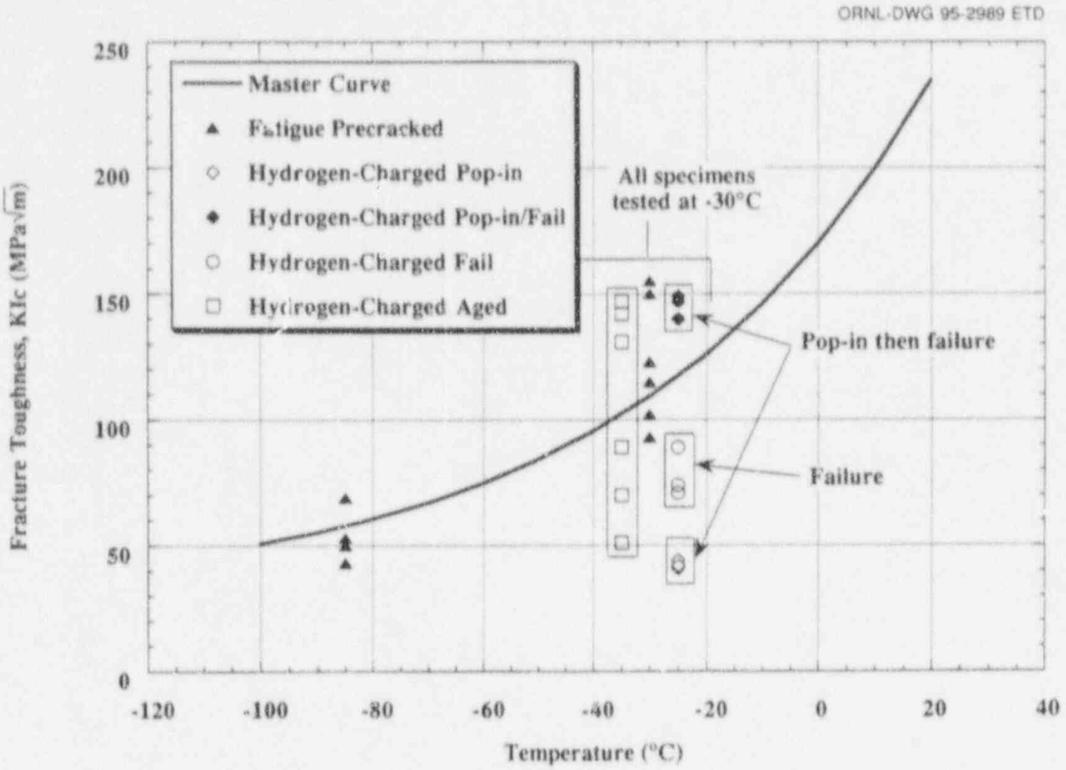

Figure 2.8 Comparison of toughness values determined from 1T CT specimens with either chevron-grooved fatigue precracked flaw or EB-weld hydrogen-charged flaw

significantly greater. The conclusion from this work is that fatigue precracking to sharpen test flaws in the cruciform beams is the preferred method to achieve consistent results with minimization of scatter in the data.

2.3.2 Finite-Length Flaw Specimen Fabrication and Testing (W. J. McAfee, J. W. Bryson, and W. F. Jackson, Jr.)

The biaxial, finite-length flaw test specimen design has been described in detail previously.[5] The initial flaw geometry selected was a 1.52-cm-deep by 3.81-cm-long (0.6-in. by 1.5-in.) semiellipse. This geometry was developed based on criteria that were established for the general specimen behavior and was to be treated as a reference flaw for future tests in this series. The through-surface finite-length flaw was ram-EDM into the top surface of the test section, while the overall test section plan form, including the LDCSs, was cut from the parent plate segment using the wire EDM process. The resulting flaw width at the specimen surface is ~0.051 cm (~0.020-in.) at the widest point (center) tapering to a tip radius of ~0.007 cm (~0.003-in.) These dimensions were determined by machining several development flaws, which were then sectioned to measure the final flaw configuration. Figure 2.9 clearly shows the number and pattern of diffusion slots being used for these specimens as well as the location of the test flaw. Component parts for six specimens have been machined. Three uniaxial assemblies, in the form used for fatigue precracking, were completed for initial testing to investigate the general response of this particular flaw/specimen configuration. The plan was to fatigue precrack and test to failure two of these specimens in this uniaxial configuration (i.e., no transverse beam arms) to determine the crack growth and compliance characteristics of the machined flaw, the general load distribution through the test section, and the failure characteristic of the specimen. The third specimen was then to be fatigue precracked, assembly completed, and tested to failure under biaxial loading. Figure 2.10 shows one of these specimens with the instrumentation layout used for these tests. A total of ten foil strain gages and three clip gages were used. The strain gages mounted on the test section (8) were to verify the field of surface strain distribution around the flaw as compared to analyses. Those on the beam arms were for verification of applied loading. The clip gages were to measure both compliance change during fatigue precracking and CMOD during the failure test.

Preparatory to testing, FEAs were performed to assist in selection of fatigue loading. Figure 2.11 shows the geometry used as the basis for these pretest analyses. As noted above, the reference flaw geometry was a 1.52-cm-deep by 3.81-cm-long (0.6-in. by 1.5-in.) semiellipse. The material

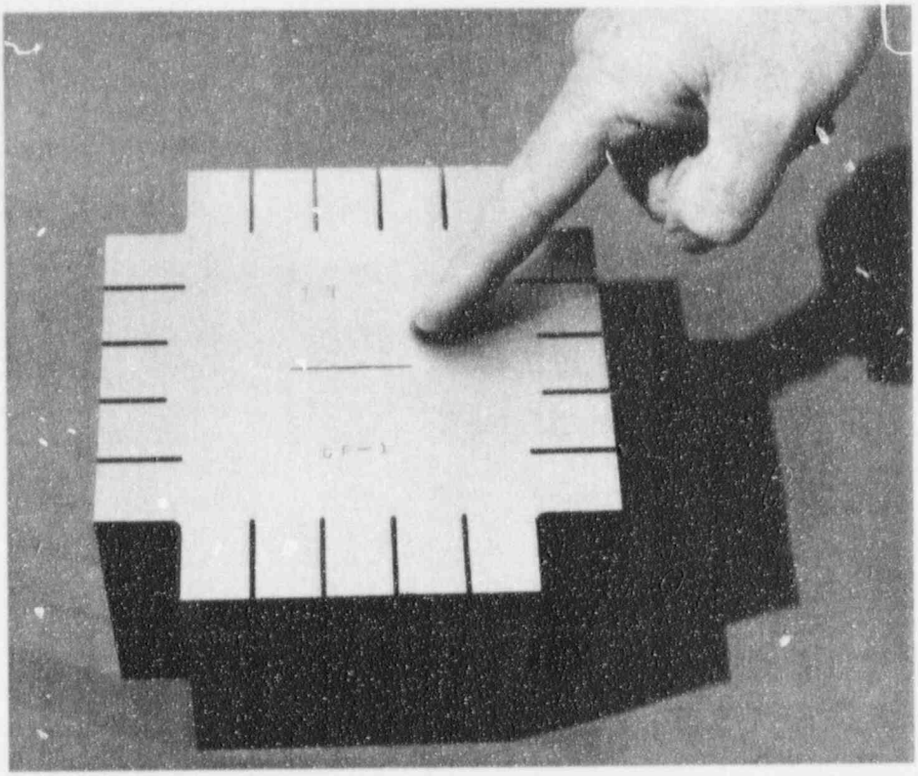

Figure 2.9 Overview of finite-length flaw test section showing details of test flaw and pattern of LDCSs

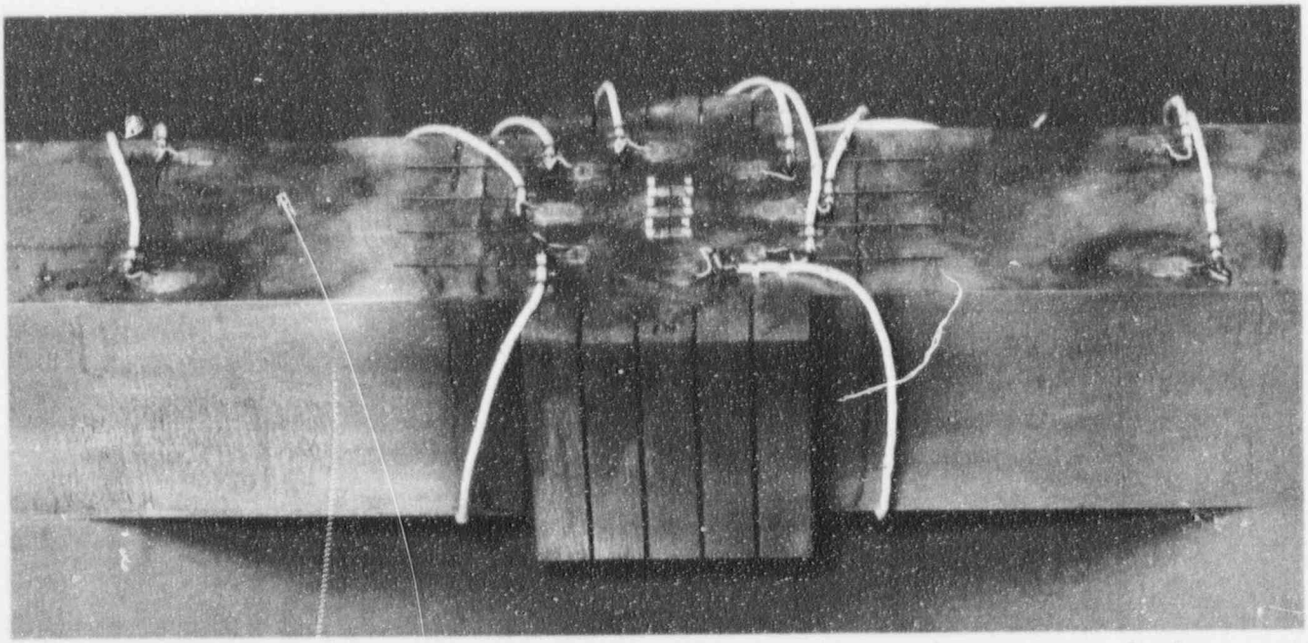

Figure 2.10 First finite-length flaw specimen in uniaxial configuration instrumented preparatory to development test

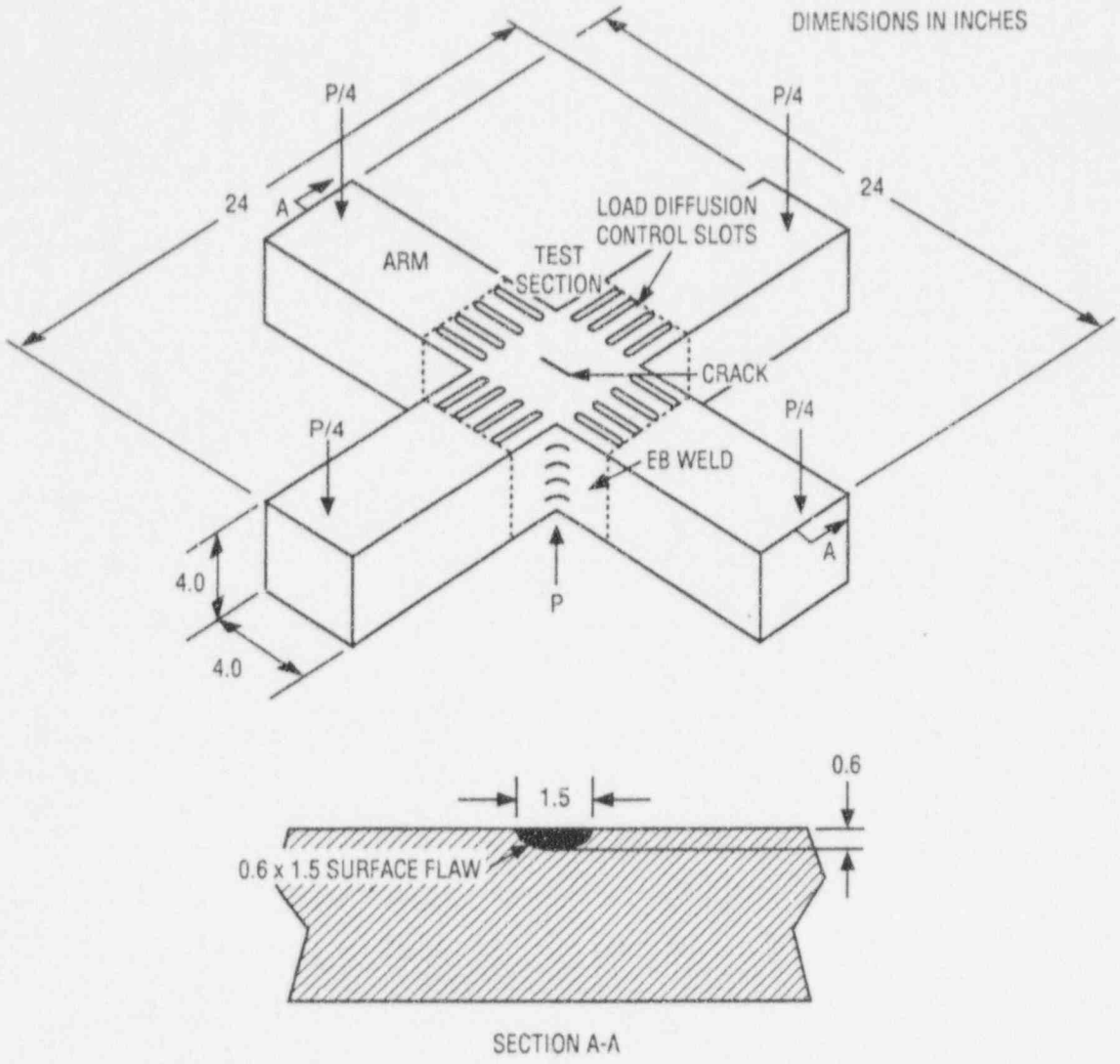

Figure 2.11 Schematic of finite-length flaw specimen showing dimensions, load points, and flaw geometry used in analyses

properties used were the same as those used in previous analyses for the biaxial beams. Figure 2.12 shows results for the variation of K_J along the crack front at different load levels under uniaxial loading. These were elastic-plastic analyses using the code ABAQUS. For a ΔK in the range of 27.5 to 38.5 MPa$\sqrt{m}$ (25 to 35 ksi$\sqrt{in.}$), which was the desired range for fatigue precracking, the load range was selected to be 65 to 75 kips (see Fig. 2.12). For an estimated minimum failure toughness of 90 MPa$\sqrt{m}$ (81 ksi$\sqrt{in.}$), this load range results in a maximum K not exceeding 38.5 MPa$\sqrt{m}$ (35 ksi$\sqrt{in.}$) and meeting the requirements of ASTM E399.[6]

The first of these specimens, CF-4, was fatigue prec: cked and tested to failure at temperature of –31°C (–23°F) to determine flaw growth behavior for this geometry. The failure temperature was selected based on the 1TCT specimen data for this material (see Fig. 2.7). The fatigue growth characteristics for the flaw were very regular because essentially uniform growth was achieved around the full periphery of the flaw front. This may be seen in Fig. 2.13, which shows the fracture surface for this specimen. The amount of flaw growth was less than had been estimated based on the pretest analyses, ~0.6 mm (0.024 in.) compared to a target of 1.27 mm (0.050 in.). In addition, the specimen underwent substantial plastic deformation before failure such that a reliable estimate of toughness could not be made. Three possibilities seemed to exist for such plasticity behavior: (1) the material yield was less than had been anticipated, (2) the flaw had not grown sufficiently to adequately form a sharp metallurgical notch, or

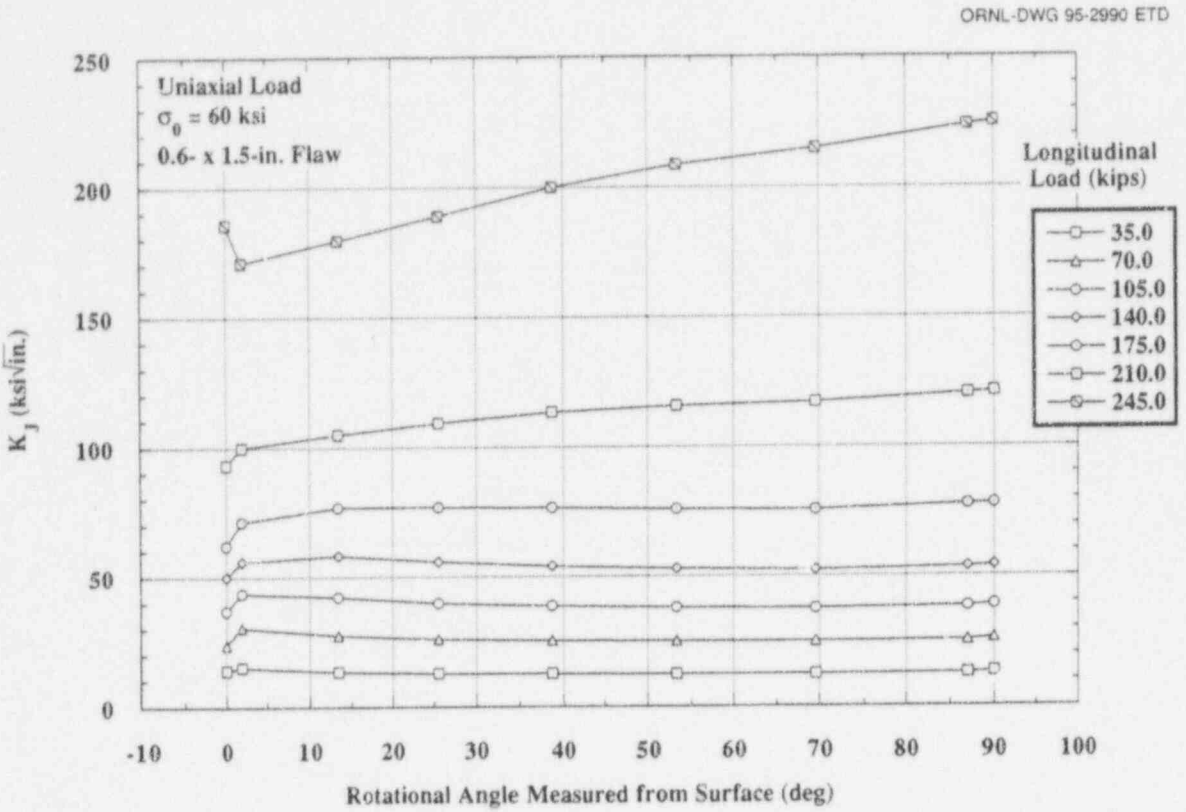

Figure 2.12 Calculated variation of K_J with angular location around flaw front for different levels of uniaxial applied load; 15.2- by 38.1-mm (0.6- by 1.5-in.) finite-length flaw with 414-MPa (60-ksi) yield strength

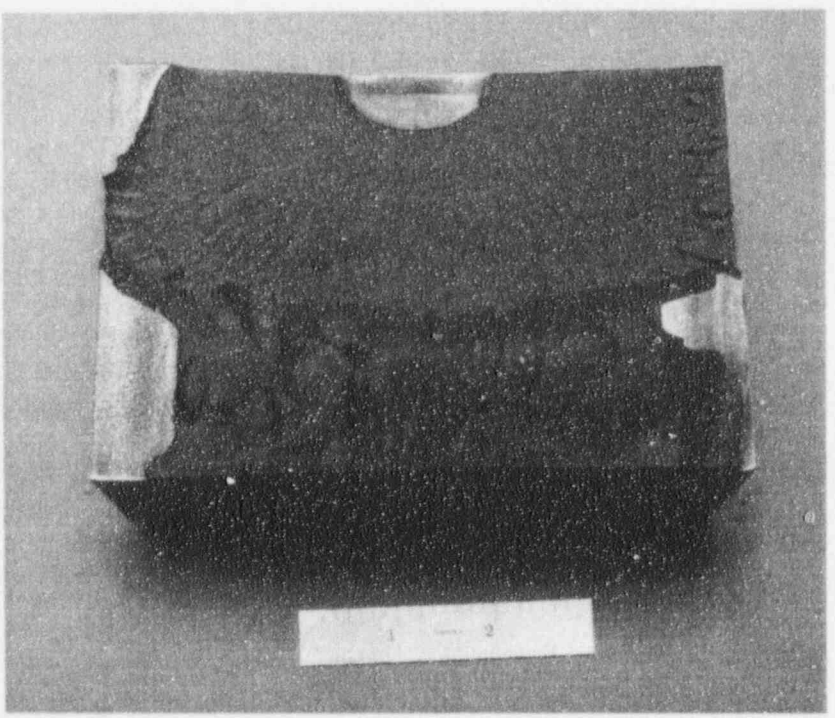

Figure 2.13 Fracture surface of finite-length flaw specimen CF-4

(3) the flaw size was in the region of transition from fracture to plastic collapse. To evaluate the second hypothesis, a second specimen, CF-1, was fatigue precracked to a change in compliance approximately twice that measured for CF-4 and was then tested to failure under the same conditions as Specimen CF-4. Specimen CF-1 behaved in a similar manner because it underwent significant plastic deformation before fracture. Examination of the fracture surface revealed ~3 mm (0.12 in.) of flaw growth for this specimen, which would have been more than sufficient to form a sharp flaw.

Hypothesis (1) was examined by performing additional FEAs of the finite-length flaw specimen. An elastic-plastic analysis of the specimen geometry was performed assuming an initial yield of 620 MPa (90 ksi). The results for this analysis showing the variation of K_J along the crack front at different load levels under uniaxial loading are given in Fig. 2.14. The primary observations from these analyses were that increasing yield causes a decrease in accumulated plasticity, as would be expected, and caused an increase in applied load required to achieve a specified K value. Thus, assuming a failure toughness in the range 90 to 150 MPa$\sqrt{m}$ (82 to 137 ksi$\sqrt{in.}$), increasing the yield strength would require an increase in applied load to failure to a level that might exceed the capacity of the biaxial fixture.

Increasing the flaw size, Hypothesis (3), was considered as a means of achieving the required balance between flaw-tip K, material toughness, and load capacity. A 19- by 53-mm (0.75- by 2.1-in.) semielliptic flaw was analyzed using an assumed material yield of 620 MPa (90 ksi). The results for this increased flaw size, shown in Fig. 2.15, indicate a significant increase in calculated K for a specified load. When applied to the case of 1:1 biaxial loading (Fig. 2.16), the load levels required to achieve the probable K values at failure were projected to be near the capacity of the test fixture.

It was concluded from the test results and the supporting analyses that, for this set of development finite-length flaw specimens, the flaw size should be increased to increase K at the flaw tip, and the test temperature should be lowered to increase the material yield and to lower the material toughness. To perform a test that will be a fracture toughness test rather than a plastic collapse test, a toughness/yield strength ratio near unity seems to be required. For Plate 14 material and the modified flaw geometry, this ratio may be achieved near a test temperature of –60°C (–75°F). At –60°C, Plate 14 yield strength is in the range of 448 to 517 MPa (65 to 75 ksi). As an upper bound, an additional analysis was performed using the new geometry and assuming a yield of 517 MPa (75 ksi); these results are shown in Fig. 2.17. Referring to Fig. 2.7, for a test

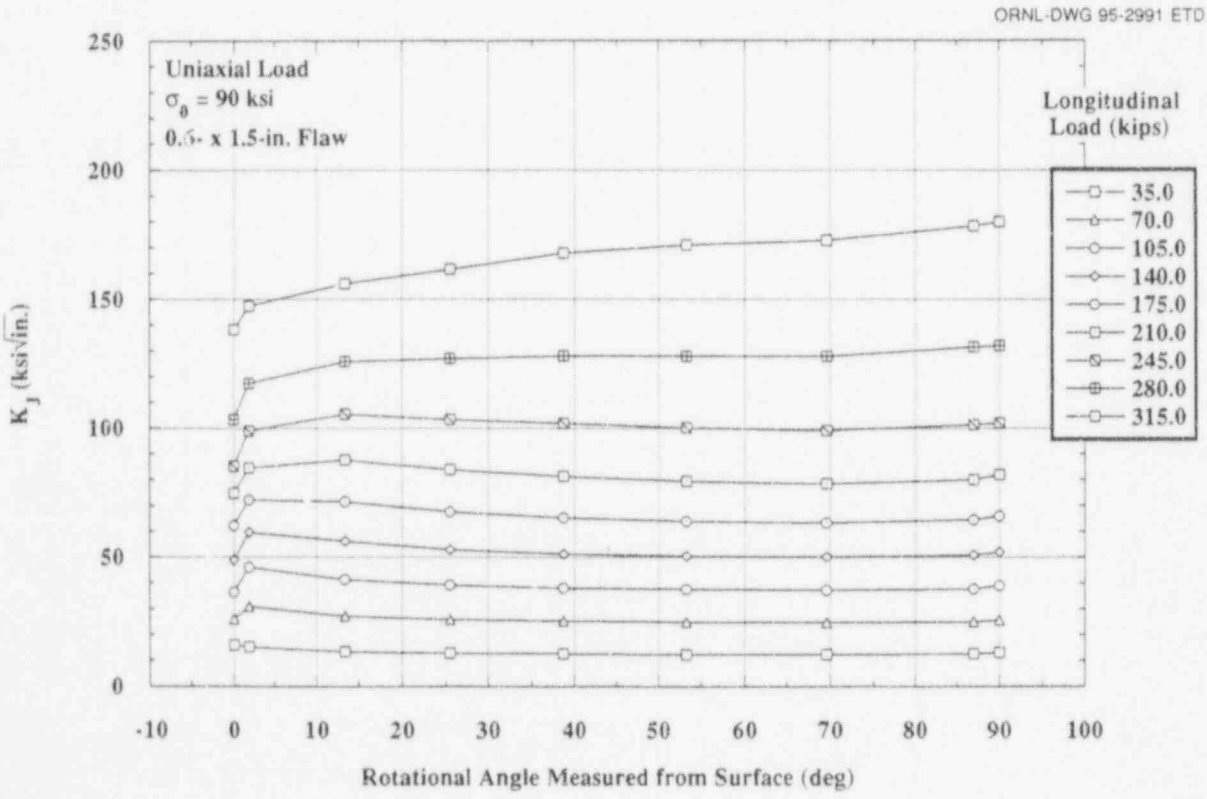

Figure 2.14 Calculated variation of K_J with angular location around flaw front for different levels of uniaxial (0:1) applied load; 15.2- by 38.1-mm (0.6- by 1.5-in.) finite-length flaw, 621-MPa (90-ksi) yield strength

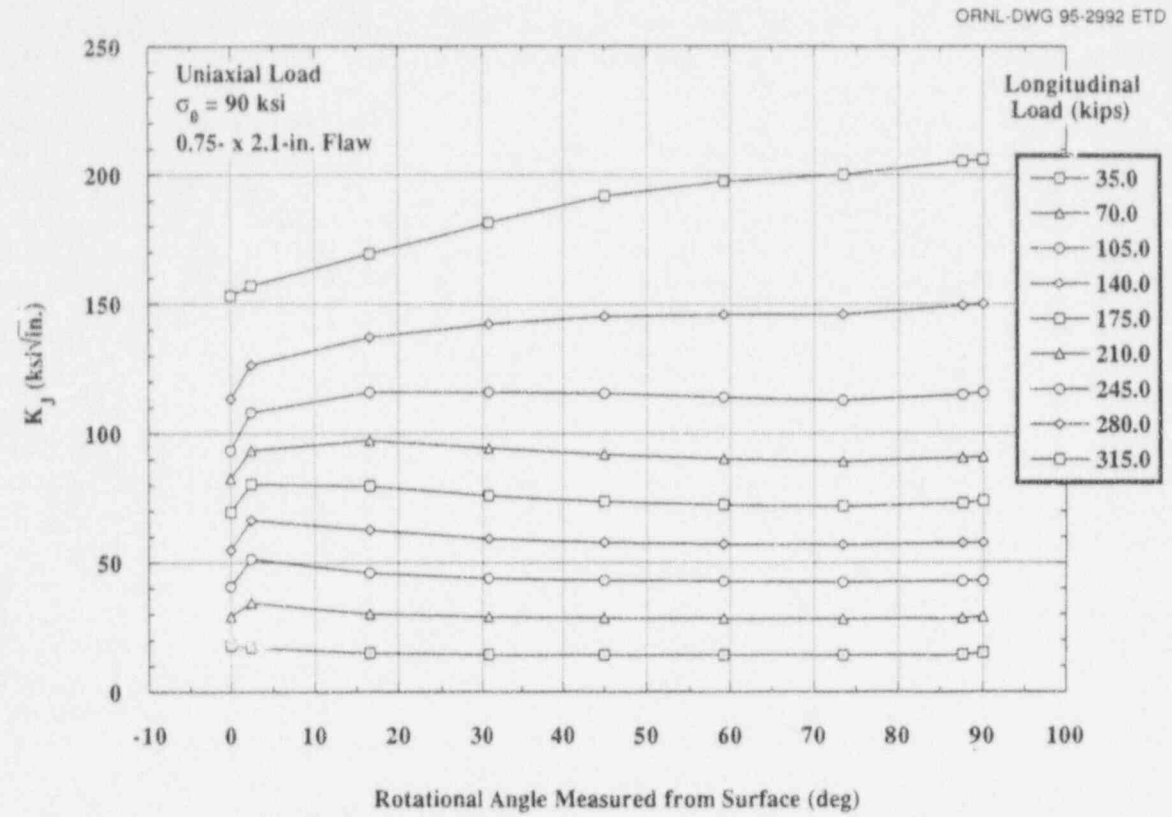

Figure 2.15 Calculated variation of K_J with angular location around flaw front for different levels of uniaxial (0:1) applied load; 19.1- by 53.3-mm (0.75- by 2.1-in.) finite-length flaw with 621-MPa (90-ksi) yield strength

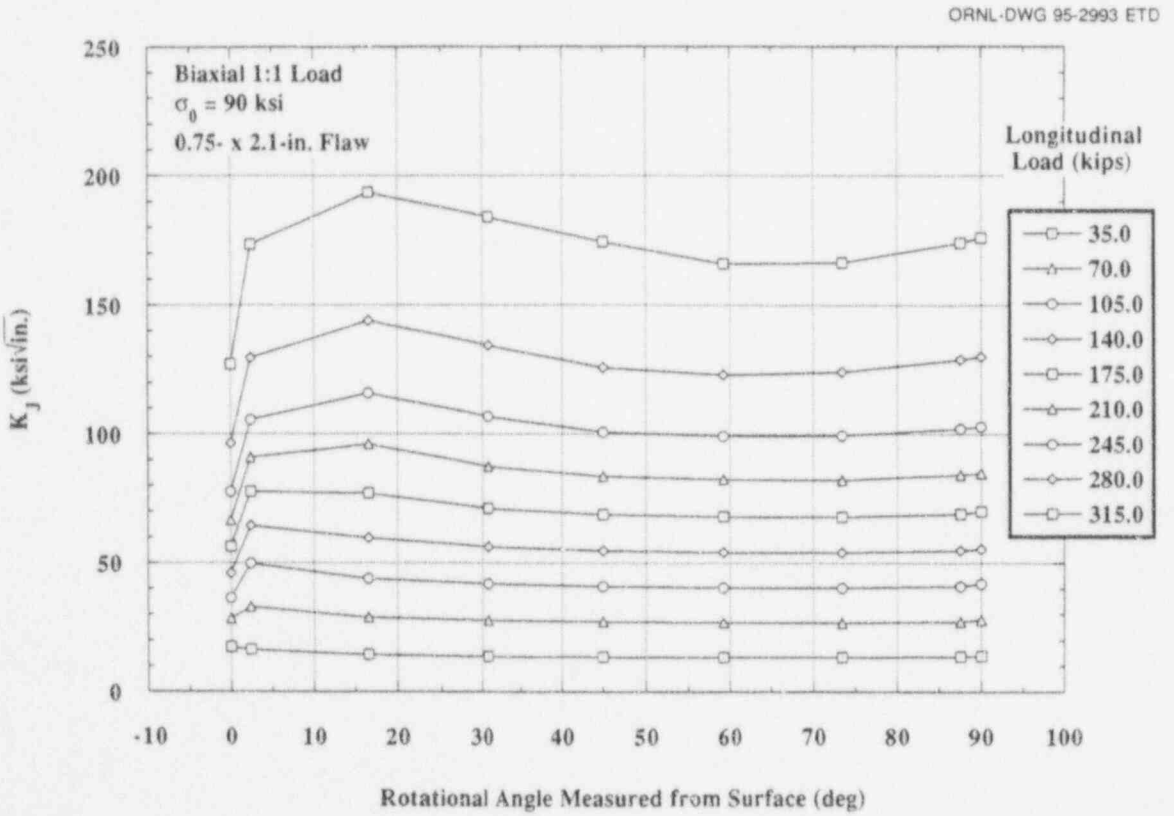

Figure 2.16 Calculated variation of K_J with angular location around flaw front for different levels of biaxial (1:1) applied load; 19.1- by 53.3-mm (0.75- by 2.1-in.) finite-length flaw with 621-MPa (90-ksi) yield strength

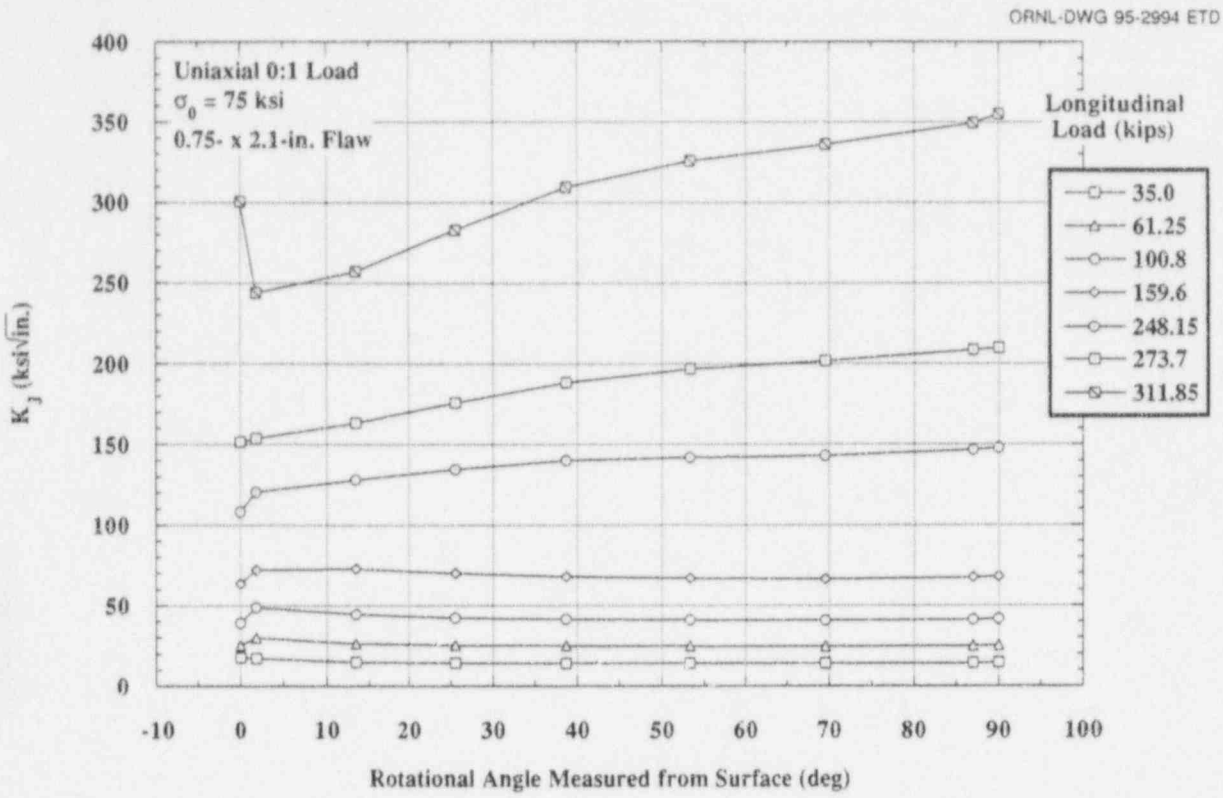

Figure 2.17 Calculated variation of K_J with angular location around flaw front for different levels of uniaxial (0:1) applied load; 19.1- by 53.3-mm (0.75- by 2.1-in.) finite-length flaw with 517-MPa (75-ksi) yield strength

temperature of –60°C, toughness values in the range of 50 to 100 MPa$\sqrt{m}$ (46 to 91 ksi$\sqrt{in.}$) would be predicted. Figure 2.17 would indicated failure of the finite-length flaw specimen to occur with limited amounts of plasticity and well within the load capacity of the test fixture.

The remaining four specimens in the series are currently being remachined to a 17.8- by 50.8-mm (0.7- by 2.0-in.) semielliptic flaw. This flaw will be extended 0.050-in. uniformly by fatigue precracking. These four specimens will be tested as two under uniaxial (0:1) load and two under biaxial (1:1) load.

References

1. R. D. Cheverton et al., Martin Marietta Energy Systems, Inc., Oak Ridge National Laboratory, *Pressure Vessel Fracture Studies Pertaining to the PWR Thermal-Shock Issue: Experiments TSE-5, TSE-5A, TSE-6*, USNRC Report NUREG/CR-4249 (ORNL-6163), June 1985.*

2. *Modern Steels and Their Properties, Carbon and Alloy Steel Bars*, Sixth Edition, Bethlehem Steel Corporation, Bethlehem, Pennsylvania, 1967.

3. T. R. Wilshaw et al., "A General Model to Predict the Elastic-Plastic Stress Distribution and Fracture Strength of Notched Bars in Plane Strain Bending," *Eng. Fract. Mech.* 1, 191–211 (1968).

4. J. A. Joyce and R. E. Link, *The Effect of Electric Discharge Machined Notches on the Fracture Toughness of Several Structural Alloys*, USNRC Report NUREG/CR-5981 (CDNSWC/SSM-61-93/01), September 1993.*

5. W. E. Pennell et al., Martin Marietta Energy Systems, Inc., Oak Ridge National Laboratory, *Heavy-Section Steel Technology Semiannual Progress Report, March–September 1993*, USNRC Report NUREG/CR-4219, Vol. 10, No. 2 (ORNL/TM-9593/V10&N2), 1995.

6. ASTM E 399-92, "Standard Test Method for Plane-Strain Fracture Toughness Testing of Metallic Materials," *Annual Book of ASTM Standards*, Vol. 03.01, American Society for Testing and Materials, Philadelphia, Pennsylvania, 1992.‡

*Available for purchase from the National Technical Information Service, Springfield, VA 22161.
†Available in public technical libraries.
‡Available from American National Standards Institute, 1430 Broadway, New York, 10018, copyrighted.

3 Evaluation of Cladding Effects

B. R. Bass

3.1 Introduction

During this report period, advances were made in Task H.3 to provide the measured data and analytical models that are essential for developing (1) a quantitative description of cladding effects on the fracture behavior of shallow finite-length surface cracks in RPVs and (2) a basis for improved treatment of surface crack geometries in fracture assessment procedures applied to pressurized-thermal-shock (PTS) transients, to pressure-temperature (P-T) limit transients, and to cracks detected during in-service inspections.

3.2 Full-Thickness Clad-Beam Testing Program (B. R. Bass, J. A. Keeney, and W. J. McAfee)

This section describes preliminary results from an HSST testing program designed to quantify fracture toughness for shallow cracks in material for which metallurgical conditions are prototypic of those found in RPVs. In the initial phase, three full-thickness clad beam specimens taken from the RPV of a canceled nuclear plant were fabricated at ORNL and tested at the NIST, Gaithersburg, Maryland.* These tests were performed to investigate the influence of metallurgical gradients, weld inhomogeneities, and the cladding process on the fracture toughness of material containing shallow cracks. Specifically, fracture toughness data were generated from three-point arc-bend specimens (229- by 226-mm cross section and ~1300-mm chord length) fabricated from full-thickness RPV clad, weld, and plate material. Through-clad shallow cracks in these beams were located in weld material joining together two base-metal shell segments. Comparison of results from these tests with those from homogeneous shallow-crack test specimens provide an opportunity to quantify effects of some near surface conditions on fracture toughness. In addition, the effective fracture toughness from these large beams can be compared with the toughness as determined by current ASME Sect. XI rules.[1]

3.2.1 Details of Test Specimen

The full-thickness clad beam specimens were fabricated from an RPV shell segment that was available from a

*NIST Test Report for Full-Thickness Clad Beam Fracture-Toughness Test Bendbar 1 tested April 6, 1993 (report dated March 10, 1994); Bendbar 2 tested January 13, 1994 (report dated March 10, 1994); and Bendbar 3 tested February 24, 1994 (report dated March 21, 1994).

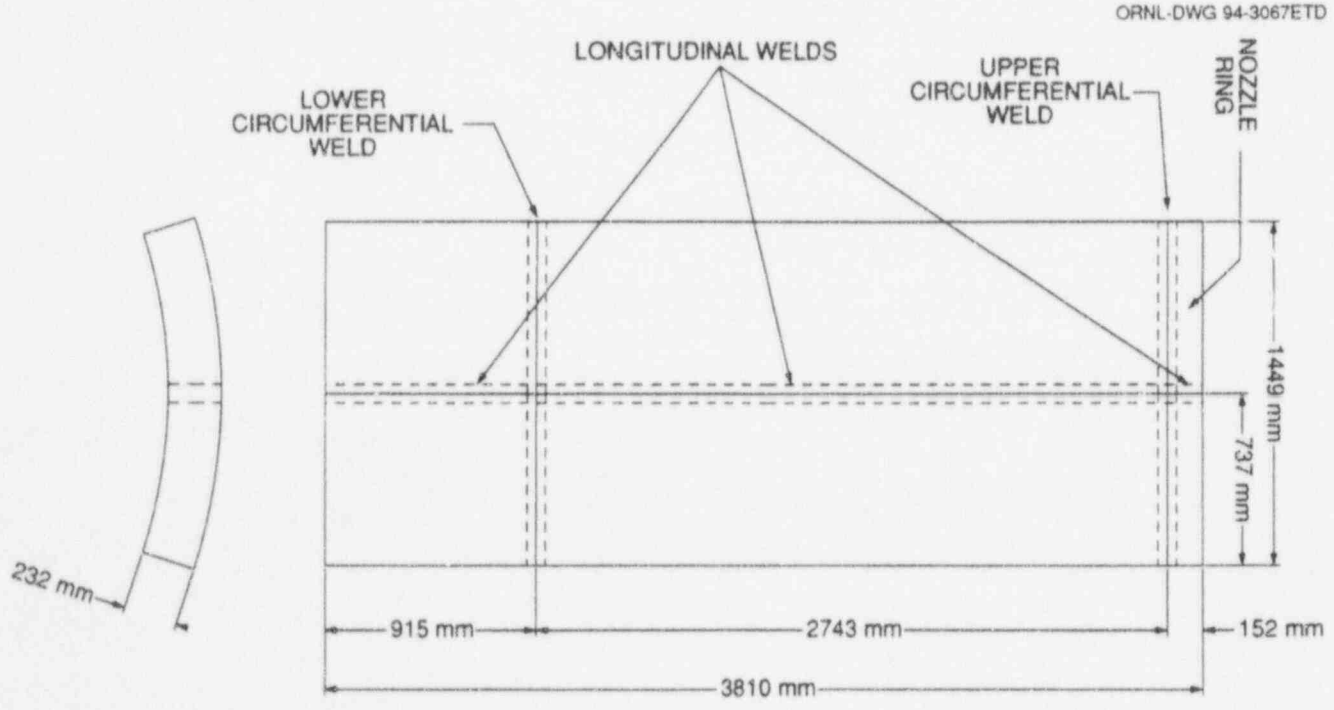

Figure 3.1 Sketch of RPV shell segment used as source material for full-thickness clad beam specimens

canceled pressurized-water reactor (PWR) plant (the plant was canceled during construction, and the vessel was never in service). The material is A 533 B steel with a stainless steel clad overlay on the inner surface. A sketch of the vessel shell segment is shown in Fig. 3.1. The shell segment includes two circumferential welds and one longitudinal weld. The "lower" circumferential weld (see Fig. 3.1) connects two shell courses, and the "upper" circumferential weld connects a shell course with the nozzle ring. The longitudinal weld is located near the midwidth of the shell segment and runs from the "upper" circumferential weld through the lower end of the shell segment. The welds are submerged-arc welds (SAWs) with A 533 B class 1 filler metal. The plate material, clad overlay, and weldment are prototypic of a production-quality RPV. The shell has a nominal inner radius of 2210 mm (87 in.) and a thickness of 232 mm (9.125 in.).

Because the initial series of three specimens was intended to investigate the fracture behavior of the longitudinal weld, the test beams were cut in the circumferential direction of the shell. The specimens were saw-cut from a master blank and then machined to final dimensions incorporating handling, load contact, and flaw details. A sketch of the specimen geometry is shown in Fig. 3.2. The specimen was designed to be tested in three-point bending with a load span (S) of 1219.2 mm (48 in.). Flat, parallel load contact points were machined on the top and bottom surfaces of the beam (see Fig. 3.2) to remove surface irregularities and to ensure uniform load application across the width of the beam. The centerline of the weld was located and used as a reference in machining the specimen details such that a radial plane, nominally passing through the center of the weld, would be a plane of symmetry for the specimen. The flaw was machined to lie in this plane. The flaw was machined into the beam using the wire EDM process and extended from the shell inner surface, that is, the clad surface, to predetermined depths into the beam. Using the EDM process, flaws with very narrow width (0.5 mm) and uniform depth can be machined into thick sections with minimum impact on the surrounding material. Heating and the associated potential for introduction of surface residual stresses is minimized, and only small amounts of material are removed. The final dimensions for each clad beam (CB) specimen are shown in Table 3.1. One deep-flaw specimen (CB-1) and two shallow-flaw specimens (CB-2 and CB-3) were produced. The crack depth (a) listed for each beam is the final depth after fatigue precracking. Part of the test procedure was to sharpen the flaw by fatigue precracking to achieve ~2.5 mm (0.1 in.) of flaw growth.

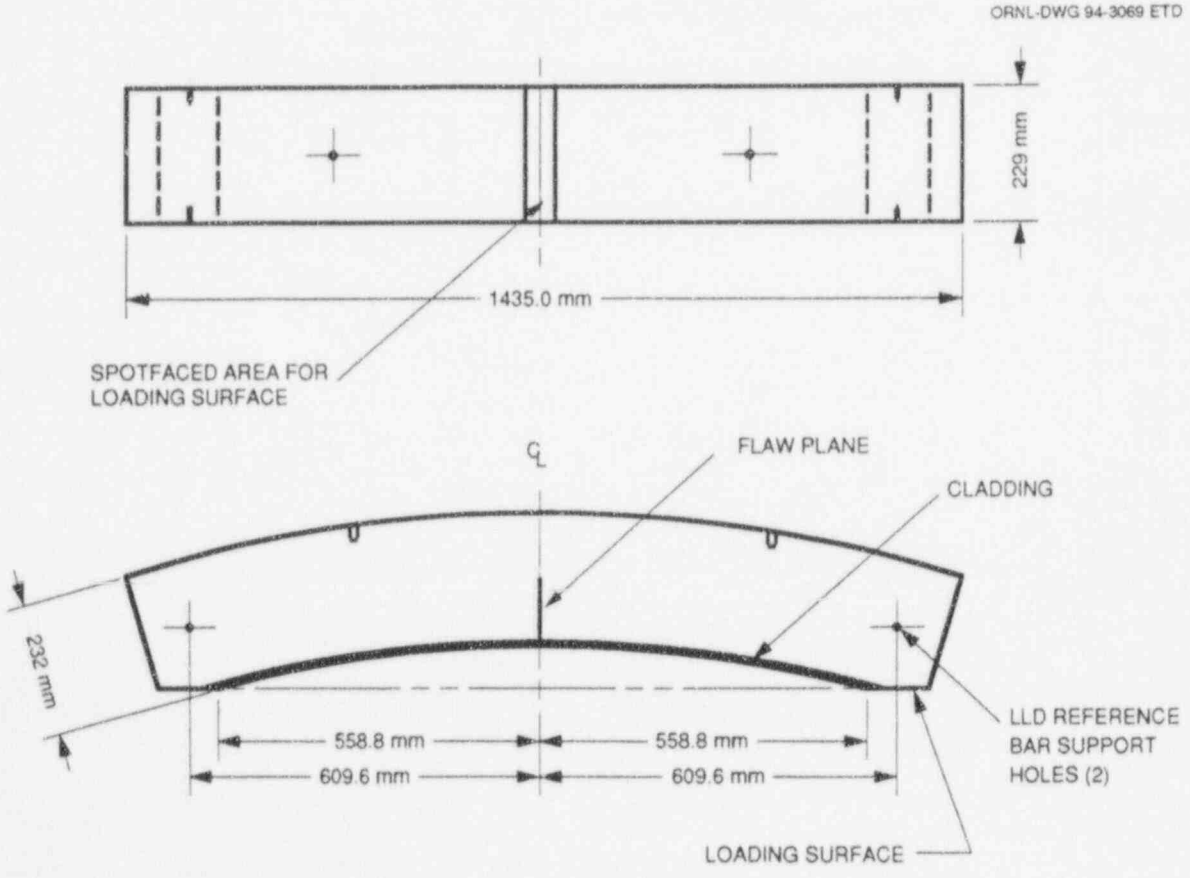

Figure 3.2 Sketch of full-thickness clad beam specimen

Table 3.1 Parameters defining specimen geometry of full-thickness clad beam specimens

	CB-1[a]	CB-2	CB-3
Load span, S (mm)	1219.2	1219.2	1219.2
Thickness, B (mm)	230.2	230.2	229.6
Width, W (mm)	225.7	224.3	224.3
Crack depth, a (mm)	117.5	10.8	23.7
Ratio, a/W	0.50	0.05	0.10

[a]Used as development beam.

3.2.2 Characterization of Circumferential Weld

This section describes the characterization of the SAW used in the full-thickness clad beam tests. As described in Sect. 3.2.1, the shell contained both axial and circumferential welds. Macrographs of the circumferential and axial welds are shown in Fig. 3.3(*a*) and (*b*), respectively. The macrographs show the individual weld passes and the cladding on the inside of the vessel. The dark streaks on the circumferential weld are due to the cladding being entrained during the flame-cutting of this particular section.

In the course of cutting the beam blanks, the upper circumferential weld was made available for the characterizations. Tests using the ABI technique indicate that the tensile properties of the axial and circumferential weld are similar. The characterization of the circumferential weld included CVN tests, RT_{NDT} determinations (defined in Ref. 2), and tensile tests.

The specimens used for the preliminary characterization, listed in Table 3.2, were machined from the circumferential weld, as shown in Fig. 3.4. The nomenclature used to define specimen orientation with respect to the major rolling direction and the thickness is standardized[3] for plates but not for welds. For the purpose of these characterizations, a method similar to that for plates was used for welds; this method consists of one- or two-letter identifiers. The letters "L" and "S" were used for directions parallel to the welding direction and thickness direction, respectively. The letter "T" was used to indicate a direction normal to both L and S. Using this method, the first letter given is the longitudinal axis of a specimen that is also normal to the fracture plane. One letter was sufficient to define the orientation of tensile specimens. For CVN specimens, a second letter was added indicating the direction of crack propagation. The CVN specimens shown in Fig. 3.4 are in the "T" orientation. Because the specimen is square in cross section, the specimens could be configured to be either T-L or T-S by properly orienting the notch. These letter designations are shown in Fig. 3.4.

3.2.2.1 Results of Testing CVN Specimens in the L-S and T-L Orientations

The three full-thickness beam specimens were tested in the T-S orientation, and, accordingly, CVN tests were performed in that orientation. The determination of RT_{NDT} required the use of T-L oriented CVN specimens because the T-S orientation for the axial weld corresponds to the T-L orientation for the circumferential weld. The CVN impact test results obtained for both orientations were the impact energy, lateral expansion, and percent shear fracture appearance (SFA). The 10 × 10 × 55-mm CVN specimen used for these tests is recommended by the American Society for Testing and Materials (ASTM) Standard Method for Notched Bar Impact Testing of Metallic Materials (E 23).[3]

Detailed results from the Charpy tests are shown in Figs. 3.5 and 3.6 for the T-S and T-L orientations, respectively. Approximately 20 specimens from the midthickness of the weld metal were tested in each of the T-S and T-L orientations. A regression fit of a hyperbolic tangent equation to the experimental data was performed, and Table 3.3 gives the resulting parameters. For the regression fit, the lower-shelf energy (LSE) was prescribed to be 2.7 J (2 ft-lb). This value of the LSE is based on an average of five CVN impact tests at –196°C (–321°F) on material from the WF70 Midland weld.[4] The 20-, 41-, and 68-J impact energy transition temperatures were calculated from the resulting hyperbolic tangent equation. Table 3.3 also contains the drop-weight NDT temperature and related energy level, as well as the RT_{NDT}. Details of the determination of NDT temperature and RT_{NDT} are given later.

The CVN impact energy in the T-S orientation is compared to that in the T-L orientation in Fig. 3.7. From this figure and Table 3.3, it can be seen that, for this weld, there is no significant directional difference in the CVN impact energy behavior.

For the purposes of determining the transition temperature shift of irradiated RPV steels, the NDT temperature is generally assumed to correspond to the 41-J (30 ft-lb) CVN impact energy level for 1/4t, T-L orientation material. At midthickness, the temperature corresponding to the 41-J energy level is ~27°C (49°F) higher than the drop-weight NDT temperature. The temperature corresponding to the 20-J (15 ft-lb) energy level would have been a better correlation to the NDT temperature.

ORNL-PHOTO 8168-94

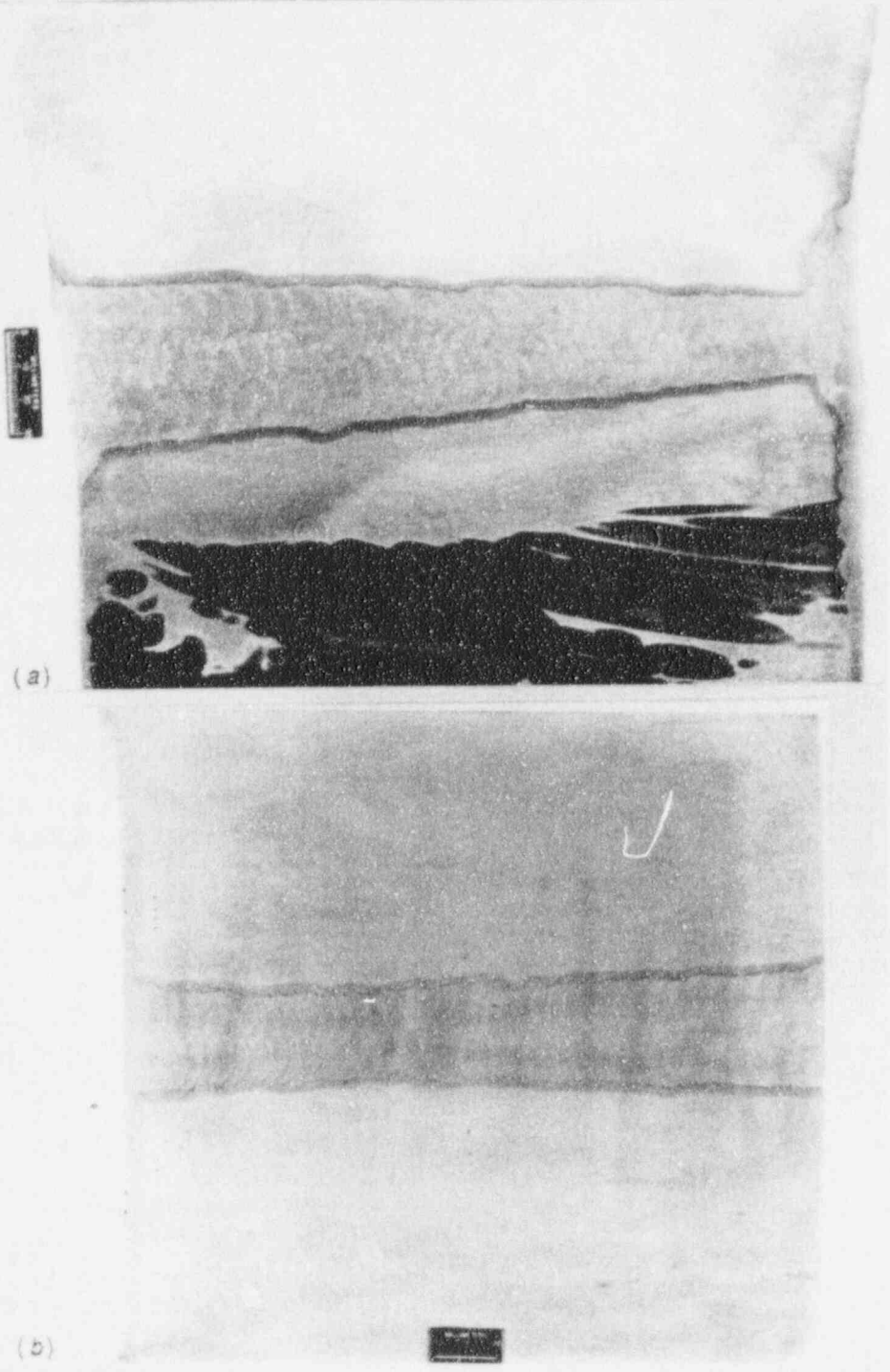

Figure 3.3 Details of welds used in full-thickness clad beam studies: (*a*) axial weld and (*b*) circumferential weld

3.2.2.2 Determination of the Reference Temperature RT_{NDT}

In accordance with Subarticle NB-2330 in Sect. III of the *ASME Boiler and Pressure Vessel Code*,[2] the reference temperature RT_{NDT} is the higher of (1) the drop-weight NDT temperature or (2) (T – 33)°C, where T is the temperature at which T-L orientation Charpy specimens attain at least a 68-J (50-ft-lb) impact energy and a lateral expansion of 0.89 mm (35 mils).

The drop-weight testing was performed in accordance with the ASTM Test for Conducting Drop-Weight Test to Determine Nil-Ductility Transition Temperature of Ferritic Steels (E 208),[3] and the results are shown in Table 3.4. The

Table 3.2 Specimens machined for characterizing the circumferential weld for the full-thickness clad beam specimens

	CVN		P-3 drop weight[a]	6.35-mm gage diameter tensile
Orientation	T-S	T-L[a]	NA[b]	T
Number of specimens	17	23	10	6
Specimen identification	SNU01 through SNU17	SNU18 through SNU40	SNU01 through SNU10	SNU01 through SNU06

[a]Required for RT_{NDT} determination.
[b]NA = not applicable; according to ASTM E 208-91, paragraph 7.2, the drop-weight NDT is generally considered to be insensitive to specimen orientation with respect to rolling or forging direction.

NDT temperature is defined in ASTM E 208 to be the highest temperature at which a specimen breaks, providing that two tests at a temperature 5°C higher show no-break performance. Thus, the NDT temperature is –50°C (–58°F). The specimen size used was P-3 and, in accordance with ASTM E 208, had a single pass crack-starter weld bead. The results from CVN impact tests at the temperature –17°C (NDT + 33) in the T-L orientation indicated that the minimum 68-J energy level was not attained for three specimens. The 68-J energy level and the 0.89-mm lateral expansion requirement were achieved at a temperature of 10°C (50°F), which resulted in an RT_{NDT} of –23°C (–10°F).

3.2.2.3 Tensile Testing

The results of tensile testing two specimens from midthickness, circumferential weld material at each of three temperatures are given in Table 3.5. The values of total elongation

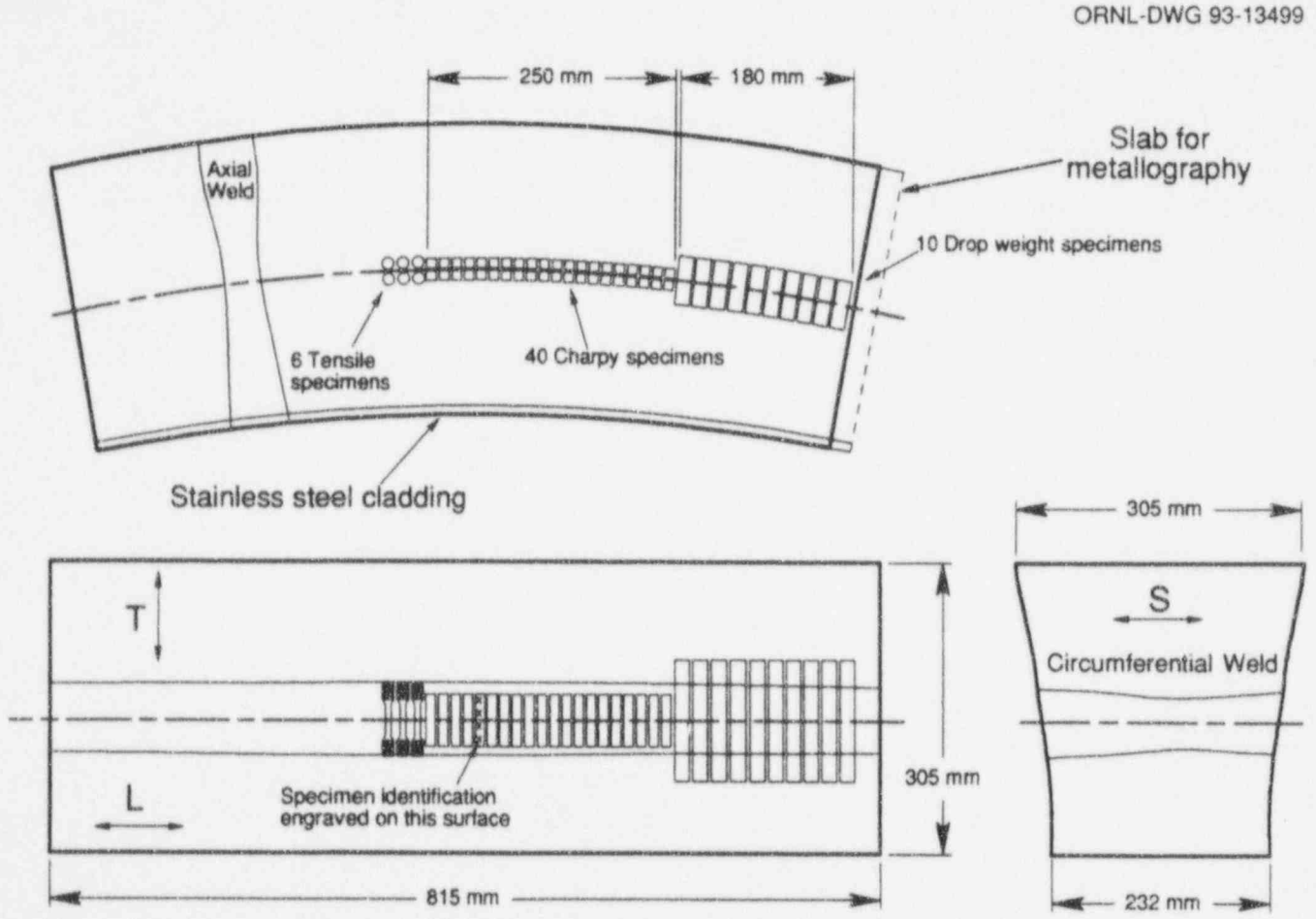

Figure 3.4 Cut-up characterization block containing circumferential weld of unused RPV showing location of tensile, CVN, and drop-weight specimens

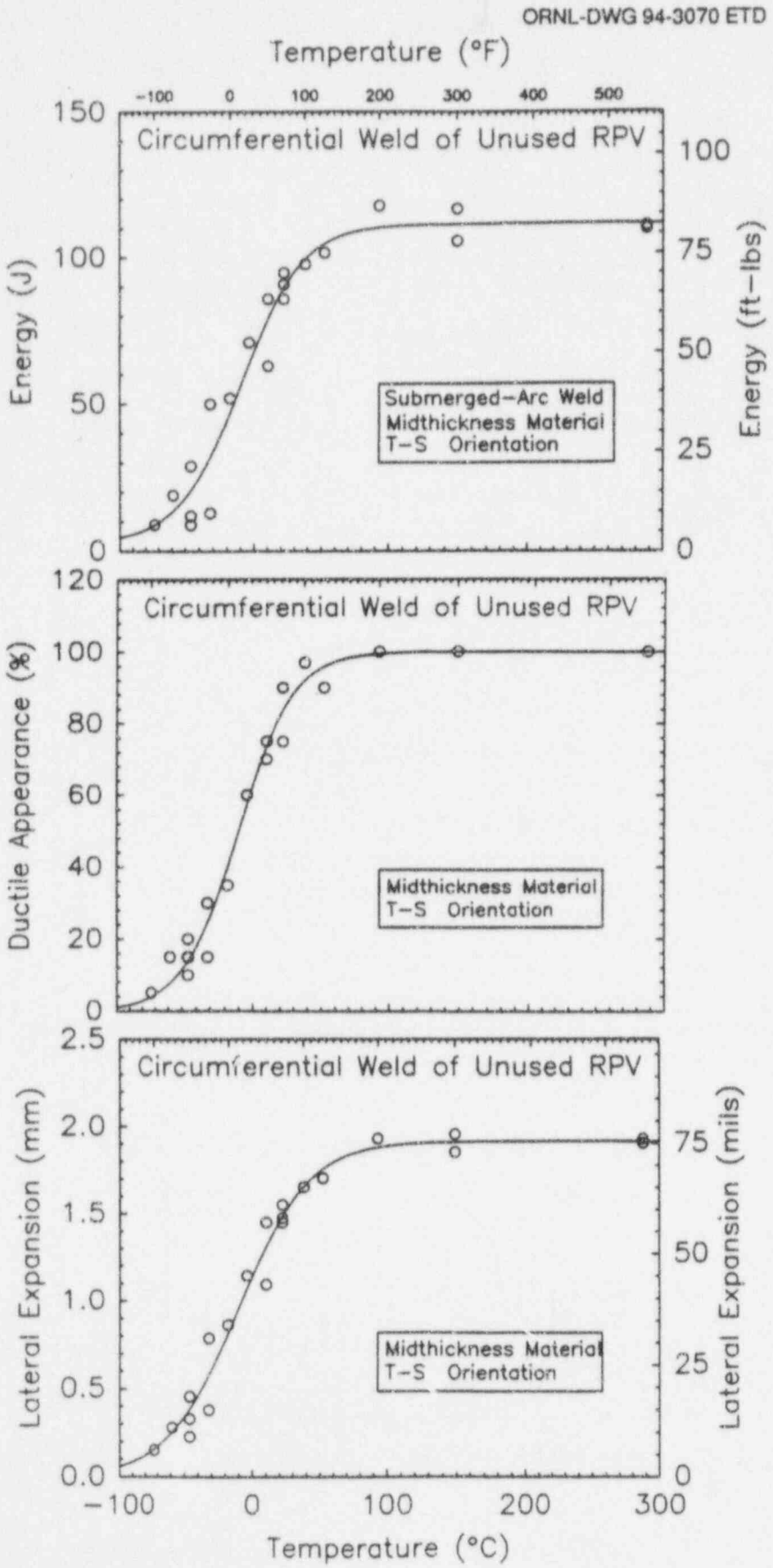

Figure 3.5 CVN impact test results on specimens machined in T-S orientation from midthickness of circumferential weld of unused RPV: (*a*) CVN impact energy, (*b*) percent SFA, and (*c*) lateral expansion

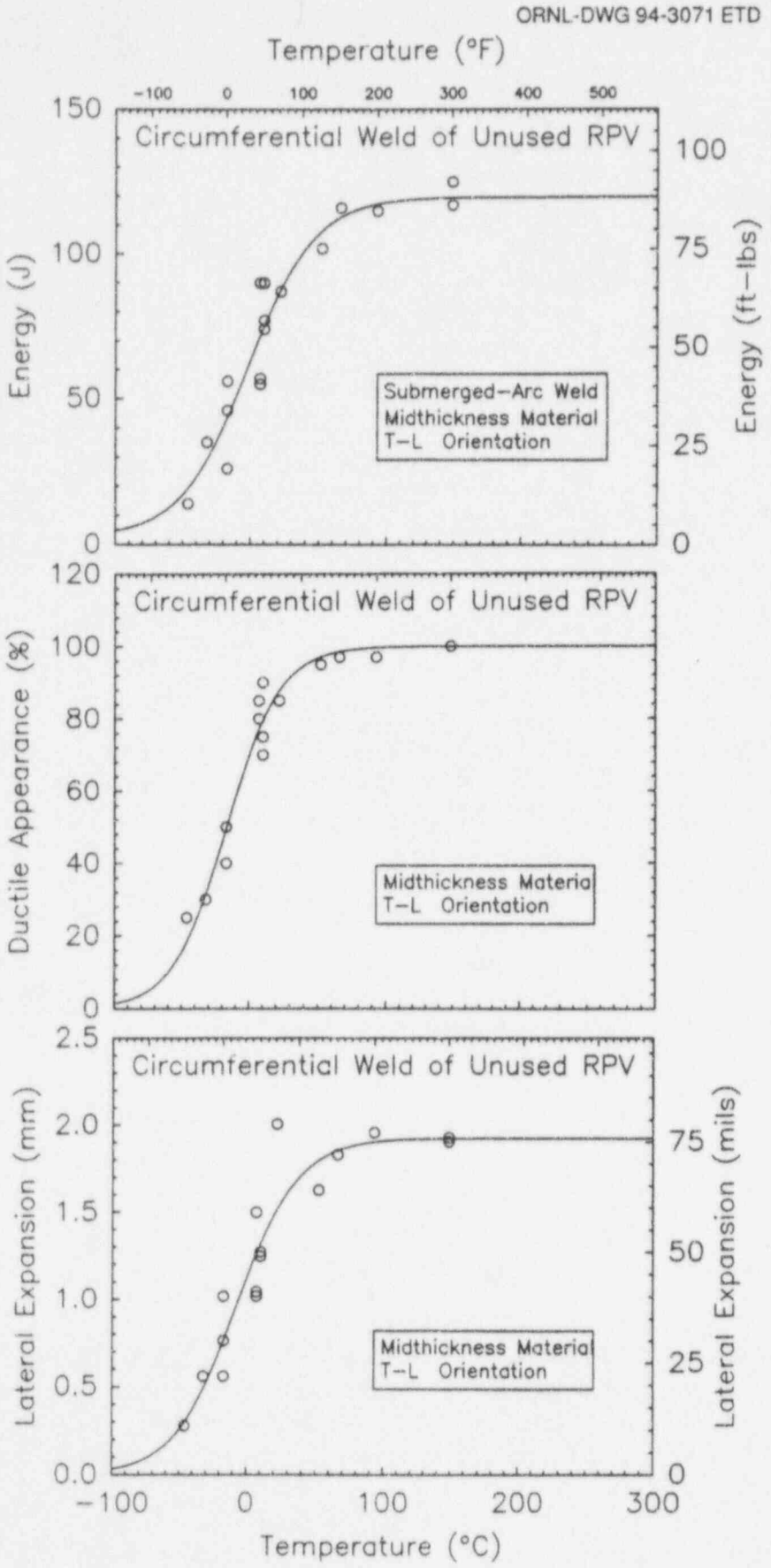

Figure 3.6 CVN impact test results on specimens machined in T-S orientation from midthickness of circumferential weld of unused RPV: (*a*) CVN impact energy, (*b*) percent SFA, and (*c*) lateral expansion

Table 3.3 Summary of test results to determine the CVN impact energy in the T-S and T-L orientations, drop-weight NDT temperature, and RT_{NDT} of midthickness material from the circumferential weld of an unused RPV

Tanh fit parameters[a]			Temperature [°C(°F)] of an energy level			NDT[b]	RT_{NDT}	Energy level [J(ft-lb)] at	
USE [J(ft-lb)]	MTT [°C(°F)]	TZW [°C(°F)]	20 J	41 J	68 J	[°C(°F)]	[°C(°F)]	NDT	RT_{NDT}
				T-S orientation					
111.8 (82.5)	–9.21 (15.4)	90.6 (163.1)	–47 (–53)	–23 (–9)	0 (32)	–50 (–58)	–23 (–10)	18 (13)	41 (30)
				T-L orientation					
119.7 (88.3)	–1.742 (28.9)	97.9 (176.3)	–45 (–49)	–19 (–2)	4 (39)	–50 (–58)	–23 (–10)	17 (13)	37 (27)

[a] The following equation was used to fit the data: Energy = (USE + 2.7)/2 + [(USE – 2.7)/2]•Tanh[(T – MTT)/(TZW/2)], where USE = upper-shelf energy, 2.7 = lower-shelf energy, MTT = midtransition temperature, and TZW = transition zone width. The 2.7 J is the lower-shelf energy and was determined experimentally from five tests conducted at liquid nitrogen temperature (–196°C) on a submerged-arc weld.

[b] According to ASTM E 208-91, paragraph 7.2, the drop-weight NDT is generally considered to be insensitive to specimen orientation with respect to rolling or forging direction.

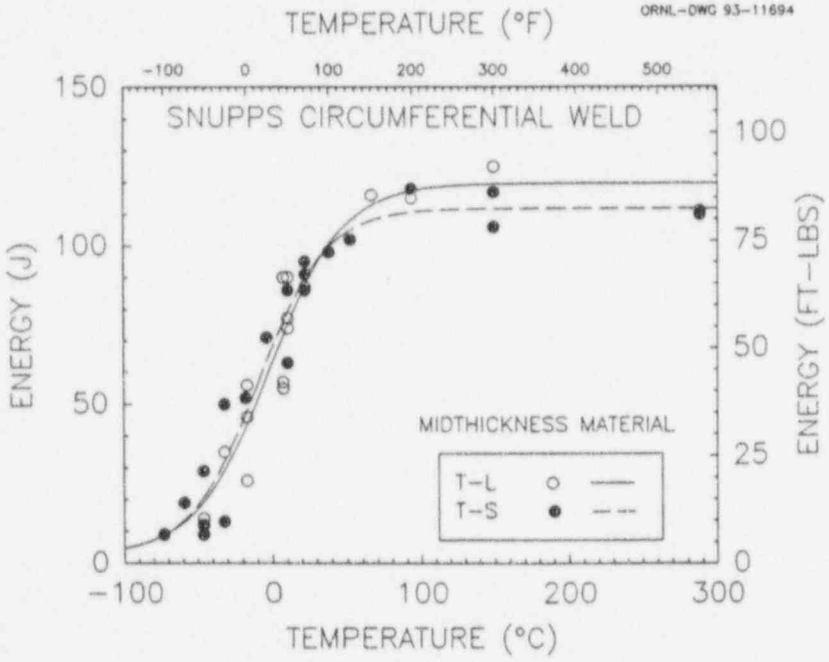

Figure 3.7 Comparison of the CVN-impact energy in T-S orientation to that in T-L orientation for midthickness material from circumferential weld of unused RPV

Table 3.4 Results of drop-weight testing P-3 size specimens from the circumferential weld between nozzle ring to shell course (Specimens were machined from midthickness material and the crack-starter bead was a single pass weld as defined in ASTM E 208)

Specimen ID	Test temperature (°C)	Test results		
		Break	No break	NDT[a] (°C)
SNU09	–50	√		
SNU08	–45		√	
SNU10	–45		√	
SNU06	–40		√	
SNU02	–30		√	
				–50

[a]NDT is defined in E 208-91 to be the highest temperature at which a specimen breaks, and at least two tests at a temperature 5°C higher show no-break performance.

Table 3.5 Tensile properties of midthickness material from the circumferential weld of an unused RPV [The axis of the specimens was normal to the welding direction (T-orientation), and the gage diameter was 6.35 mm (0.25 in.)]

Specimen	Temperature [°C(°F)]	Strength [MPa(ksi)]		Elongation (%)		Reduction of area (%)
		0.2% Yield	Ultimate strength	Uniform	Total	
SNU03	–80 (–112)	664 (96.3)	768 (111.4)	11	25	64
SNU06	–80 (–112)	652 (94.6)	761 (110.4)	11	26	64
SNU02	–25 (–13)	600 (87.0)	712 (103.2)	9	23	65
SNU05	–25 (–13)	596 (86.4)	703 (102.0)	10	24	67
SNU01	23 (73)	565 (82.0)	672 (97.5)	—	18	63
SNU04	23 (73)	565 (81.9)	665 (96.4)	8	23	66

were determined by measuring the change in length of the entire specimen and dividing that change in length by the length of the reduced section.

The yield and ultimate strengths shown in Table 3.5 are plotted in Fig. 3.8 as a function of temperature and were regression fit with an Irwin-type equation:[5]

$$\sigma_0 = 390 + \frac{51,650}{T+273} \quad , \quad -80 \le T \le 25°C \; ; \qquad (3.1)$$

and

$$\sigma_u = 488 + \frac{52,830}{T+273} \quad , \quad -80 \le T \le 25°C \; ; \qquad (3.2)$$

where σ_0 and σ_u are the yield and ultimate strengths in megapascals, respectively, and T is the temperature in degrees Celsius.

A 25-mm (1-in.) extensometer was attached to the gage length of the specimens to record the loads and extensometer output. The engineering stresses and strains calculated from the digital output are shown in Fig. 3.9 and were used in the analysis of the full-thickness clad beam tests.

The ABI technique was used to determine whether the yield strengths of the circumferential weld[6] and the axial weld were similar. Three ABI indentations were made at the midthickness location for both welds. The tensile tests previously described were performed on midthickness

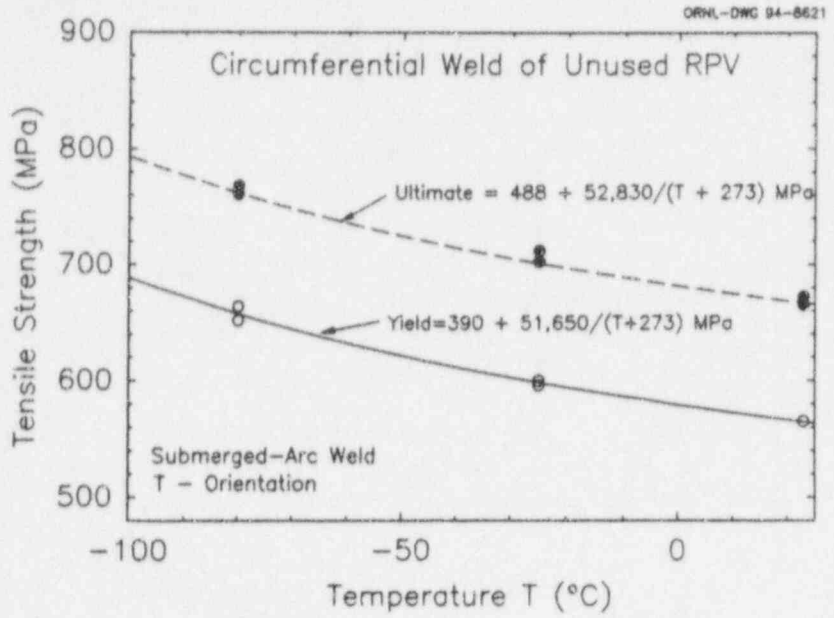

Figure 3.8 Yield and ultimate tensile strengths of T-orientation specimens for midthickness material from circumferential weld of unused RPV

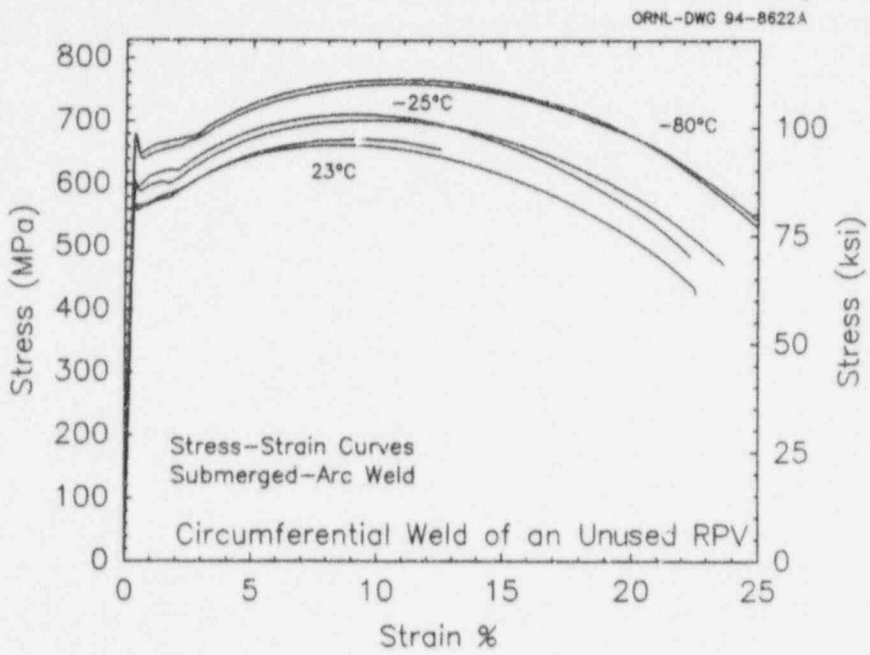

Figure 3.9 Stress-strain behavior at different temperatures of SAW metal from midthickness of circumferential weld

material from the circumferential weld. The comparative results are shown in Table 3.6. The ABI-derived yield strengths for the circumferential weld averaged 508 MPa (73.7 ksi) and ranged from 490 to 531 MPa (71 to 77 ksi) compared to an average of 565 MPa (82.0 ksi) for the two tensile specimens tested at room temperature. The average and range of ABI values for the axial weld were 515 MPa (74.7 ksi) and 510 to 524 MPa (74 to 76 ksi), respectively. It was thus concluded that the tensile properties for both welds are similar.

These impact and tensile data were used to develop a consistent set of properties needed for the clad beam test data evaluation and FEAs. These properties are shown in Table 3.7. The ABI technique was used to determine the yield stress for the base and clad material. The

Table 3.6 Yield strength derived at room temperature from ABI for midthickness material from the circumferential and axial welds of an unused RPV

ABI Identification	Yield [MPa(ksi)]
Circumferential weld	
21	503 (73)
22	531 (77)
23	490 (71)
Average	508 (73.7)
Axial weld	
11	524 (76)
13	510 (74)
14	510 (74)
Average	515 (74.7)

Table 3.7 Material properties at test temperature of –25°C

	Base metal	Weld metal	Cladding
Modulus of elasticity (E), MPa	200,000	200,000	152,000[a]
Poisson's ratio (ν)	0.3	0.3	0.3
Yield stress (σ_0), MPa	440[b]	599[c]	367[b]
Ultimate stress (σ_u), MPa	660[d]	704[e]	659
RT_{NDT}, °C		–23	
NDT, °C		–50	

[a]Measured E value from S. K. Iskander et al., Martin Marietta Energy Systems, Inc., Oak Ridge National Laboratory, "Experimental Results of Tests to Investigate Flaw Behavior of Mechanically Loaded Stainless Steel Clad Plates," NUREG/CR-5785 (ORNL/TM-11950), April 1992.
[b]σ_0 measured by ABI technique.
[c]Evaluated from $\sigma_0 = 390 + 51{,}650/(T + 273)$ where T is the material temperature.
[d]σ_u measured by Rockwell B indentation technique.
[e]Evaluated from $\sigma_u = 488 + 52{,}830/(T + 273)$.

tabulated yield stress for the weld material is 36% higher than the yield stress for the base material. The weld material exhibits a significant overmatch in yield stress as compared to the yield stress for the base material.

3.2.3 Test Equipment and Procedures

The full-thickness clad beam tests were performed at NIST using the available 53.4-MN (12-million pound) servo-hydraulic test machine. It was necessary to modify the existing facility or procure special components to perform the required tests. Because the 53.4-MN actuator does not have dynamic capability, a 2.67-MN (600-kip) actuator was procured for use in fatigue precracking the specimens. To avoid the possibility of warm prestressing, the test specification[7] dictated that the specimen not be disturbed after fatigue precracking. A fatigue system was designed that permitted removal of the 2.67-MN actuator after precracking without disturbing the general test set-up. The fracture test was then performed using the 53.4-MN actuator. A three-point bend fixture with span and load capacity sufficient to perform these tests was designed and fabricated. This fixture was designed for a load capacity of at least 15 MN (3370 kips), which was calculated to be in excess of that required for these tests. The fixture was designed to meet the general requirements of ASTM E-399 (arc-bend chord-supported tests).[3] Special large-range crack-opening-displacement gages and associated electronics were obtained specifically for these tests. In addition, dual data acquisition systems (DASs) were purchased to provide redundancy and minimize the possibility of data loss during the tests. The load and DAS components were installed, calibrated, and functionally validated before the failure tests. All instruments making critical measurements have calibrations traceable to NIST. Because the tests were performed at a low temperature, an environmental chamber was fabricated to completely enclose the test article and load-contact points to facilitate control of both time- and spatial-dependent specimen temperature variations.

The total test sequence for the set of three beams involved three phases: (1) a shakedown and demonstration phase, (2) the fatigue precracking phase, and (3) the failure test phase. A complete series of validation tests was performed before beginning the fracture tests. As indicated by the footnote in Table 3.1, the deep-flaw specimen was designated as a development beam for this series. The primary purpose of the development beam test was to verify and validate the testing procedures for the two remaining tests. The development beam was sent to NIST in the blank form, that is, prior to final machining and without a notch or crack. It was instrumented with 16 thermocouples, shown schematically in Fig. 3.10, to check out the temperature control system. Two of the thermocouples located on the back surface of the specimen (outer surface of shell) were recessed 114.3 mm (4.5 in.) deep to measure interior specimen temperatures for comparison with those measured on the surface. The beam was mounted in the test facility with the environmental enclosure in place; it was then cooled as it would be for an actual fracture test, and measurements of cooling rate and temperature distribution were made. Cooling was achieved by a spray of liquid nitrogen (LN_2) onto the beam surface. In general, during cooldown, there was considerable variation in the temperature record at different locations due to LN_2 spraying directly on the thermocouples. When the desired temperature had been

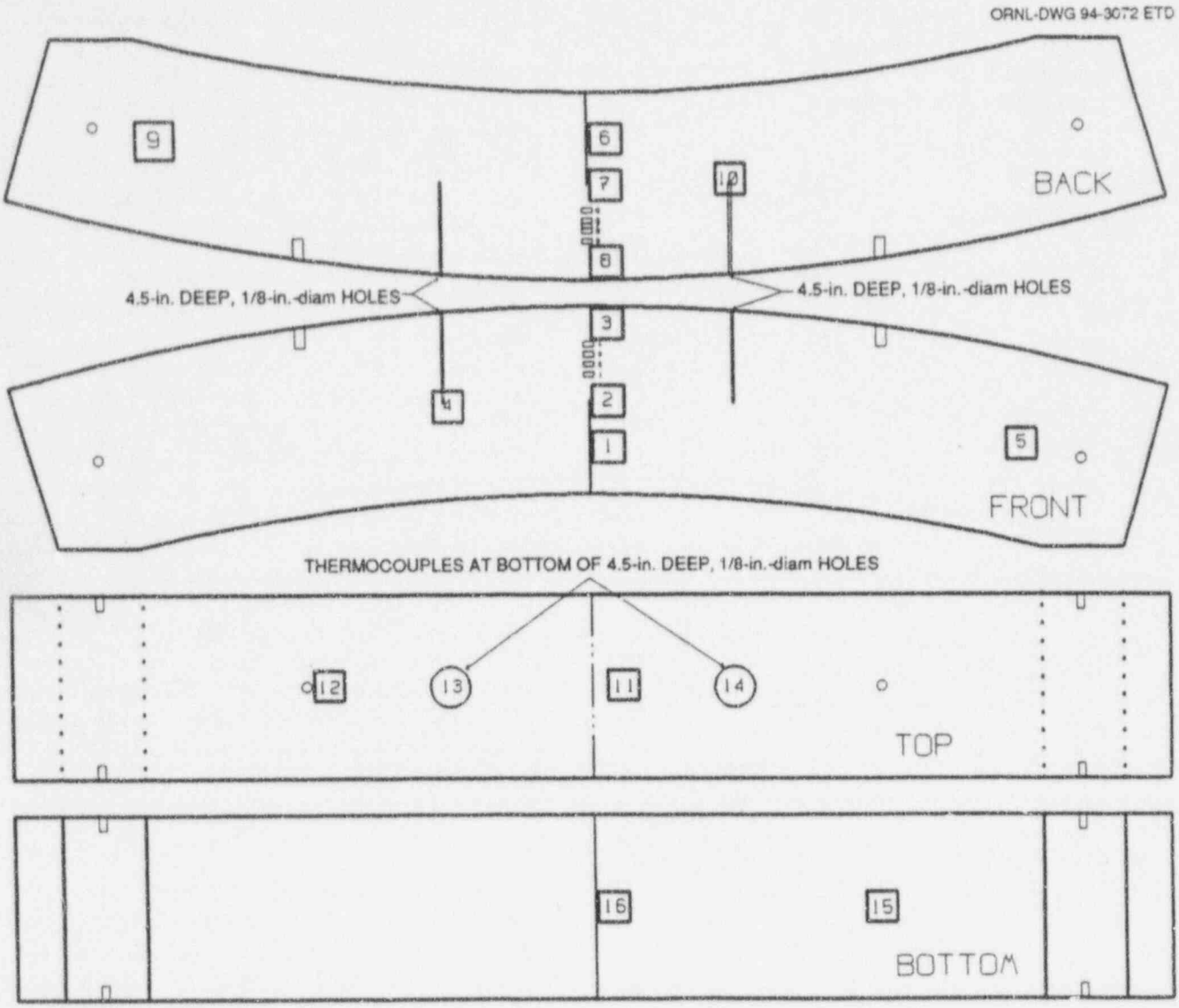

Figure 3.10 Full-thickness clad beam specimen thermocouple configuration used in demonstration of temperature control (as provided by NIST)

negatively exceeded by several degrees, the LN_2 spray was stopped, and the beam was allowed to come to thermal equilibrium. Within 1 h, all thermocouples, including those embedded in the beam, were reading within 1 to 2°C of one another. The beam then warmed up at a rate of ~3.5°C/h while maintaining or improving the temperature uniformity. Three demonstration tests of this type were performed. Based on the results, a procedure was developed whereby the desired test temperature would be negatively exceeded by ~5°C, the LN_2 spray would be stopped, and the beam would be allowed to thermally equilibrate and warm to the test temperature. This was acceptable since the rate of change in temperature was much less than the time interval required to perform the fracture tests. When these tests were complete, this beam was sent to the machine shop for final machining into the fracture test specimen CB-1.

When CB-1 was returned as a test specimen, it was fully instrumented with crack-opening-displacement gages and surface strain gages. In addition, a specially designed fixture was used to measure LLD. The specimen was then installed in the test fixture, and a careful inspection was performed to determine that the load-contact points mated properly. For the first test (CB-1), the LLD fixture was also installed. For subsequent tests, the LLD fixture was left off during fatigue precracking because the LLD assembly restricted viewing of the crack tip for determination of crack growth. Figure 3.11 shows CB-1 in the test fixture in preparation for the fatigue precracking phase. Figure 3.12 illustrates the test specimen, loading fixture, and the load transfer configuration.

ORNL-PHOTO 5588-93

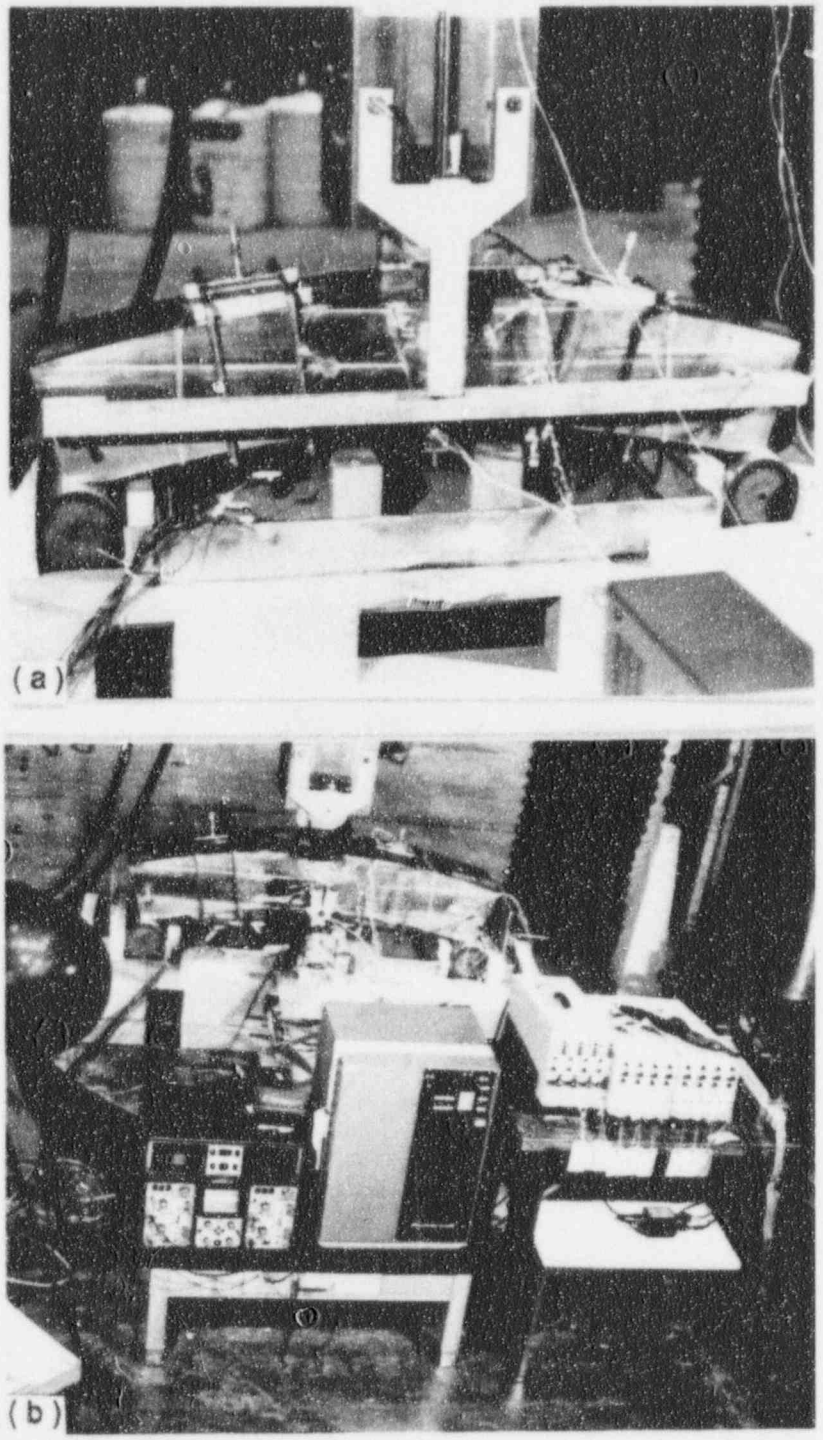

Figure 3.11 (*a*) **Full-thickness clad beam specimen CB-1 shown mounted in test fixture during fatigue precracking, and** (*b*) **sample, bridge amplifiers, and some of the data collection system shown in relative positions**

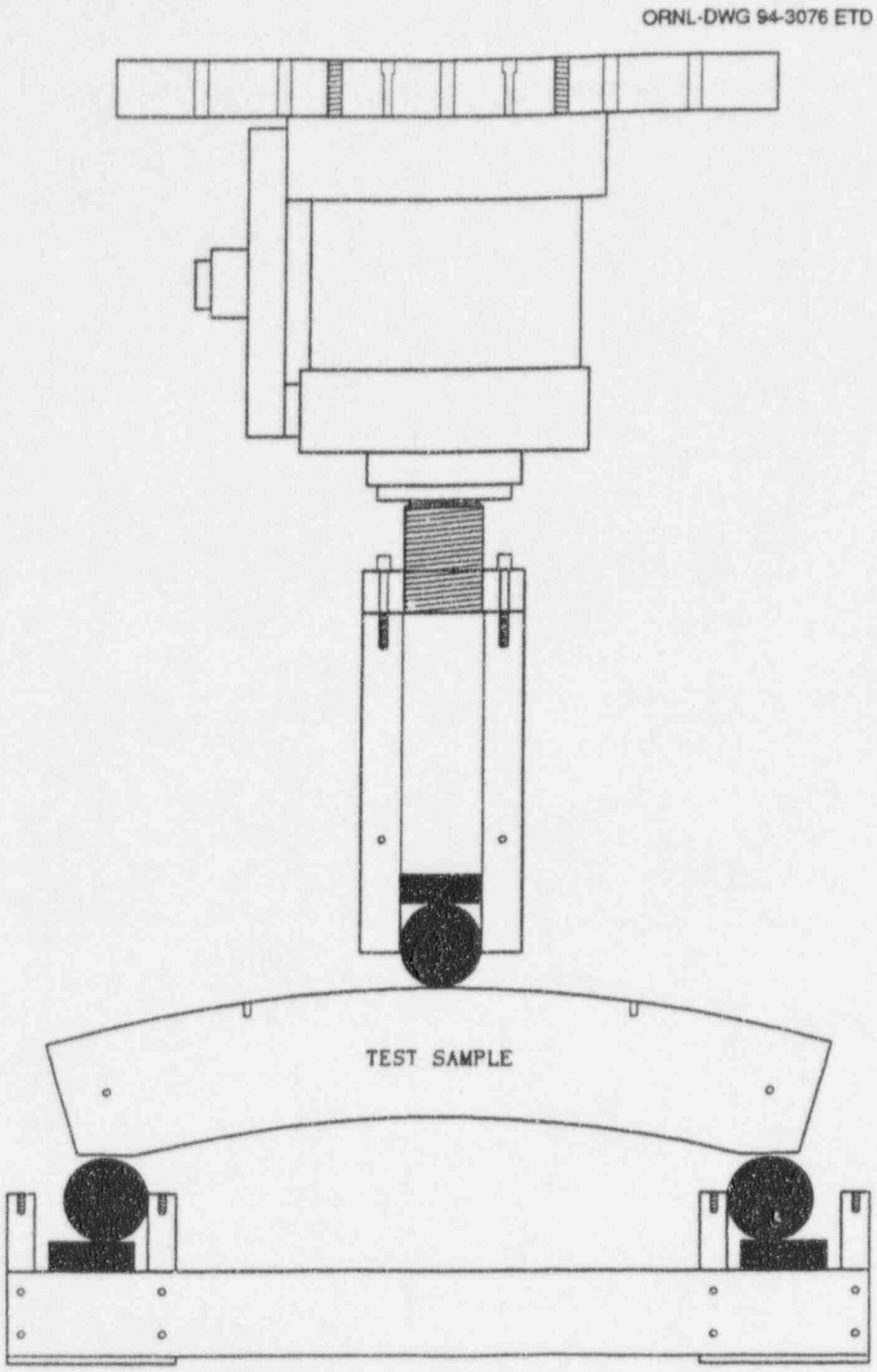

Figure 3.12 Schematic of load system and test beam

Fatigue precracking of CB-1 was initially carried out at room temperature by cycling between 23 and 227 kN (5 and 51 kips), which corresponds to a stress-intensity factor (SIF) range of 25 MPa$\sqrt{m}$ (23 ksi$\sqrt{in.}$). After 6510 cycles at frequencies in the range of 0.1 to 0.3 Hz, no fatigue crack appeared to have developed. The loading was increased to a range of 27 to 273 kN (6 to 61 kips), corresponding to DK = 30 MPa$\sqrt{m}$ (27 ksi$\sqrt{in.}$). An additional 3,525 cycles were run (10,035 total) with no visible sign of crack growth. The load range was increased a third time, 45 to 318 kN (10 to 71 kips), corresponding to DK = 33 MPa$\sqrt{m}$ (30 ksi$\sqrt{in.}$), and a crack initiated from the EDM flaw at a total of 11,400 cycles. The load range was then reduced to 55 to 282 kN (12 to 63 kips), DK = 28 MPa$\sqrt{m}$ (25 ksi$\sqrt{in.}$). At this load range, an additional 19,000 cycles were required to grow the flaw the specified 2.5 mm. During the fatigue precracking phase, data were taken using all load, displacement, and strain

instrumentation to verify correct function. The amount of crack growth was verified by posttest measurements on the fracture surface. The fatigue precracking parameters for the test beams are summarized in Table 3.8.

Table 3.8 Fatigue precracking parameters for full-thickness clad beam specimens

	CB-1	CB-2	CB-3
Temperature, °C	20.0	20.0	20.0
P_{max}/P_{min}	7–10	7–10	7–10
K_{max}, MPa$\sqrt{m}$	33	33	33
ΔK, MPa$\sqrt{m}$	28	28	28

For the fracture phase, the manifold for spraying the LN_2 onto the beam surface was mounted around the specimen, and the environmental chamber was used to enclose the assembly. Once the specimen was completely enclosed, it was cooled to the test temperature (–25°C) per the procedures just discussed. The specimen was then loaded to fracture under stroke control using a constant LLD rate. Specimen CB-1 failed at a load (P) of 1232.5 kN (277 kips). The fracture surface for this specimen is shown in Fig. 3.13. The fracture surface can be divided into three parts. The upper part is the machined flaw surface, where the uniformity or straightness of the crack front is clearly visible. The second part is the crack-growth surface due to fatiguing. Note that, with the exception of portions of the crack front near the beam sides, the flaw growth was very uniform. The third part is the fracture surface itself, which shows a cleavage fracture. While there are multiple initiation sites, the first initiation location appeared to be near the center of the crack front. The same failure test procedure and the same general instrumentation layout was used for all three specimens. The fracture surfaces for specimens CB-2 and CB-3 are shown in Figs. 3.14 and 3.15, respectively. The general features are similar to those for CB-1.

ORNL-PHOTO 8082-94

Figure 3.13 Fracture surface of full-thickness clad beam specimen CB-1

ORNL-PHOTO 8085-94

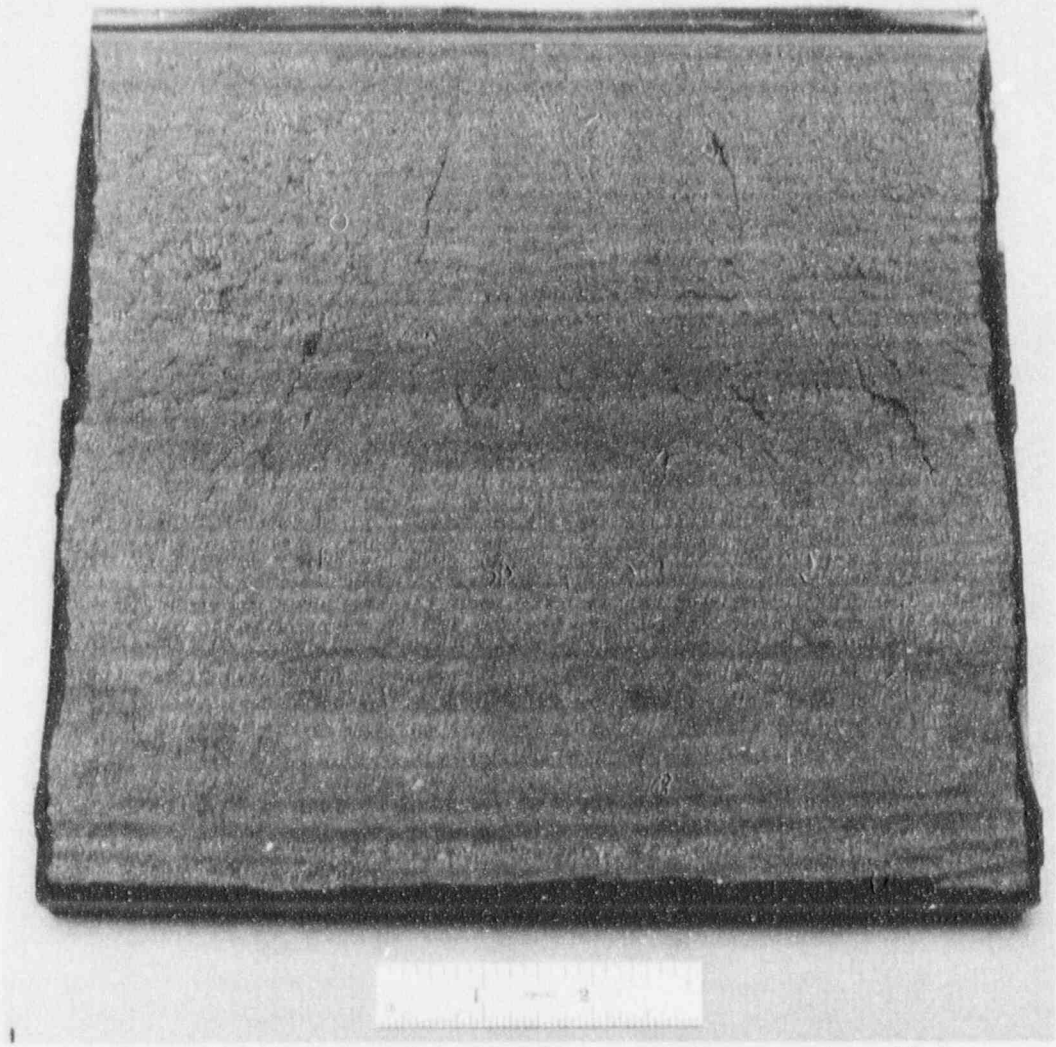

Figure 3.14 Fracture surface of full-thickness clad beam specimen CB-2

ORNL-PHOTO 8086-94

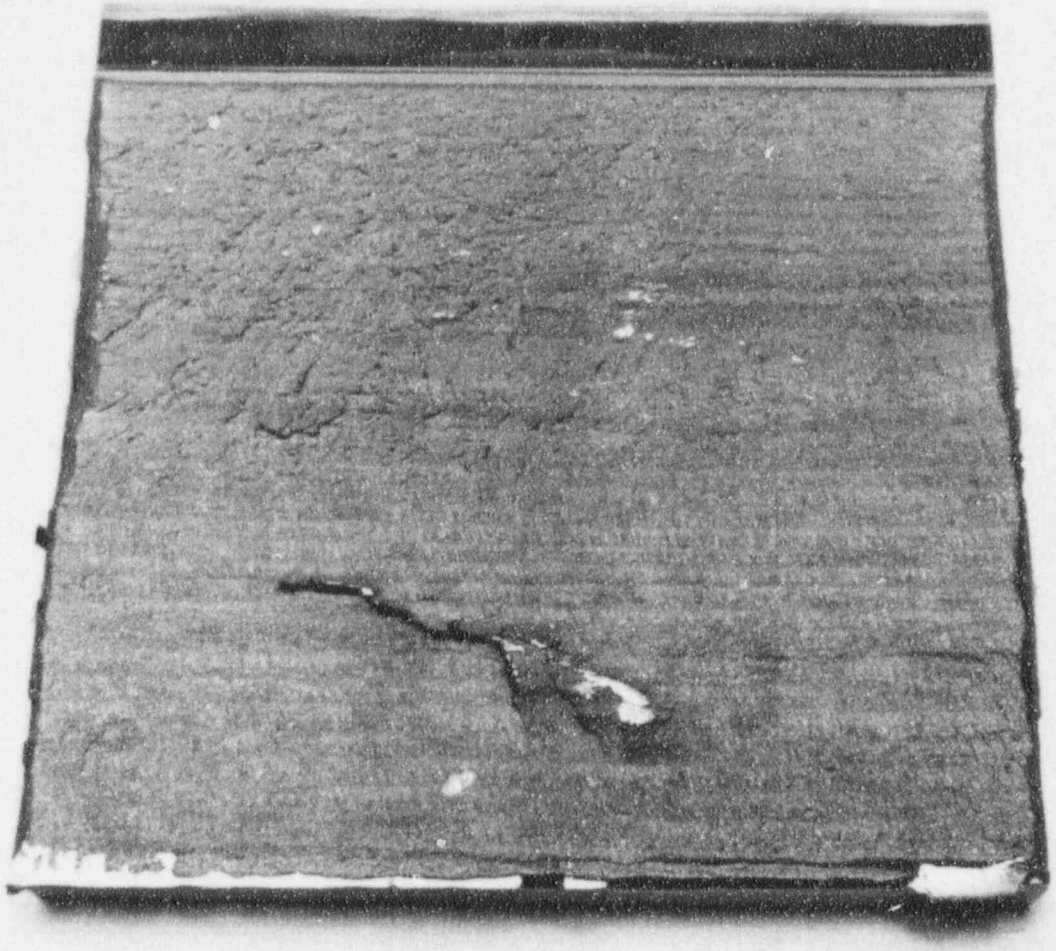

Figure 3.15 Fracture surface of full-thickness clad beam specimen CB-3

3.2.4 Test Results and Comparison with Existing Data

The P vs displacement curves for each of the three beams are shown in Fig. 3.16 for LLD and in Fig. 3.17 for CMOD, respectively. These curves depict the inelastic behavior in the shallow-crack specimens as fracture conditions are approached. The conditions of each specimen at failure are listed in Table 3.9. The plastic component of the area under each P vs displacement curve (defined as U_{pl} for LLD and A_{pl} for CMOD) and the corresponding h-factors, η^{ℓ}_{pl} and η^{c}_{pl}, are also included in Table 3.9. Toughness data for the clad beam specimens were calculated using the techniques described in Ref. 8. The P vs CMOD method,[9] considered the more accurate of the techniques examined for determining fracture toughness of shallow-crack specimens, is the primary method used for the clad beam analysis. The critical J-integral values were converted to critical elastic-plastic, SIFs (K_{Jc}), using the plane strain formulation. The toughness values determined for the tests, along with the parameters used to estimate the toughness, are included in Table 3.9. These data should be regarded as preliminary, since the potential effects of residual stresses and material gradients in the heat-affected zone (HAZ) (associated with the cladding) were not considered in the toughness determinations.

The fracture toughness data given in Table 3.9 for prototypic submerged-arc pressure vessel weld material are compared in Figs. 3.18–3.21 with single-edge-notch bending (SENB) and biaxial cruciform data for A 533 B steel* previously generated in testing programs by ORNL[8–10] and by CDNSWC.[11] (These fracture toughness data for A 533 B plate material and pressure vessel weld material are also tabulated in Appendix A of Ref. 12.) In Figs. 3.18 and 3.19, the data are plotted as a function of the reference temperature, $T - RT_{NDT}$. For the deep-crack data

*W. E. Pennell, ORNL, letter to S. N. M. Malik, USNRC, March 18, 1994.

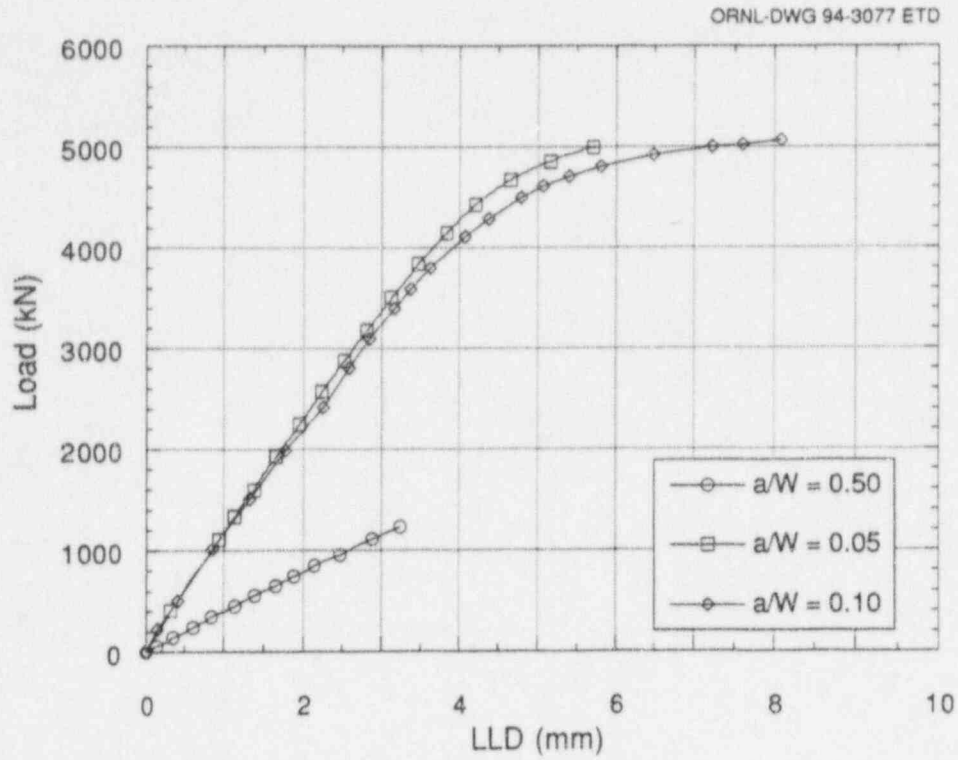

Figure 3.16 Load vs LLD response for clad beam specimens

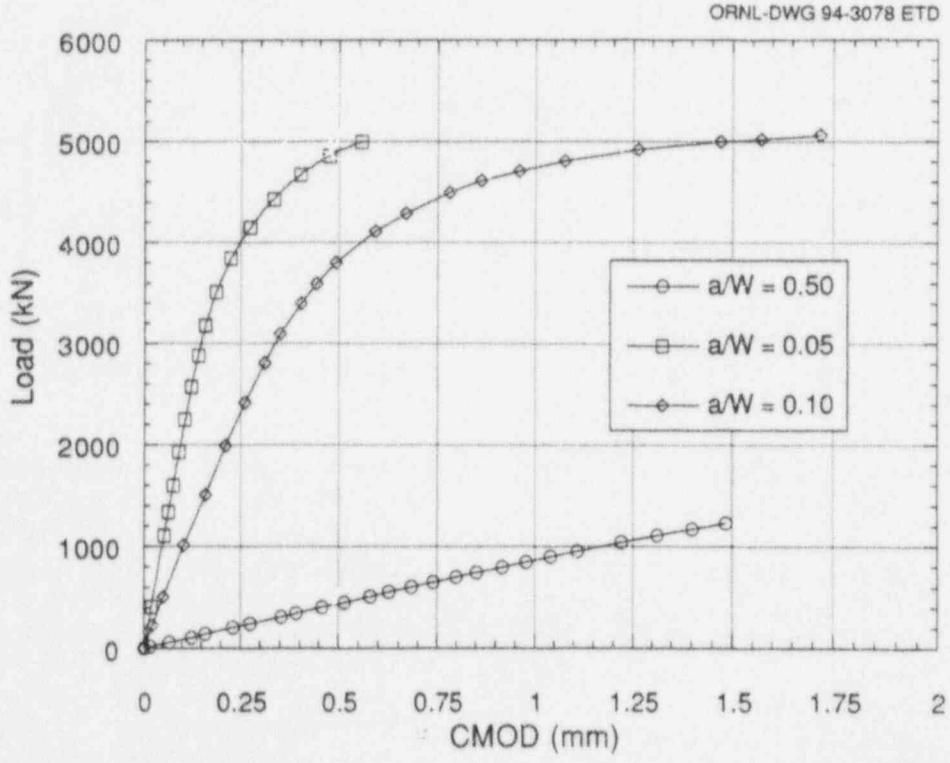

Figure 3.17 Load vs CMOD response for clad beam specimens

Table 3.9 Summary of results from the full-thickness clad beam testing program

	CB-1	CB-2	CB-3
a/W	0.50	0.05	0.10
Temperature, °C	−25.5 ± 1.0	−25.0 ± 1.0	−25.5 ± 1.0
Stroke rate, mm/min	2.49	8.38	6.89
Time to failure, s	230	366	440
Failure conditions			
P, kN	1232.5	5002.3	5060
LLD, mm	3.236	5.767	8.083
CMOD, mm	1.485	0.567	1.718
U_{pl}, kN-mm	135	6427	16879
A_{pl}, kN-mm	88	1473	5486
η-factors			
η^{ℓ}_{pl}	1.37	0.79	1.05
η^{c}_{pl}	2.26	4.16	4.08
Fracture toughness			
Elastic component			
J_{el}, kN/m	131.3	110.6	230.5
K_I, MPa$\sqrt{m}$	173.0	154.5	223.1
P vs CMOD			
J_{pl}, kN/m	8.1	124.7	486.0
Total J, kN/m	139.4	235.3	716.5
K_{Jc}, MPa$\sqrt{m}$	173.5	225.4	393.3
P vs LLD			
J_{pl}, kN/m	7.4	103.8	384.8
Total J, kN/m	138.7	214.4	615.3
K_{Jc}, MPa$\sqrt{m}$	173.1	215.2	364.5

(Fig. 3.18), a single curve is adequate to define a lower bound to all three of the deep-crack fracture toughness data sets. For the shallow-crack data (Fig. 3.19), the lower-bound curve to the CDNSWC data is substantially lower than the lower-bound curve to the HSST data and nearly coincident with the lower-bound curve of the combined deep-crack data set.

The choice of the reference temperature can potentially influence interpretation of the shallow-crack toughness data in Fig. 3.19. Reference 2 defines RT_{NDT} in terms of both the NDT and the temperature (T_{c_V}) at which the lower-bound Charpy energy from three tests is not less than 68 J (50 ft-lb). For a given material, one of these temperatures (NDT or T_{c_V}) will be the controlling temperature in determining RT_{NDT}. Examination of the reference temperature data for the materials represented in Figs. 3.18 and 3.19 reveals that RT_{NDT} is controlled by NDT for the CDNSWC data and by T_{c_V} for the welds in the full-thickness clad beams tested at NIST. The RT_{NDT} values of the two source plates, HSST plates CE-WP and 13B,[10] used in generating the HSST A 533 B data are controlled by NDT and T_{c_V}, respectively. A proposed solution* to this problem is to adopt a common reference temperature for comparing the various data sets. In Figs. 3.20 and 3.21, the parameter NDT is employed as the reference temperature.

*W. E. Pennell, ORNL, letter to S. N. M. Malik, USNRC, March 18, 1994.

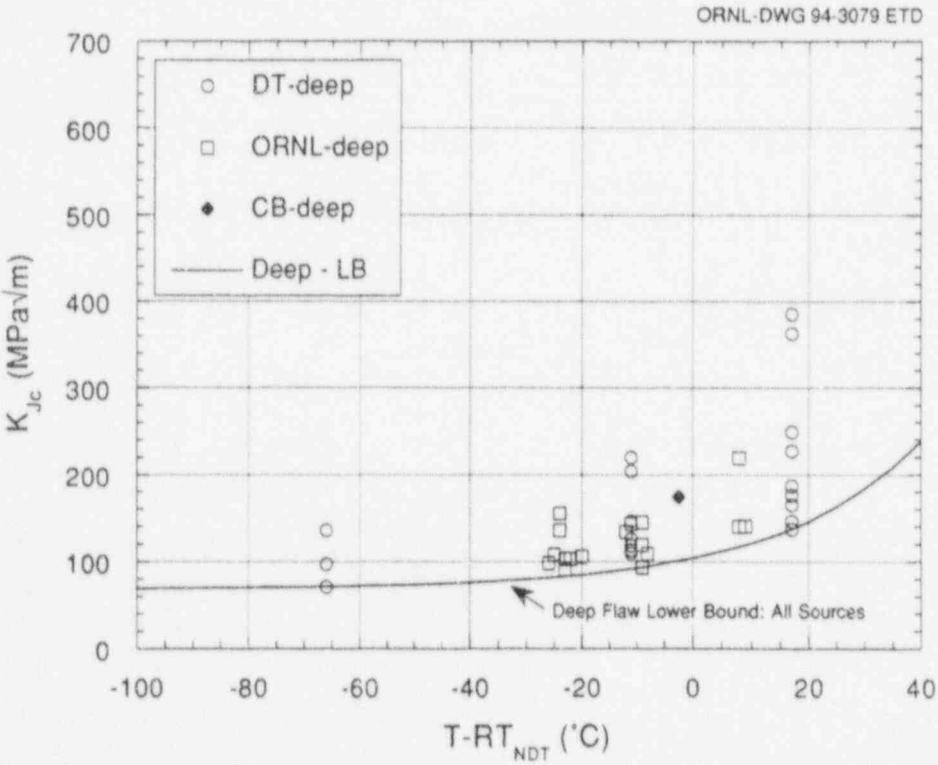

Figure 3.18 Deep-crack fracture toughness results as function of normalized temperature T − RT_{NDT}. Note: DT = David Taylor, CB = clad beam, and LB = lower bound

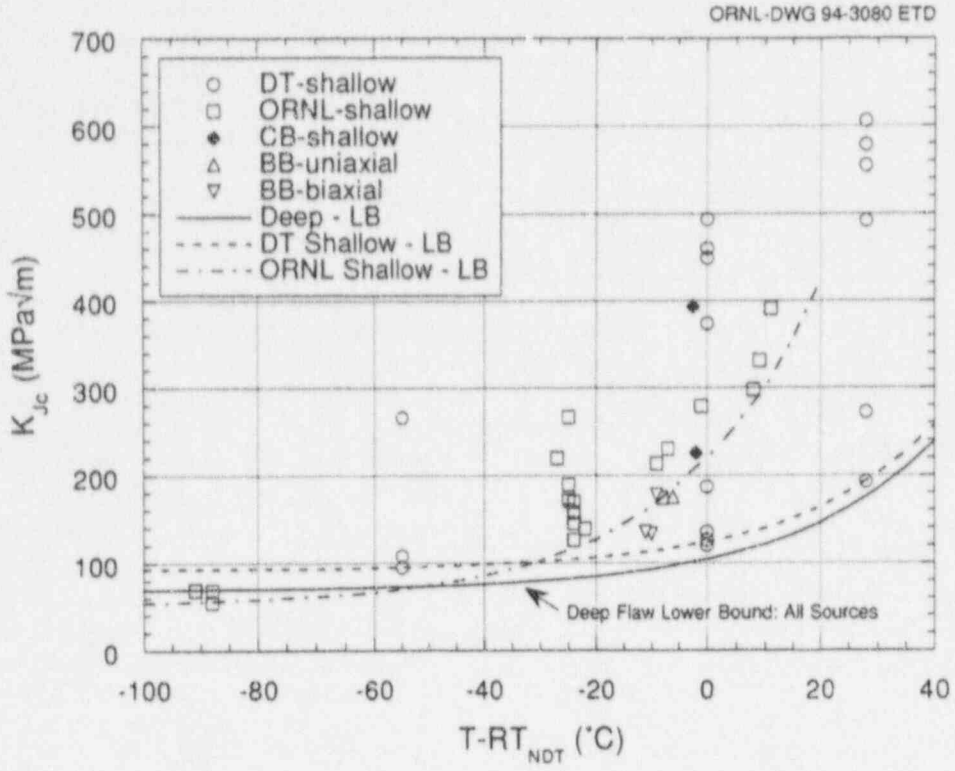

Figure 3.19 Shallow-crack fracture toughness results as function of normalized temperature T – RT_{NDT} . Note: BB = biaxial beam

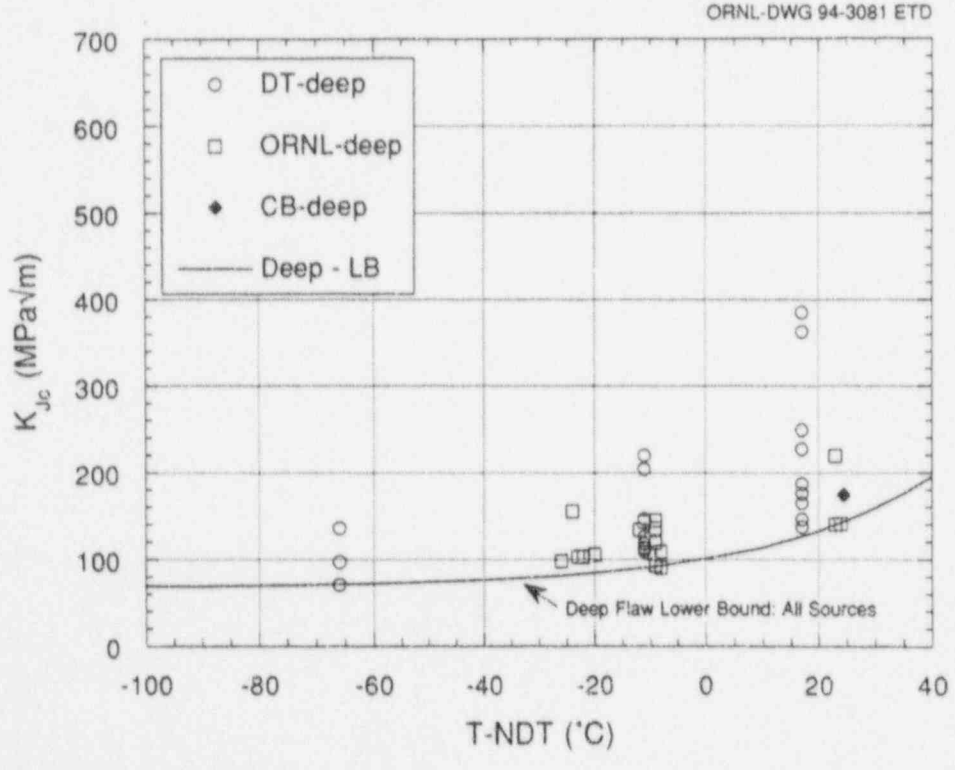

Figure 3.20 Deep-crack fracture toughness results as function of normalized temperature T – NDT

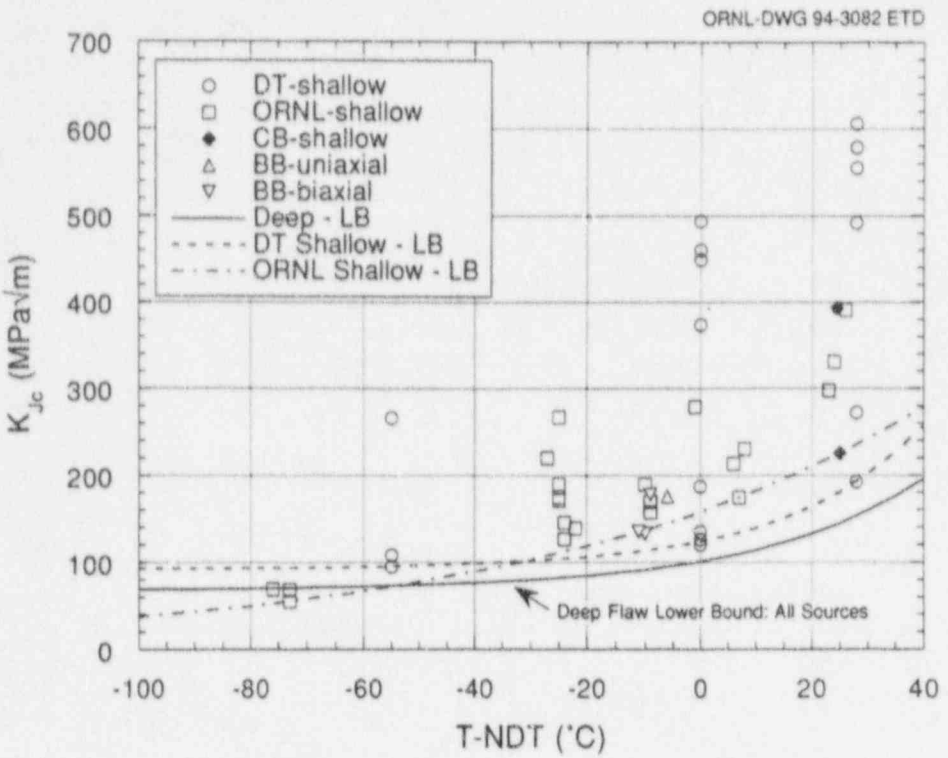

Figure 3.21 Shallow-crack fracture toughness results as function of normalized temperature T – NDT

Figure 3.20 indicates that a single curve still defines the lower bound to the deep-crack fracture toughness data sets. In Fig. 3.21, lower-bound curves to the shallow-crack HSST data and to the CDNSWC data are still distinctly separated, but to a lesser degree than in Fig. 3.19 for the comparison based on RT_{NDT}. The results in Fig. 3.21 indicate that, while the loss of constraint associated with shallow cracks elevates the mean fracture toughness, the increased data scatter in the transition region tends toward the same lower bound associated with highly constrained deep-crack toughness data.

The crack tip in clad beam specimen CB-2 (a/W = 0.05) was located at a depth of ~10 mm, which is near the boundary of the cladding HAZ in the weld metal. In Fig. 3.21, the fracture toughness result for specimen CB-2 defines the lower bound of the HSST shallow-crack toughness data at the higher temperatures, when NDT is the normalizing parameter. Although material property data are not available for confirmation, the potential exists that metallurgical conditions in the cladding HAZ region significantly influenced the relatively low initiation toughness measured in the CB-2 test.

A comparison of the shallow- and deep-crack lower-bound curves for the ORNL data only, plotted vs $T - RT_{NDT}$ in Fig. 3.22 and vs T – NDT in Fig. 3.23, indicates that there is less of a separation between the shallow- and deep-crack lower-bound curves at a particular K_{Jc}. Figure 3.22 shows, by the horizontal arrow, that for a K_{Jc} of 150 MPa$\sqrt{m}$, the temperature shift $[\Delta(T - RT_{NDT})]$ is 35°C, which is close to the temperature shift [Δ(T – NDT)] of 31°C in Fig. 3.23 for the same toughness.

In the next report period, analyses of the test data will be described, including comparisons of test data with FEA results and applications of toughness estimation techniques. Also, applications to the clad beam data of the stress-based constraint characterizations developed by O'Dowd and Shih and by Dodds and Anderson will be included.

3.2.5 Additional Testing

Additional full-thickness clad beam tests are planned to complete the investigation of fracture toughness of shallow cracks located in prototypical full-thickness weld and plate material. Two clad beam specimens will be fabricated to duplicate the CB-2 and -3 shallow-crack tests in weld metal. Shallow-crack fracture toughness results from these specimens should provide additional data that are essential to a better understanding of the effects of metallurgical conditions in the region of the clad HAZ. Three additional specimens will be available for testing of shallow cracks in the A 533 B plate material and to respond to further testing needs derived from results of the existing test matrix.

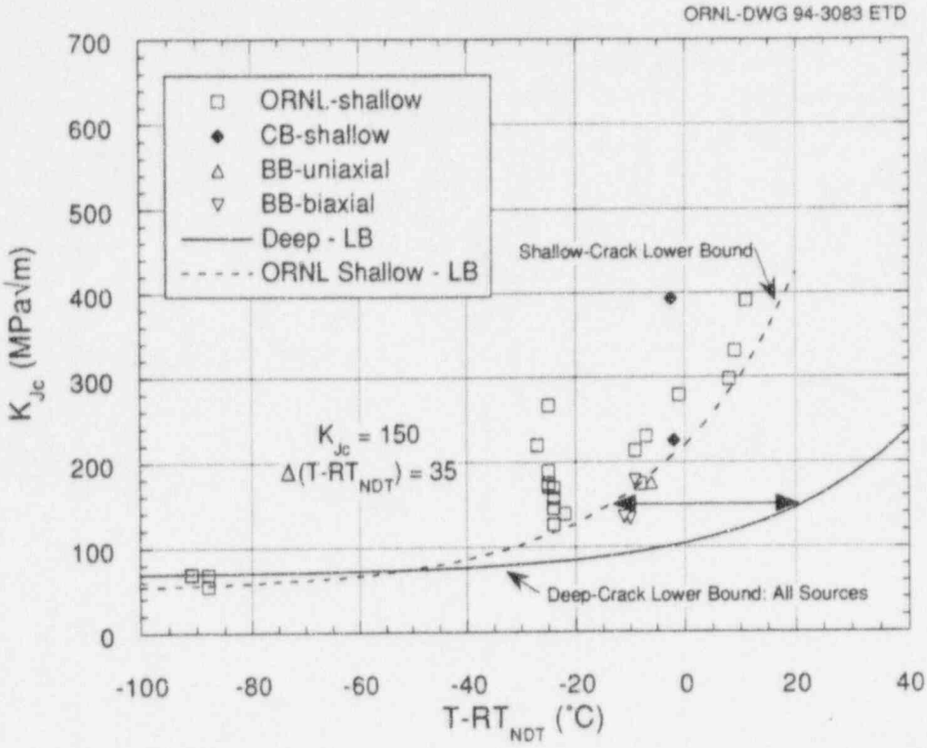

Figure 3.22 HSST shallow-crack fracture toughness results as function of normalized temperature T – RT_{NDT}

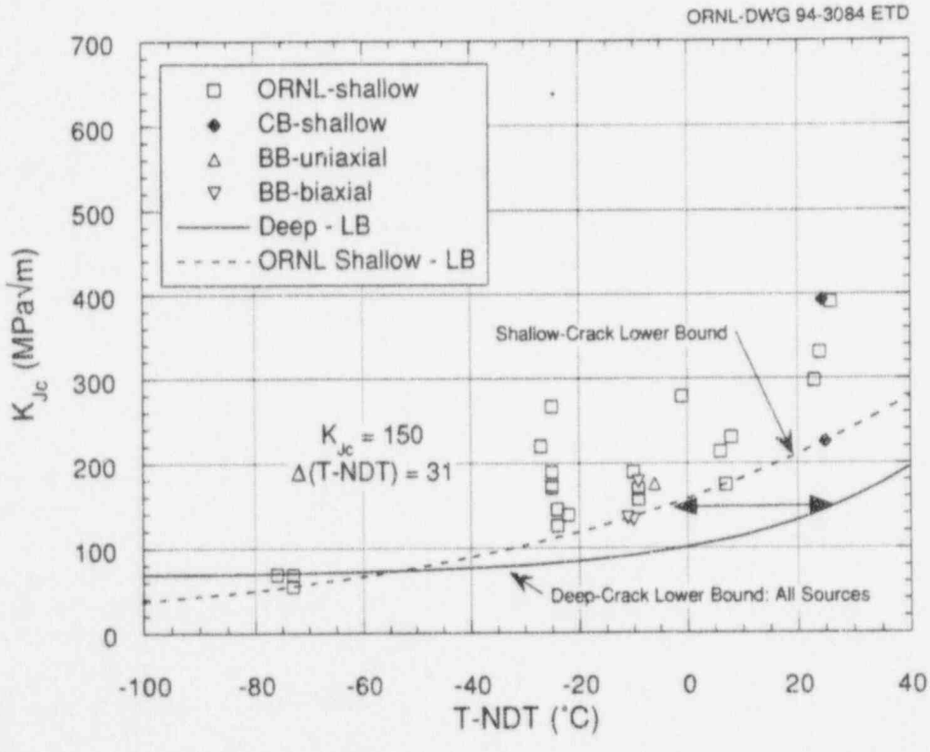

Figure 3.23 HSST shallow-crack fracture toughness results as function of normalized temperature T – NDT

3.3 Quasi-Static Clad Yielding Model Development (J. A. Kenney and T. L. Dickson)

Work was begun on the formulation and validation of a clad yielding model that can be incorporated into linear-elastic fracture mechanics (LEFM) influence coefficient methodology. Conventional practice in assessments of RPVs assumes a thermoelastic (TE) constitutive model and base-metal fracture toughness properties for the discrete clad region. However, crack initiation studies indicate that incorporation of clad yielding into the assessment models reduces the crack-driving forces for shallow flaws. Also, ductile fracture toughness of cladding may prevent longitudinal propagation of many finite-length shallow flaws. These studies imply that the failure probability may be significantly reduced when clad mechanical and fracture toughness properties, including the effects of irradiation, are incorporated into the calculations.

Influence coefficient methodology based on LEFM concepts is generally used to perform deterministic and probabilistic RPV assessments. As a near-term refinement in the assessment methodology, a generic model is being developed that incorporates the clad yield stress into the calculations, while permitting the LEFM influence coefficient approach to be retained in the presence of the clad nonlinear response. An empirical approach utilizing a matrix of clad vessel solutions is being employed to construct the model. Validation of the model predictions will be done using available test data and analyses.

In preliminary studies, a validation problem was defined to benchmark direct finite-element solutions from ABAQUS[13] with the FAVOR[14] code. The problem consisted of a clad RPV containing a shallow inner surface crack (c/a = 2; a/W = 0.05) and subjected to PTS loading. For the elastic case, the ABAQUS and FAVOR solutions were in good agreement, with <1% difference.

In the next phase, elastic-plastic analyses were performed with ABAQUS to provide clad vessel solutions for use in a generic model based on an empirical approach. The vessel was subjected to a constant internal pressure loading of 1 ksi and the following thermal transient:

$$T = T_f + (T_i - T_f) \cdot \exp(-b \cdot t) \ , \qquad (3)$$

where T, T_i, and T_f are current, initial, and final temperature, respectively; b is the decay constant; and t is the transient time. For these analyses, T_i = 288°C (550°F), b = 0.15, h = 2840 W/m^2·K (500 Btu/h·ft^2·°F), while T_f ranges from 66 to 121°C (150 to 250°F). In these first analyses, T_f was set at 66°C (150°F) for the most severe transient, and a comparison was made between TE and thermo-elastic-plastic (TEP) K_I values through time for each position around the crack front. The TEP K_I values dropped dramatically below the TE values at the inner surface (≈40%), were larger than the TE K_I values in the base metal near the claddiing (≈7%), and then were slightly less than the TE K_I values (≈3%). The next set of analyses will be for the same flaw, but T_f will be set to 121°C (250°F) (the least severe transient to be analyzed).

Future work will include TE and TEP analyses over a range of flaw depths, clad thicknesses, and flaw geometries. This will facilitate the development of an empirical correlation that has sufficient generality to correct LEFM K_I solutions for the effect of clad plasticity as would be required for prototypical PTS scenarios. This correlation will be incorporated into the FAVOR code.

3.4 Cladding Method Development

A methodology is being developed for producing weld overlay cladding that meets testing requirements for the clad cruciform specimens to be tested under subtask H.3.4. At a specified test temperature, tearing toughness properties of the cladding should exhibit a relationship to cleavage toughness properties of the base material, which is similar to that in an irradiated RPV near end-of-life. This relationship should be established at a reference temperature ($T - RT_{NDT}$) where the base material exhibits toughness values representative of irradiated conditions. The materials will be used to fabricate composite cruciform specimens for testing at a specified temperature where the cladding and base material properties have the desired relationship.

During this report period, a special heat of type 316 stainless steel (National Fusion Reference Heat X15893) was investigated. It has a K_{Jc} and a tearing modulus of ~80 MPa$\sqrt{m}$ and 15, respectively, at room temperature and in the T-L orientation. In the L-T orientation the corresponding values are 300 to 400 MPa$\sqrt{m}$ for K_{Jc} and 120 to 180 for tearing modulus. Thus, this material could be used in the T-L orientation to study lower bounds.

Also, three sets of wrought stainless-steel material were obtained from Rolled Alloys, Incorporated, for evaluation as surrogates for irradiated cladding. Heat treatment was necessary to degrade the toughness to simulate irradiated properties. Two sets of 1/2 T(CT) compact-tension specimens were tested. These specimens were machined in two different orientations from austenitic stainless steel (AL 6XN) that was aged at 815°C (1500°F) for 10 and

100 h, respectively. The specimens failed by unstable fracture, which made this heat treatment unsuitable as a surrogate for irradiated cladding. Target initiation toughnesses were 50 to 100 kJ/m^2 for J_{Ic} and ~180 for tearing modulus. One specimen, aged 10 h, had corresponding values of 32 kJ/m^2 and 90, respectively. The remaining specimens failed after too few loading/unloading cycles and did not give a J-R curve. This material, in the unaged condition, was an austenitic stainless steel with a room-temperature CVN impact energy in excess of 300 J, indicating a very high initiation toughness and tearing resistance.

Because of difficulties associated with achieving the target toughness properties using heat treatment, deterministic analyses will be performed with the FAVOR code to investigate whether the tearing toughness of irradiated cladding should be considered an issue in meeting the goals of the clad testing program. Thus, the objective is to determine from the FAVOR analysis whether irradiated cladding is predicted to experience ductile tearing in a prototypic vessel subjected to a severe PTS transient. If the stainless steel cladding is predicted not to experience tearing during the experiment, then it can be concluded that a relatively high tearing toughness of the cladding should not be an issue in achieving the objectives of the clad cruciform testing program.

Results from the FAVOR deterministic analyses will be included in the next report period.

3.5 Validation Through International Participation

During this report period, analyses of the EdF clad beam experiments (DSR3 and DD2) were performed under the HSST Program. These analyses were carried out in support of Phase II of the Project for Fracture Analysis of Large-Scale International Reference Experiments (FALSIRE). Project FALSIRE is organized by the Fracture Assessment Group of the Organization for Economic Cooperation and Development/Nuclear Energy Agency's Committee on the Safety of Nuclear Installations Principal Working Group No. 3 to assess various fracture methodologies through interpretive analyses of selected large-scale fracture experiments. The HSST Program is also providing analytical results for the ORNL biaxial cruciform beam specimen BB-4 and the AEA Technology (United Kingdom) spinning cylinder experiment SC-4. The analyses for BB-4 have been completed and are described in Refs. 8 and 9. The FALSIRE II reference experiments are being analyzed by over 20 different international organizations, and comparative results will be presented at the FALSIRE II Specialists' Workshop to be held in Atlanta, Georgia, during November 1994.

3.5.1 French Clad Beam Experiments—DSR3 and DD2 (J. A. Keeney)

An experimental program is under way at EdF to provide data for evaluating different methods of fracture analysis used in RPV integrity assessments.[15–17] Experimental results are being compared with analysis predictions to validate different methods of fracture analysis and to evaluate their conservatism. Also, the effects of stainless steel cladding are being examined. The focus of these studies is a series of clad beams containing subclad cracks tested in four-point bending. The tests were performed at low temperatures (–170°C) to simulate severe radiation embrittlement and to investigate the effects of cladding on cleavage fracture in the base metal. Test conditions were representative of near end-of-life for the base metal, but not for the cladding. Two of the clad beam tests (DSR3 and DD2) are being utilized in Phase II of Project FALSIRE.

3.5.2 Test Description

The central part of each beam is A 508 class 3 steel with an RT_{NDT} of –40°C. The fabricated specimen DSR3 has dimensions of 120 × 145 × 1700 mm, with a 4.5-mm layer of cladding on the top surface produced by an automatic SAW process. Specimen DD2 has dimensions of 119.2 × 145 × 1700 mm with a 6.0-mm layer of cladding. The cladding is applied in two layers, the first of which is 309L stainless steel, followed by a second layer of 308L stainless steel. The beams contain a small subclad crack (approximately semielliptical) with a depth of 13 mm and length of 40 mm for DSR3 and a depth of 4.5 mm and length of 48 mm for DD2. The cracks were generated by fatigue-precracking. After the cladding process, a stress relief heat treatment was applied at 600°C for 8 h. The cladding layer had relatively low yield stresses and relatively high toughness. Data collected during the tests are load, load-point displacement, strains, and temperatures. Strains were measured with strain gages placed on the clad surface and on the opposite surface of the beam. Temperatures were measured with thermocouples placed on the surface and inside the specimen.

Before the mechanical test, the beam is cooled with liquid nitrogen such that the temperature (approximately –170°C) is uniform inside the specimen after the cooling. The beam is insulated to avoid significant reheating during the test. The specimens are then loaded in four-point bending, as shown in Fig. 3.24, with a 1450-mm major span and 450-mm minor span. In the DSR3 test, the load on the

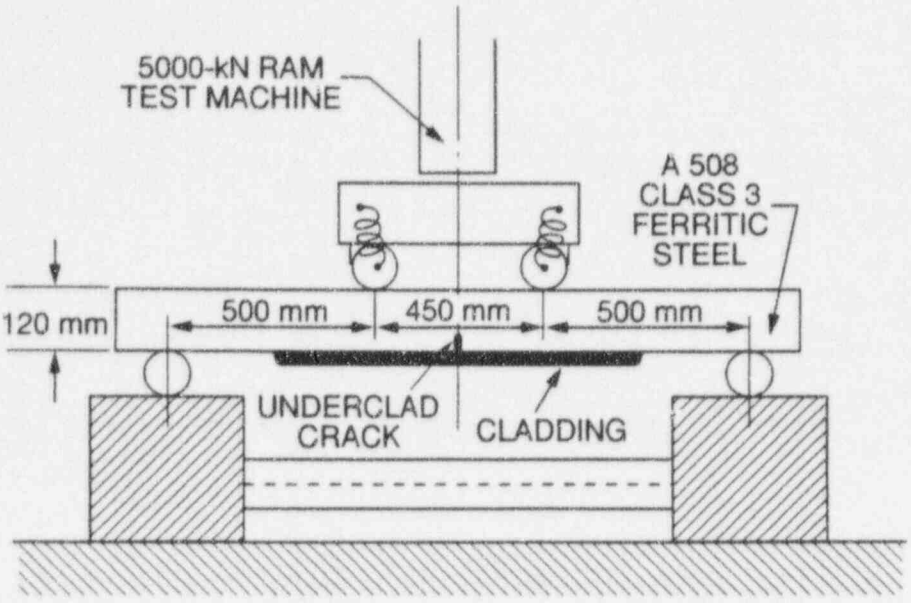

Figure 3.24 Schematic of the test frame used in four-point bending fracture experiments

beam at fracture was reported to be 695 kN. The cleavage fracture initiated in the ferritic base material, with no crack arrest. The temperature at the crack tip at the time of fracture was between –165°C and –170°C. In the DD2 test, the beam fractured at a load of 870 kN with no crack arrest. The point of cleavage initiation was located about 1.5 to 2 mm from the clad/base interface in DD2; the corresponding location in DSR3 was about 2.5 mm from the interface. Detailed information concerning the EdF clad beam testing program is given in Refs. 15–17.

3.5.3 Analysis Methods and Results

The three-dimensional (3-D) finite-element models of the clad beams were generated with the ORMGEN[18] mesh-generating program. From symmetry conditions, only one-fourth of the beam is included in the model (DSR3 is shown in Fig. 3.25). Both models consist of 16,178 nodes and 3,312 twenty-noded isoparametric elements. The measured crack front for each beam was modeled with a highly refined mesh in which the crack-tip element dimensions were on the order of 0.012 mm. Collapsed-prism elements surround the crack tip to allow for blunting and for a 1/r singularity in the strains at the crack front.

The beams were analyzed with the ABAQUS[13] finite-element program [a nuclear quality assurance certified (NQA-1) code]. The elastic-plastic small-strain analyses were performed using the material properties in Table 3.10 and the multilinear true stress-plastic strain curves depicted in Fig. 3.26.

The finite-element model was subjected to four-point bending with boundary conditions shown in Fig. 3.25. A distributed pressure load was applied over the surface of a thin strip of elements (5 mm wide), and the beam was simply supported on the opposite surface by fixing nodes in the direction opposite to the applied load. In each load step of the analyses, iterations were performed to establish global equilibrium using a force equilibrium method. Integrations of the stiffness matrix were performed with a $2 \times 2 \times 2$ Gauss point rule. The "stress-free" temperature was taken as the test temperature of the beam (residual stress and differential thermal strain effects were ignored).

Results from 3-D elastic-plastic analyses of the French clad beam experiments are summarized in Figs. 3.27–3.32. The deformation of the overall finite-element model and the crack-tip region are shown in Fig. 3.27 for DSR3 (DD2 showed similar deformation). The deformation indicates that the boundary conditions have been applied correctly. Calculated LLD, CMOD, and strains are shown in Figs. 3.28–3.32. The calculated CMOD values for both DSR3 and DD2 (Figs. 3.29 and 3.30) indicate that the largest values of CMOD are located near the clad/base interface, which is due to the cladding layer stretching and allowing the crack to open more. In Figs. 3.28, 3.31, and 3.32, the calculated and measured values of LLD and strain are compared for each test. In Figs. 3.31 and 3.32 the measured strains were normalized to zero at zero load for a better comparison with the calculated strains. The comparisons show good agreement, which indicates that the overall structural response has been modeled appropriately.

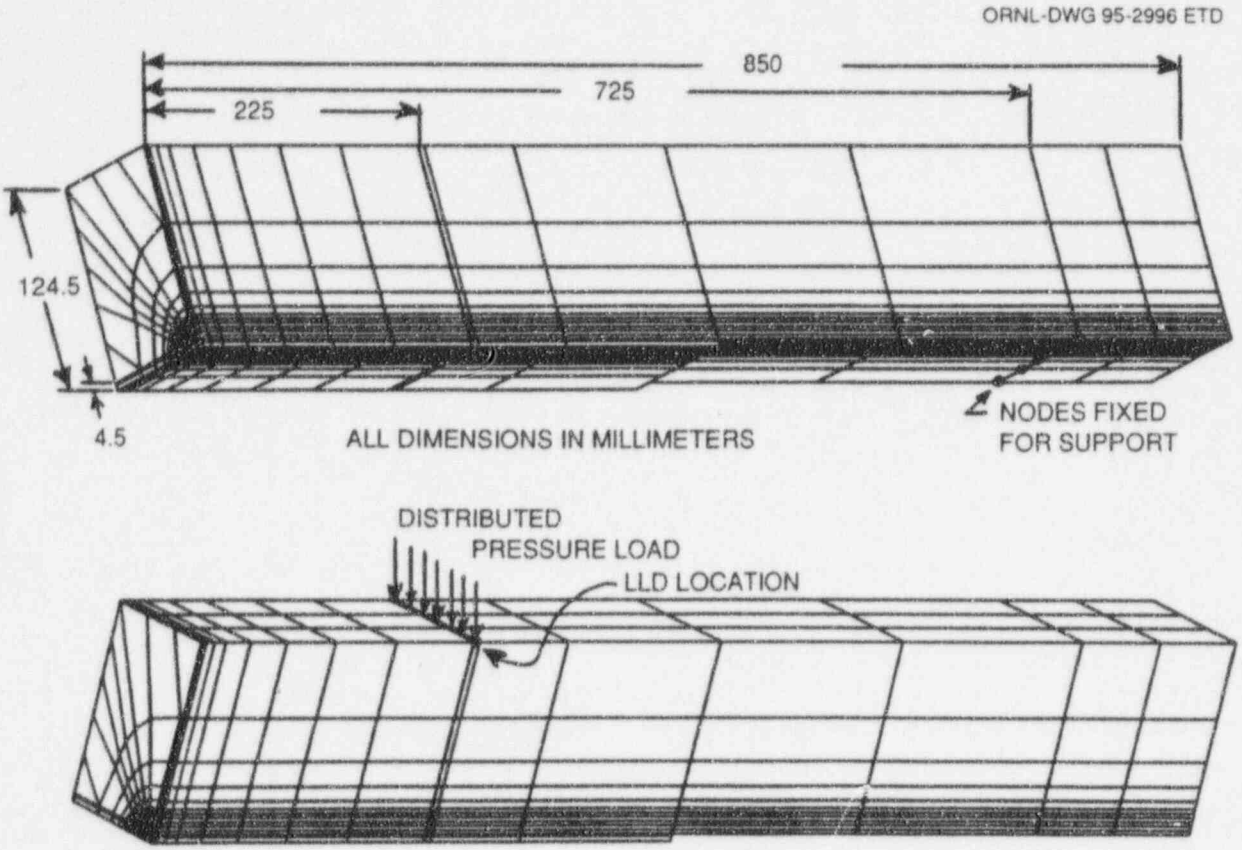

Figure 3.25 Finite-element model used in analysis of DSR3 with dimensions and boundary conditions

Table 3.10 Material properties for the French clad beam analyses

Material property	Base A 508 Class 3	Stainless steel cladding 309L and 308L
Young's modulus (E), GPa	210.0	160.0
Poisson's ratio (ν)	0.28	0.30
Yield stress (σ_y), MPa	768.0	347.0

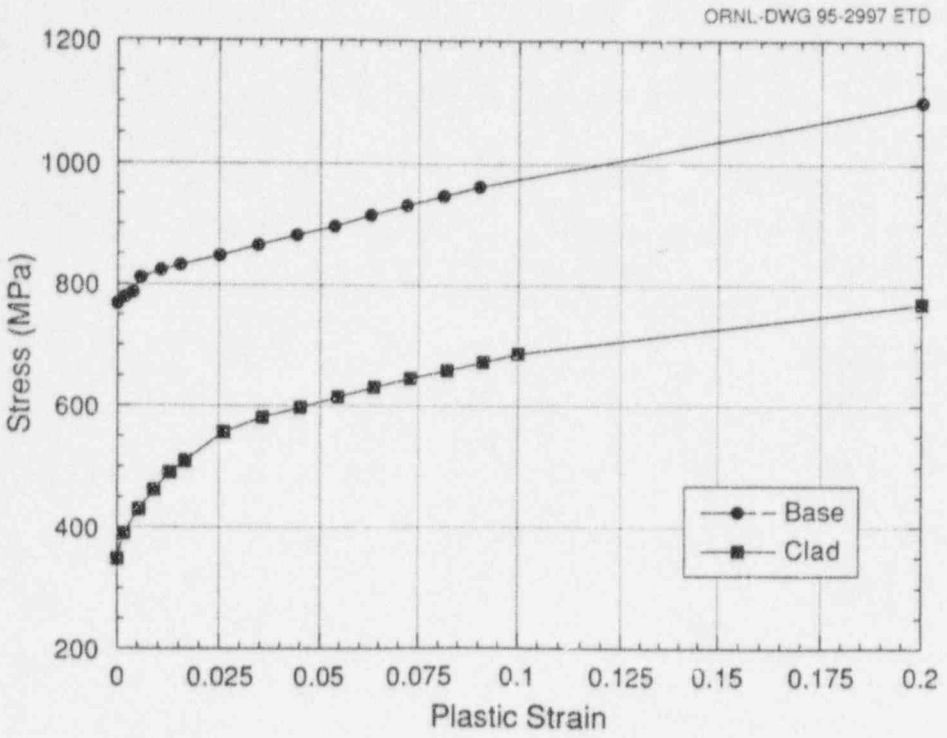

Figure 3.26 Stress-plastic strain curves at –170°C for base metal and cladding

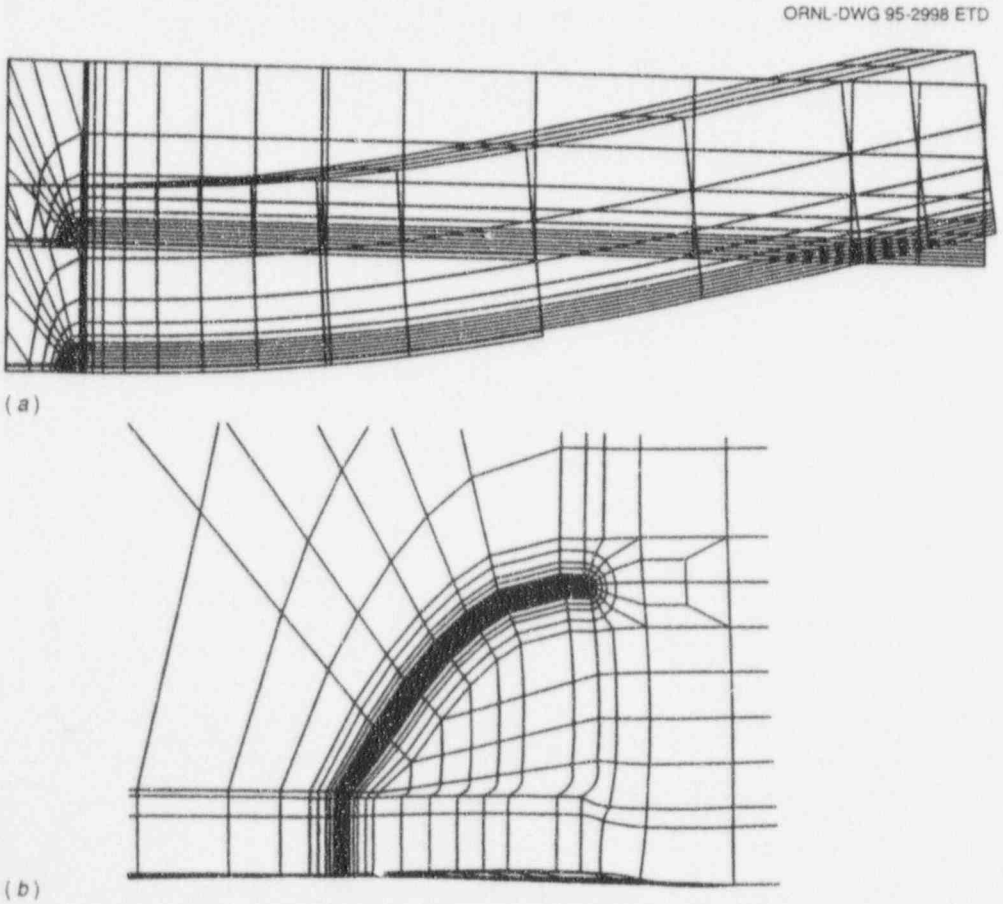

Figure 3.27 Deformation of finite-element model (DSR3) under applied initiation load of 695 kN: (*a*) 3-D model (displacement magnification factor = 10) and (*b*) crack-tip region (displacement magnification factor = 50)

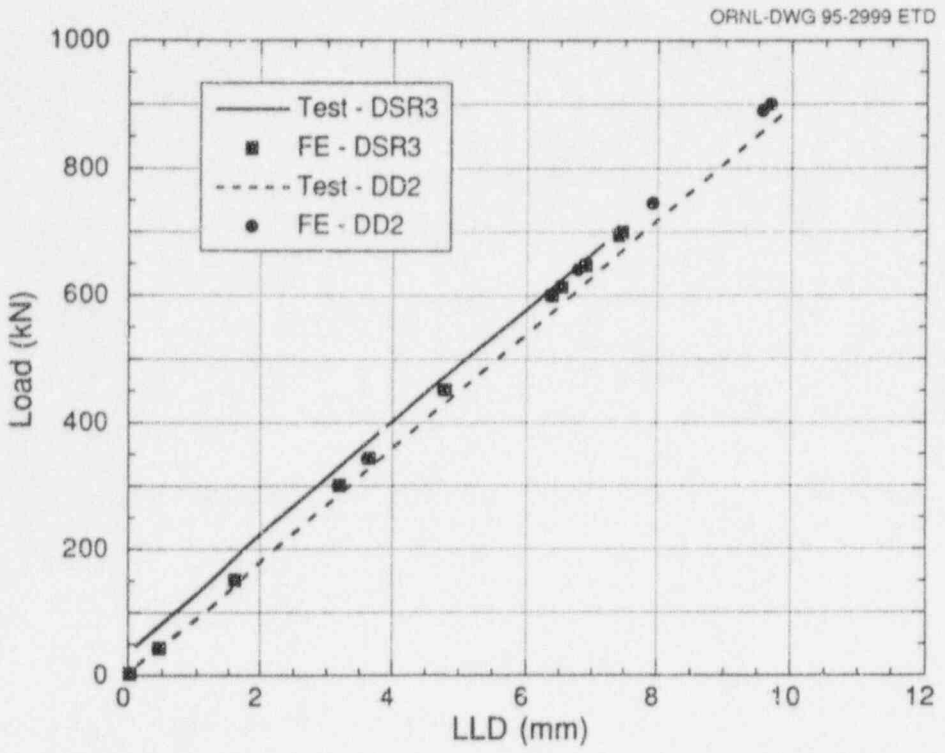

Figure 3.28 Measured and calculated load-line displacement for DSR3 and DD2

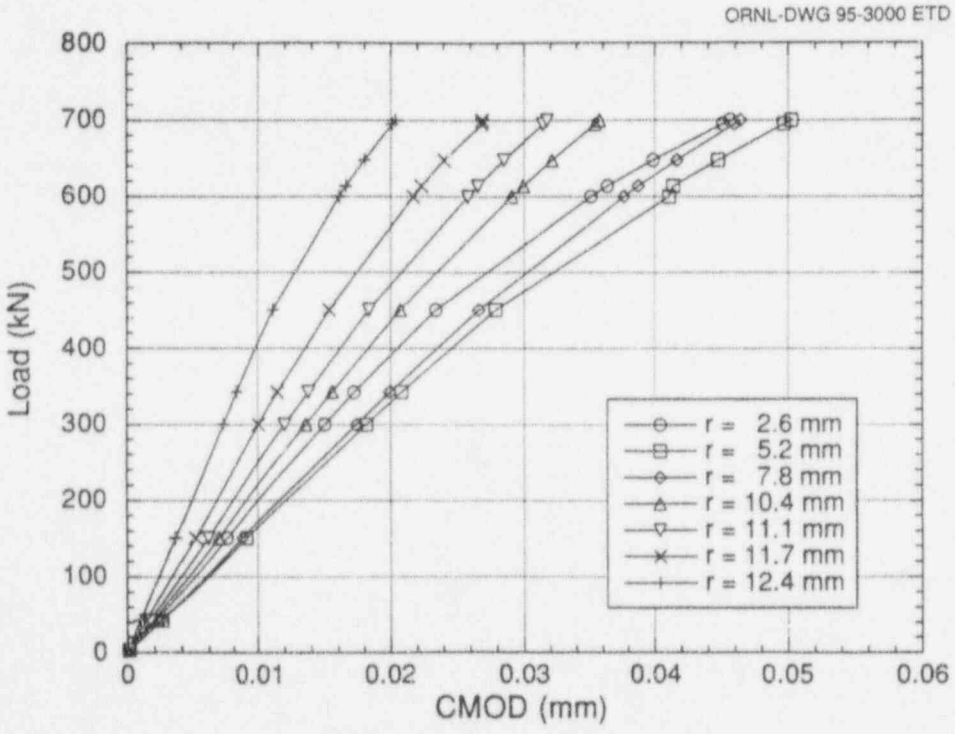

Figure 3.29 Calculated crack-mouth opening displacement for DSR3

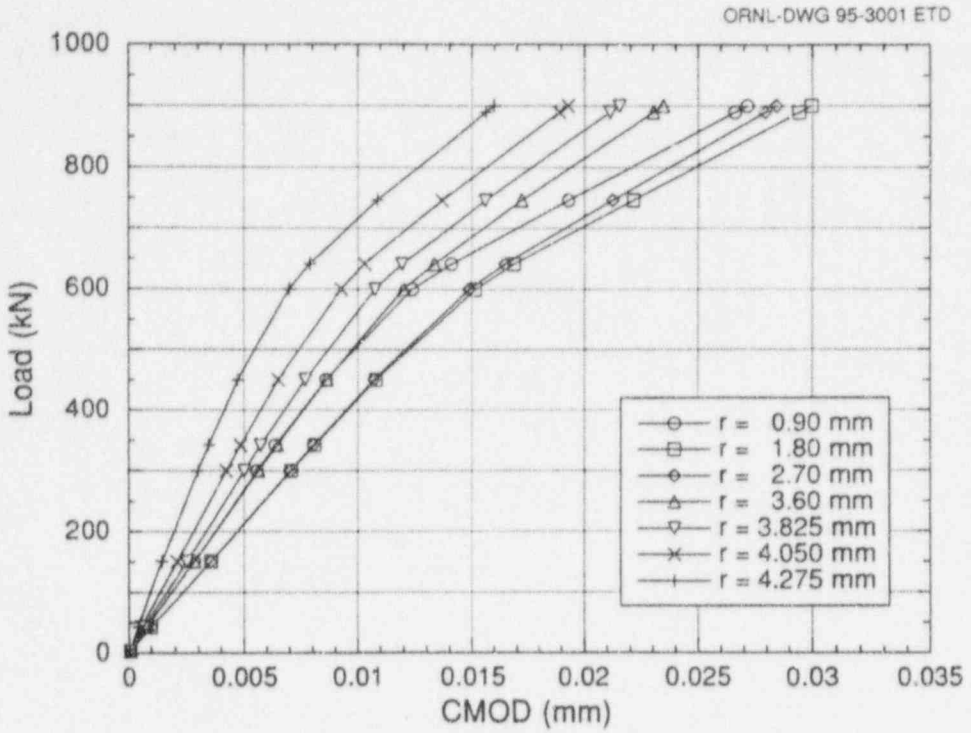

Figure 3.30 Calculated crack-mouth opening displacement for DD2

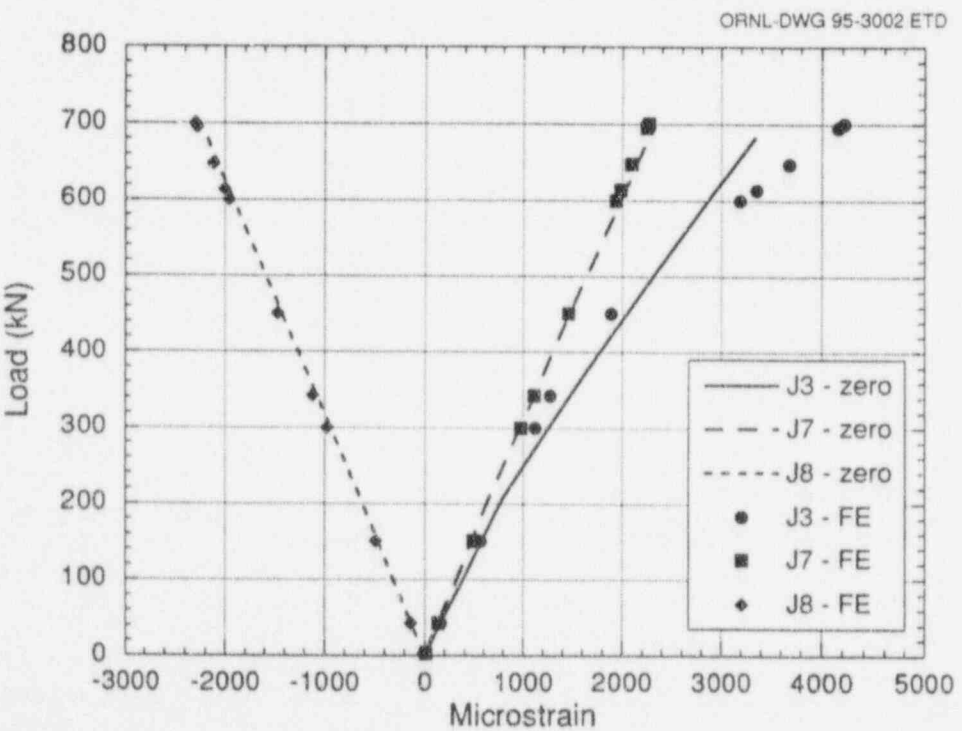

Figure 3.31 Comparison of calculated strains for DSR3 with the measured strains normalized to zero (for zero load)

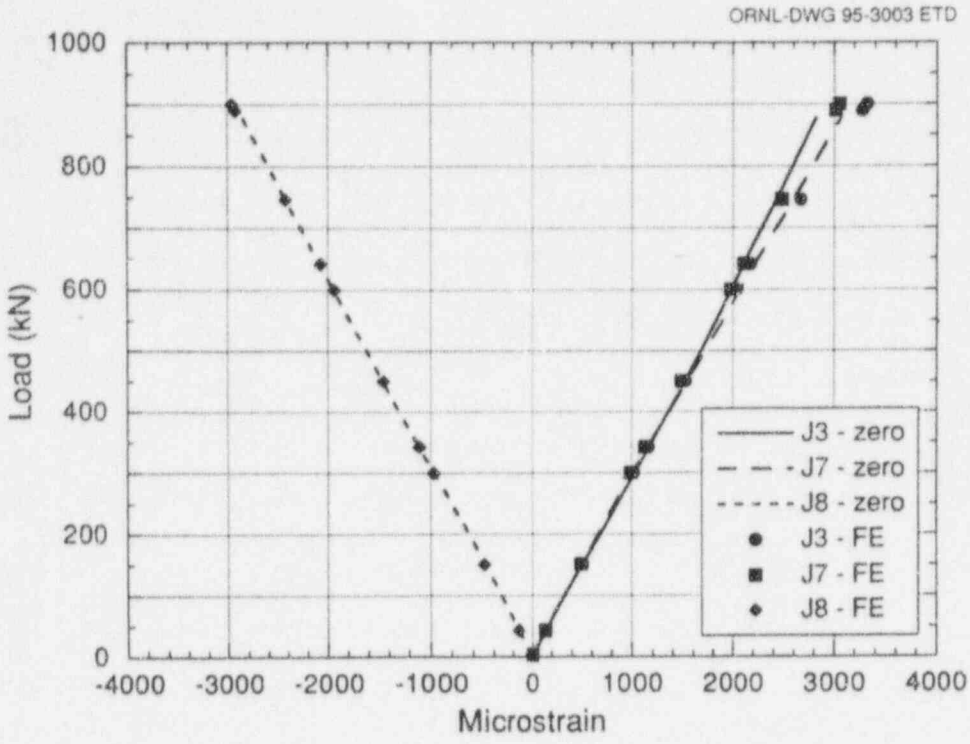

Figure 3.32 Comparison of calculated strains for DD2 with the measured strains normalized to zero (for zero load)

Results from the near-crack-tip analyses, which include comparisons of computed SIF with measured fracture toughness and evaluation of constraint parameters, will be included in the next reporting period.

References

1. "The American Society of Mechanical Engineers Boiler and Pressure Vessel Code," Section XI, "Rules for Inservice Inspection of Nuclear Power Plant Components," Appendix A, "Analysis of Flaws," Article A-4000, Material Properties, American Society of Mechanical Engineers, New York, 1989.*

2. "The American Society of Mechanical Engineers Boiler and Pressure Vessel Code," Section III, "Rules for Construction of Nuclear Power Plant Components," American Society of Mechanical Engineers, New York, 1989.*

3. Annual Book of ASTM Standards, Volume 03.01, American Society for Testing and Materials, Philadelphia, Pennsylvania, 1994.*

4. R. K. Nanstad, D. E. McCabe, R. L. Swain, and M. K. Miller, Martin Marietta Energy Systems, Inc., Oak Ridge National Laboratory, "Chemical Composition and RT_{NDT} Determinations for Midland Weld WF-70," USNRC Report NUREG/CR-5914 (ORNL-6740), December 1992.†

5. G. R. Irwin, "Linear Fracture Mechanics, Fracture Transition, and Fracture Control," *Eng. Fract. Mech.*, 1, 241–47 (1968).*

6. F. M. Haggag, "Small Specimen Test Techniques Applied to Nuclear Reactor Vessel Thermal Annealing and Plant Life Extension," *ASTM STP 1023*, ed. W. R. Corwin, F. M. Haggag, and W. L. Server, American Society for Testing and Materials, Philadelphia, 27–44 (1993).*

7. T. J. Theiss, Martin Marietta Energy Systems, Inc., Oak Ridge National Laboratory, "Specification for the Full-Thickness Clad Beam Fracture-Toughness Tests," Specification No. HSST-H10-92-001, Rev. 1, Jan. 13, 1992.‡

8. T. J. Theiss et al., Martin Marietta Energy Systems, Inc., Oak Ridge National Laboratory, "Initial Results of the Influence of Biaxial Loading on Fracture Toughness," USNRC Report NUREG/CR-6036 (ORNL/TM-12349), June 1993.†

9. B. R. Bass et al., Martin Marietta Energy Systems, Inc., Oak Ridge National Laboratory, "Biaxial Loading and Shallow-Flaw Effects on Crack-Tip Constraint and Fracture Toughness," USNRC Report NUREG/CR-6132 (ORNL/TM-12498), January 1994.†

10. T. J. Theiss, D. K. M. Shum, and S. T. Rolfe, Martin Marietta Energy Systems, Inc., Oak Ridge National Laboratory, "Experimental and Analytical Investigation of the Shallow-Flaw Effect in Reactor Pressure Vessels," USNRC Report NUREG/CR-5886 (ORNL/TM-12115), July 1992.†

11. R. E. Link and J. A. Joyce, "Experimental Investigation of Fracture Toughness Scaling Models," Constraint Effects in Fracture: Theory and Applications, *ASTM STP 1244*, ed. Mark Kirk and Ad Bakker, American Society for Testing and Materials, Philadelphia, 1994.*

12. J. A. Keeney et al., Martin Marietta Energy Systems, Inc., Oak Ridge National Laboratory, "Preliminary Assessment of the Fracture Behavior of Weld Material in Full-Thickness Clad Beams," USNRC Report NUREG/CR-6228 (ORNL/TM-12735), September 1994.†

13. *ABAQUS Theory Manual*, Version 5.2, Hibbit, Karlson and Sorensen, Inc., Providence, Rhode Island, 1992.‡

14. T. L. Dickson, "FAVOR: A New Fracture Mechanics Code for Reactor Pressure Vessels Subjected to Pressurized Thermal Shock," *PVP*-Vol. 250, *Pressure Vessel Integrity*, pp. 3–10, American Society of Mechanical Engineers (July 1993).*

15. D. Moinereau et al., "Cleavage Fracture of Plates with Small Underclad Crack: Elements Presentation and Interpretation by Fracture Mechanics," *PVP*-Vol. 213/*MPC*-Vol. 32, *Pressure Vessel Integrity*, American Society for Mechanical Engineers, 1991.*

16. D. Moinereau et al., "Cleavage Fracture of Specimens Containing an Underclad Crack," *PVP*-Vol. 223, *Pressure Vessel Fracture, Fatigue, and Life Management*, American Society for Mechanical Engineers, 1992.*

17. D. Moinereau et al., Behavior of Underclad Cracks in Reactor Pressure Vessels: Evaluation of Mechanical Analyses Used in French RPV Integrity Assessment by Cleavage Fracture Tests on Large Scale Plates, *PVP*-Vol. 250, *Pressure Vessel Integrity*, American Society for Mechanical Engineers, 1993.*

18. B. R. Bass and J. W. Bryson, Martin Marietta Energy Systems, Inc., Oak Ridge National Laboratory, "Applications of Energy Release Rate Techniques to Part-Through Cracks in Plates and Cylinders, Vol. 1, ORMGEN-3D: A Finite Element Mesh Generator for 3-Dimensional Crack Geometries," USNRC Report NUREG/CR-2997/V1 (ORNL/TM-8527), December 1982.†

---

*Available from public technical libraries.

†Available for purchase from the National Technical Information Service, Springfield, VA 22161.

‡Available for purchase from organization sponsoring the cited publication, and/or from authors, and/or recipients.

4 Ductile to Cleavage Fracture Mode Conversion

J. A. Keeney

4.1 Introduction

In the lower-to-upper transition regions of fracture toughness vs temperature behavior, RPV materials can exhibit considerable ductile flaw growth, followed by a fracture mode conversion to cleavage. The material failure by cleavage after some amount of ductile tearing can be regarded as a combined effect of a deterministic stable-tearing process (J-R curve) and a probabilistic cleavage process. Ignoring the presence of significant amounts of precleavage ductile tearing may lead to reduced accuracy in predicting cleavage initiation and resulting margins of safety. The fracture mode conversion model is needed to provide a comprehensive fracture prediction methodology for RPVs.

During this report period, work began on the characterization of precleavage tearing behavior and development of a fracture mode conversion model to take into account any precleavage ductile tearing in fracture predictions.

4.2 Metallurgical Investigations (R. K. Nanstad, D. J. Alexander, and M. C. Rao)

Metallurgical investigations are being carried out, based on existing test results, to describe the behavior of precleavage ductile tearing and mode conversion to cleavage. The physical factors involved in this phenomenon have to be taken into account in the development of a fracture mode conversion model. Also, different fractographic features are important depending on the model that is used, that is, void and inclusion volume fraction for void formation and coalescence models. The steps of this investigation will (1) identify potential sources of fracture surfaces relevant to precleavage ductile tearing (i.e., ORNL); (2) secure the fracture surfaces that are from sources other than ORNL; and (3) conduct examinations of the fracture surfaces. The initial metallurgical examination will (1) characterize the extent of crack-tip blunting prior to crack growth, (2) identify and characterize the microstructural features associated with microvoid formation and growth, (3) identify and characterize the microstructural features responsible for the mode conversion to cleavage, and (4) describe the relationship between the ductile crack morphology and the trigger points at mode conversion. The results from these investigations will be used in the development of the fracture mode conversion model.

The preliminary list of potential materials of interest to the evaluation of precleavage ductile tearing has been drafted and is now under review. The list includes plate and weld materials with relatively large data bases as well as those from some of the large structural test programs conducted within the HSST Program. The materials include

1. A 533 B from the HSST uniaxial shallow-flaw tests,
2. weld material from the NIST full-thickness clad beam tests,
3. HSSI weld 73W (unirradiated and irradiated),
4. Midland reactor beltline weld WF-70,
5. HSST Plate 13, and
6. A 508 Cl 3 used in the Material Property Council round robin.

Preliminary discussions were held with researchers at the University of California-Santa Barbara (UCSB) regarding fracture surface reconstruction with test specimens that exhibit stable ductile tearing prior to cleavage failure. UCSB has developed a hardware system, centered about a confocal microscope modified with precision x-y stages, for obtaining a digital record of the fracture surface in three dimensions. Software was also developed for processing and storage of the data, for assembly of the digital data from the conjugate surfaces, and for reconstruction of the fracture test at the submicron level. Specific fracture surfaces from previous tests performed under the HSST Program will be examined with the objective of evaluating the various metallurgical factors thought to contribute to the initiation of cleavage fracture when preceded by stable ductile tearing. These evaluations will include attempts to replicate fracture surfaces of irradiated specimens in the hot cell.

Discussions were held at NIST with Professors G. Irwin, W. Fourney, C. Schwartz, and X. Zhang (all from UM) to review the recent metallurgical studies of Prof. Irwin concerning the relationship of cleavage initiation to small-scale nonuniformities in the microstructure of pressure vessel steels. In his review, Prof. Irwin discussed the relevance of microstructural features that include carbide banding, prior-austenite grain size, ferrite grain size, carbide clusters, and carbide "clumps." He observed that the stress elevation necessary to produce a rigid-cleavage response in RPV material can be produced only with the aid of extremely high local strain rates. Furthermore, elevation of macro-scale tension by factors such as temperature reduction, constraint, and increased loading speed can increase the

chance and magnitude of a local region strain rate high enough to produce a cleavage response. The relevance of these microstructure metallurgical features to cleavage initiation and to existing analytical models of crack-tip constraint will be addressed in a letter report currently under preparation at UM.

4.3 Fracture Mode Conversion Model Development (J. A. Keeney, B. R. Bass, and J. G. Merkle)

Development of a fracture mode conversion model will be initiated in conjunction with the information obtained from the metallurgical investigations. The fracture mode conversion model will be used to predict ductile tearing preceding a cleavage crack initiation in the transition-toughness region. In developing the model, the following factors will be considered: (1) mode conversion due to an increase in stress triaxiality with crack extension (leading to a higher degree of constraint that may cause cleavage initiation) and (2) breaking of any ductile ligaments behind the advancing crack front leading to strain-rate sensitivity (i.e., rate-dependent plasticity). Initially, the following items will be considered in the model development: (1) geometry changes resulting from crack tearing extension, (2) effects of work hardening of the crack-tip modeling prior to crack resharpening, (3) void formation and coalescence models, (4) crack advance model based upon the Dodds J-R approach, (5) development of an analytical technique that would permit an "adequately refined" crack-tip model to propagate though the material with the crack-tip, and (6) cleavage conversion criteria.

Currently, a literature survey is being performed to identify the models that are available, and the information (physical features and fracture and mechanical data) needed to implement them. The results and conclusions from the literature search will be presented in a letter report* in the next report period.

Discussions were held with nuclear industry researchers at Framatome, Paris-La Defense, France, and at AEA Technology, Risley, United Kingdom, concerning (1) the French/U.K. four-party cooperative program for validation of the local approach to fracture and (2) the development of fracture models for the transition toughness region by the HSST Program. Discussions with the four-party participants focused in part on ORNL acquisition of the French/U.K. data base generated for validation of local approach models. A comprehensive report on the data base (identified as the "Synthesis Report") is being developed by EdF and will be provided to the HSST Program when completed.

Reference

1. G. R. Irwin, X. J. Zhang, and C. W. Schwartz, University of Maryland for Martin Marietta Energy Systems, Inc., Oak Ridge National Laboratory, *Small Scale Nonuniformities Related to Cleavage Initiation and Their Implications for Constraints Modeling*, USNRC Letter Report, ORNL/NRC/LTR-94/18, June 1994.†

*B. R. Bass and J. A. Keeney, Martin Marietta Energy Systems, Inc., Oak Ridge National Laboratory, "Development of Ductile Tearing-to-Cleavage Fracture-Mode Conversion Models for Reactor Pressure Vessel Steels," USNRC Letter Report ORNL/NRC/LTR-94/30 to be published.

†Available in NRC PDR for inspection and copying for a fee.

5 Fracture Analysis Methods Development and Applications

T. L. Dickson

5.1 Stress Intensity Factor Influence Coefficients

An NRC letter report entitled, *Stress-Intensity-Factor Influence Coefficients for Axially Oriented Semielliptical Inner-Surface Flaws in Clad Reactor Pressure Vessels (R_i/t =10)*, was published and distributed.[1] In this report, stress-intensity factor influence coefficients (SIFICs) are presented for axially oriented, finite-length, semielliptical inner-surface flaws with aspect ratios [total crack length (2c) to crack depth (a)] of 2, 6, and 10 in clad cylinders having an internal radius (R_i) to wall thickness (t) ratio of 10. The SIFICs are computed for flaw depths in the range of $0.01 < a/t < 0.5$ with particular emphasis on shallow flaws ($a/t < 0.1$) and cladding. SIFICs are also computed for two cladding thicknesses [t_{clad} = 3.96 mm (0.156 in.) and t_{clad} = 6.35 mm (0.25 in.)].

Work was completed on generating SIFICs for circumferentially oriented, finite-length, semielliptical inner surface flaws with aspect ratios [total crack length (2c) to crack depth (a)] of 2, 6, and 10 in clad cylinders having an internal radius (R_i) to wall thickness (t) ratio of 10. The SIFICs for the circumferential flaws are nearly identical to those generated for the companion axially oriented semielliptical flaws, particularly for the more shallow flaw depths. A letter report is currently being prepared that presents SIFICs for circumferentially oriented, finite-length, semielliptical inner-surface flaws. The report includes the recommendation that SIFICs for axially oriented, finite-length flaws may also be used for circumferential flaws for flaw depths up to 30% of the wall thickness without an appreciable loss of accuracy.

ABAQUS, a NQA-1 general finite-element code[2] with fracture mechanics capabilities, was used to generate the current data base of SIFICs for axially and circumferentially oriented finite-length flaws. ABAQUS had previously been used to generate SIFICs for infinite-length axial and continuous circumferential flaws in vessels with an internal radius (R_i) to wall thickness (t) ratio of 10.

The generation of SIFICs for axially and circumferentially oriented flaws of various aspect ratios (2, 6, 10, and infinity) for clad cylinders having an internal radius (R_i) to wall thickness (t) ratio of 10 described previously is a significant first step of a continuing task. This ongoing task has the objective of developing a comprehensive data base of accurate SIFICs for a range of axially and circumferentially oriented, inner surface flaw geometries for a range of clad vessel geometries that will envelope the commercial PWR and boiling-water reactor (BWR) vessel geometries in the United States. The incorporation of this SIFIC data base and interpolative routines into fracture analysis codes such as FAVOR will facilitate the generation of accurate fracture mechanics solutions as may be required in structural integrity assessments of any U.S. PWR or BWR vessel geometry. It is anticipated that the current SIFIC data base will be expanded in the future to include clad cylinders having an internal radius (R_i) to wall thickness (t) ratio of 15 and 20.

5.2 FAVOR

An NRC letter report entitled *FAVOR—A Fracture Analysis Code for Nuclear Reactor Pressure Vessels* was published.[3] This letter report serves as the user manual for the 9401 release of the FAVOR (Fracture Analysis of Vessels: Oak Ridge) computer code. In compliance with the current regulatory criteria, FAVOR performs vessel integrity analyses of embrittled RPVs subjected to PTS transient conditions. The 9401 release of FAVOR is limited to infinite-length axial and continuous circumferential flaw geometries. This is the initial distribution of the FAVOR code. The letter report and the code (executable files that will run on a 486 PC) were distributed to several domestic commercial and research organizations active in the field of nuclear RPV integrity assessment. An objective of releasing FAVOR at this time is to solicit critical feedback from a community of people familiar with performing fracture analyses of nuclear RPVs.

A future release of FAVOR, currently under development, includes the implementation of SIFICs for axially and circumferentially oriented, finite-length, semielliptical inner surface flaws (aspect ratios of 2, 6, and 10) for clad RPVs with an internal radius to wall thickness ratio of 10. This vessel geometry corresponds to a high percentage of the commercial PWR vessels operating in the United States.

The development version of FAVOR calculates the SIF (K_I) and the fracture initiation toughness (K_{Ic}) at ten angular locations around the semielliptical crack front at each transient time step for each flaw depth. The FAVOR solutions that utilize the SIFIC data base and superposition methods provide SIFs that are within 1 to 2% of direct

ABAQUS 3-D finite-element solutions. The K_{Ic} variation around the crack front due to both the through wall temperature and embrittlement variation is accounted for. K_I and K_{Ic} are calculated at 0°, which corresponds to the inner surface of the vessel, and at 90°, which corresponds to the deepest point of the flaw. K_I and K_{Ic} are also calculated at each 10° elliptical angle increment between the inner surface and the deepest point of the flaw. Cleavage fracture is predicted when K_I/K_{Ic} (K-ratio) ≥ 1.0 at any of the angular positions around the crack front. The angular location on the crack front of a semielliptical flaw that has the maximum K-ratio (and which would be the location of initiation in cleavage) varies with flaw depth, transient time, and embrittlement level. The inclusion of this consideration to a Monte Carlo probabilistic fracture analysis adds a level of complexity. This consideration, along with some other subtle, yet fundamental considerations, is currently being addressed in the implementation of finite flaw capability into FAVOR.

Some fracture analysis results recently generated with the development version of FAVOR are discussed below. These results are from deterministic and probabilistic fracture mechanics (PFM) analyses of a prototypical commercial U.S. PWR vessel geometry (internal radius of 86 in., wall thickness of 8.5 in., and clad thickness of 0.156 in.) subjected to the calculational reference transient used in the NRC/Electric Power Research Institute (EPRI) PTS benchmark exercise;* that is, a constant pressure of 1.0 ksi, a stylized exponential decay thermal transient with an initial coolant temperature of 550°F, a final coolant temperature of 150°F, a decay constant of 0.15, and a constant heat transfer coefficient of 500 BTU/h-ft^2-°F.

Figure 5.1 illustrates the variation of the angular location around the crack front at which the maximum K_I/K_{Ic} (K-ratio) occurs as a function of transient time for different levels of embrittlement. This particular plot is for a semi-elliptical inner surface flaw with an aspect ratio of 6 with a depth that is 10% of the wall thickness (a = 0.85 in.). RT_{NDTs} is the value of RT_{NDT} at the inner surface of the vessel as calculated by Regulatory Guide 1.99, Rev. 2 (Ref. 4), +2σ of 59°F. The various levels of RT_{NDTs} are calculated by varying the level of neutron fluence while holding copper and nickel at constant values of 0.23 and 0.73 wt %, respectively.

*B. A. Bishop, Draft for Review: Benchmarking of Probabilistic Fracture Mechanics Analyses of Reactor Vessels Subjected to Pressurized Thermal Shock (PTS) Loading, EPRI Research Project 2975-5, March 1993.

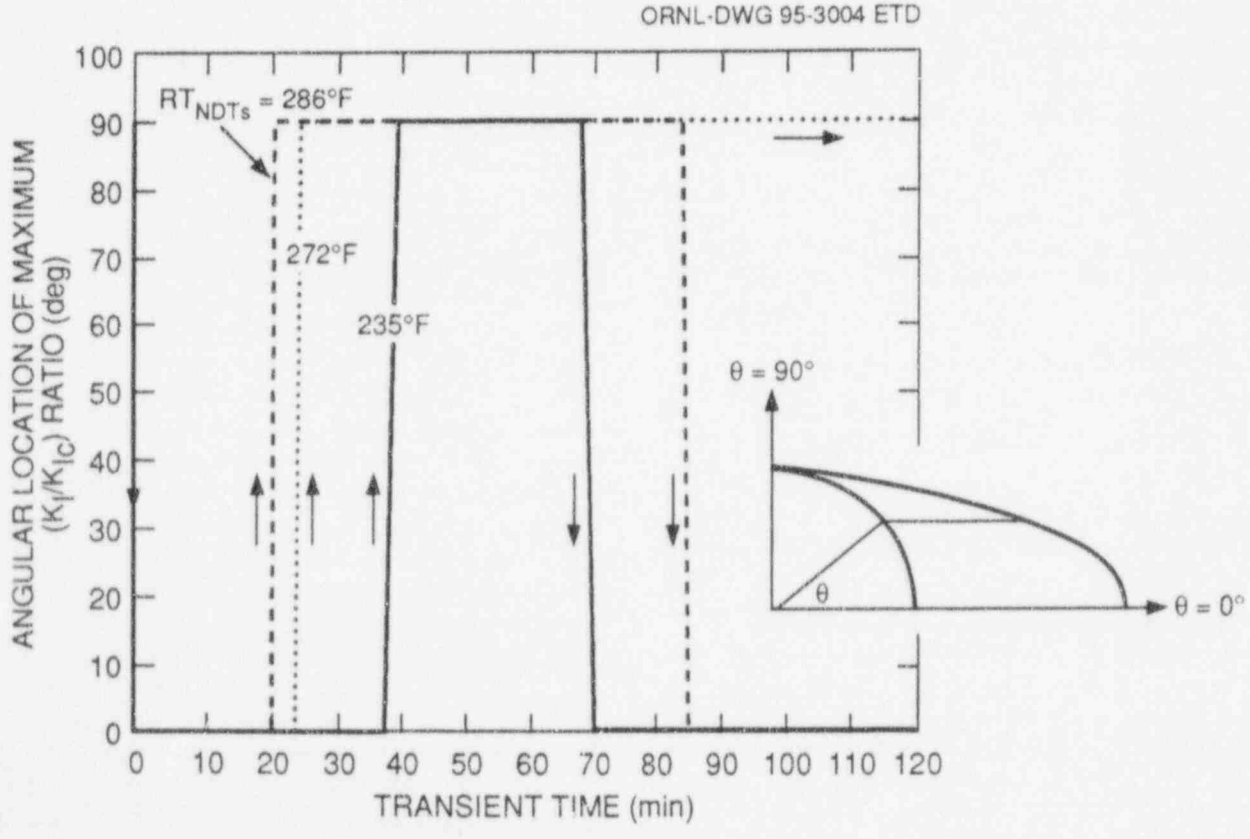

Figure 5.1 Angular location of maximum K ratio for 6:1 flaw of depth a/W = 0.1 varies as a function of transient time and inner surface RT_{NDT}

For all values of RT_{NDTs}, at time = 0 when the load is pressure induced, the maximum K-ratio occurs at the deepest point of the flaw (angular location of 90°). Very early in the transient, the location of the maximum K-ratio moves to the inner surface (angular location of 0°). For RT_{NDTs} = 235°F, at a transient time of 37 min, the angular location of the maximum K-ratio moves back to the deepest point and remains there until 70 min, when it moves back to the surface for the remainder of the transient. For RT_{NDTs} = 272°F, the maximum K-ratio moves from the inner surface to the deepest point at 24 min and stays there for the remainder of the transient. For RT_{NDTs} = 286°F, at a transient time of 20 min, the angular location of the maximum K-ratio moves from the inner surface to the deepest point and remains there until 85 min, at which time it moves back to the surface where it remains for the remainder of the transient.

Figure 5.2 illustrates that the angular location around the crack front at which the maximum K_I/K_{Ic} ratio occurs varies as a function of both crack depth and transient time for a specific embrittlement level. In this particular case, RT_{NDTs} = 272°F, including +2σ of 59°F.

From the sampling of transient conditions examined thus far, the fact that the location on the crack front at which cleavage fracture would occur varies with flaw depth, transient time, and embrittlement level, seems to be particularly true for a flaw with an aspect ratio of 6. In the case of a flaw with an aspect ratio of 2, it appears that the maximum K_I/K_{Ic} ratio always occurs at the surface. For the case of a flaw with an aspect ratio of 10, it appears that the K_I/K_{Ic} ratio occurs at the deepest point for most flaw depths, transient times, and embrittlement levels.

Figure 5.3 illustrates incipient RT_{NDTs} (the minimum value of RT_{NDTs} at which cleavage fracture is predicted) for axially oriented flaws as a function of flaw aspect ratio for various flaw depths. Again, all analysis results are for the severe PTS benchmark transient. There are four data points for each flaw depth; aspect ratios of 2, 6, and 10; and infinite-length flaws. In Fig. 5.3, the aspect ratio of 99 corresponds to an infinite-length flaw. For shallow flaws, the incipient RT_{NDTs} varies inversely with aspect ratio. For increasing flaw depths, the incipient RT_{NDTs} varies directly with flaw aspect ratio; that is, finite flaws would initiate in cleavage earlier in the vessel life than would an infinite flaw.

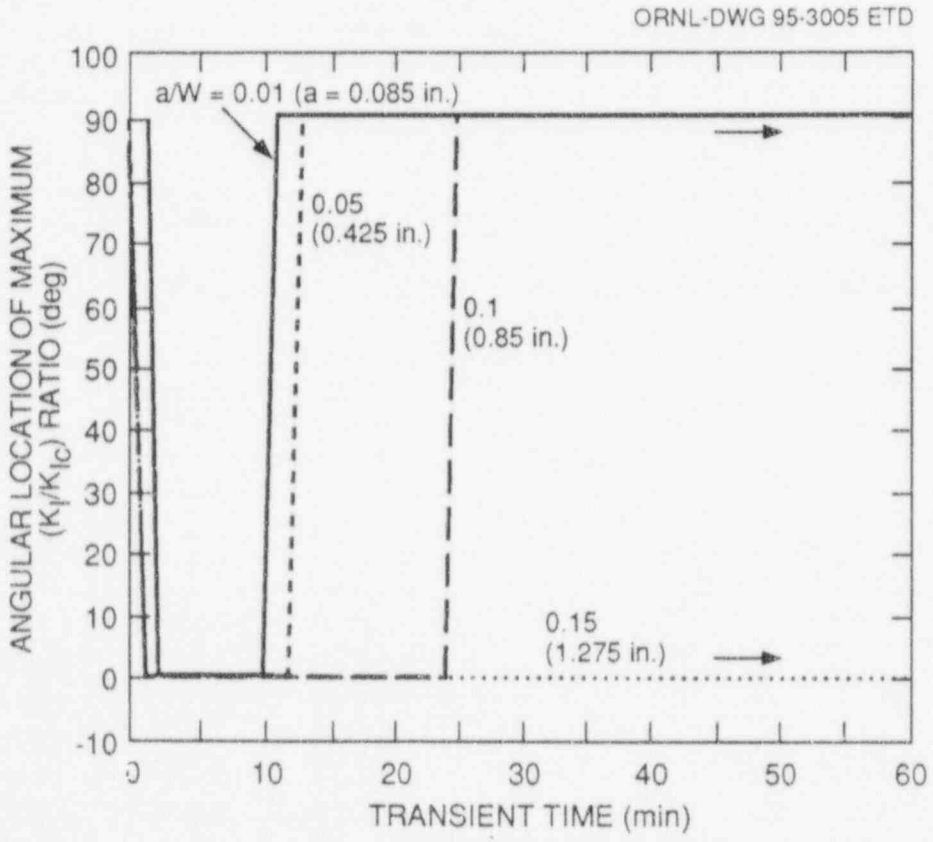

Figure 5.2 Angular location of maximum K-ratio for 6:1 flaw at RT_{NDTs} = 272°F varies as a function of transient time and flaw depth

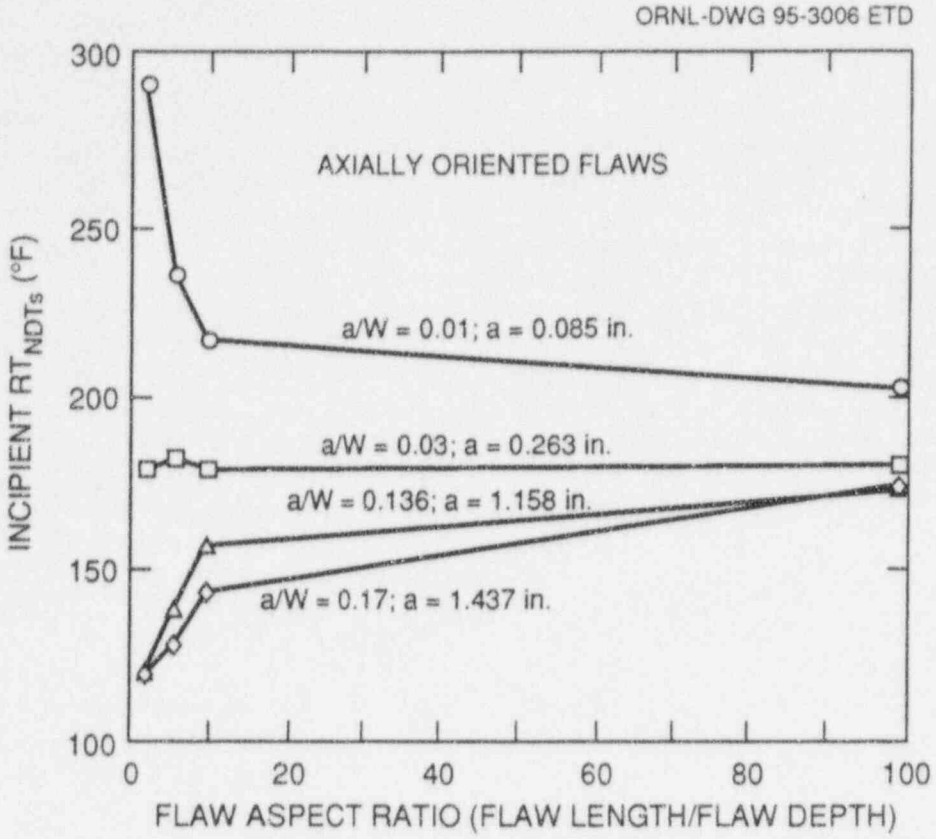

Figure 5.3 Incipient RT_{NDTs} as a function of flaw geometry for various flaw depths

Figure 5.4 illustrates the conditional probability of failure, designated as P(FIE), generated by the development version of FAVOR for axially and circumferentially oriented flaws of various aspect ratios. Again, these results were generated using the calculational reference transient used in the NRC/EPRI PTS benchmark exercise. As illustrated, for this particular analysis, P(FIE) is proportional to the flaw aspect ratio. There is approximately a factor of 2 between the two extreme cases; that is, P(FIE) for a flaw with an aspect ratio of 2 is approximately half the value for those with an infinite aspect ratio.

Also, an option has been included in the FAVOR code to probabilistically simulate the flaw aspect ratio from a uniform distribution of the available flaw aspect ratios; that is, each flaw has equal probability of having an aspect ratio of 2, 6, 10, and infinity. The values of P(FIE) obtained from these analyses correspond very closely to those values of P(FIE) for a flaw with an aspect ratio of 10.

In the PFM analyses discussed previously, the flaw density was assumed to be constant and equal to one flaw per cubic meter. The volumes of the axial and circumferential welds were assumed to be 0.028 and 0.099 m^3 (1 and 3.5 ft^3), respectively. In these PFM analyses, an initiated flaw is considered to become an infinite-length flaw, that is, the SIFs for infinite-length flaws were used in checking for crack arrest and reinitiation.

5.3 NRC Support

5.3.1 Dynamic Effects on PTS Analyses

Reactor vendor analyses and publications[5–8] have suggested that the static equilibrium description of cleavage fracture could be overly conservative with regard to predicting postcleavage events such as crack arrest and reinitiation. The static equilibrium method has traditionally been used when performing vessel fracture analyses and is the method currently incorporated in the FAVOR code. One vendor publication[5] presented an example case in which incorporating dynamic effects into the PFM analysis reduced the conditional probability of failure of an RPV subjected to a PTS by over an order of magnitude.

At the request of the NRC, analyses were performed to assess the potential impact that the inclusion of dynamic effects could have on the results of a PFM analysis of a RPV subjected to a PTS transient. From these analyses, it was concluded that the impact of the inclusion of dynamic

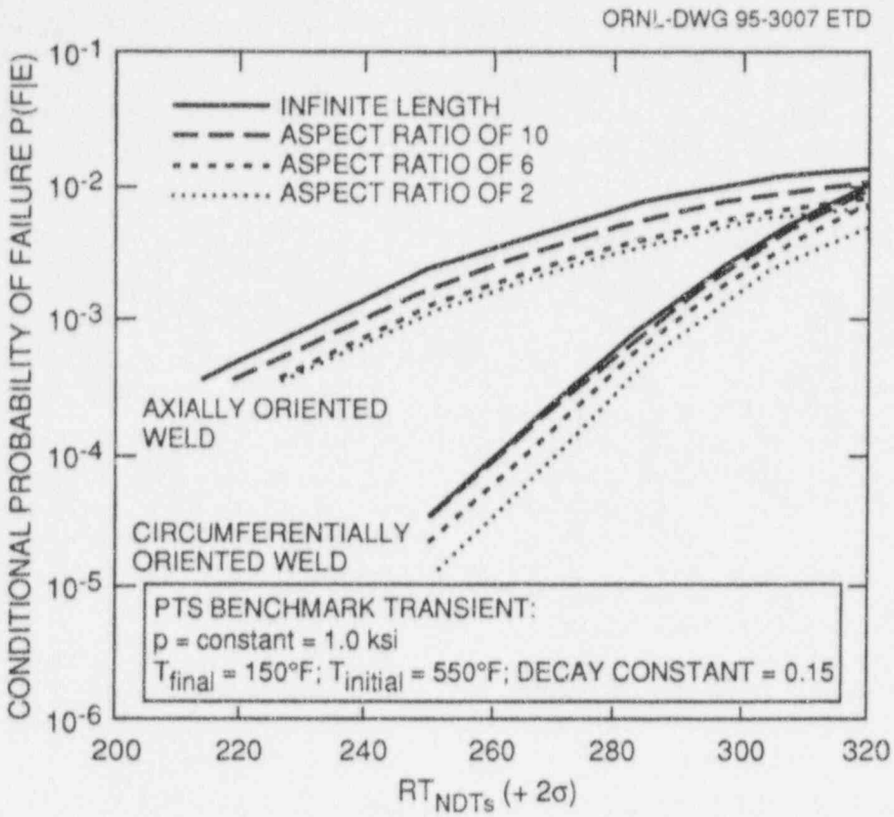

Figure 5.4 Conditional probability of failure as a function of flaw geometry

effects on a PTS analysis is largely transient dependent. The synergism of dynamic effects and thermal transients with a reheat phase considerably increases the chance that a propagating flaw will arrest and not reinitiate, potentially reducing the conditional probability of failure between 1 and 2 orders of magnitude. For those thermal transients without a reheat phase, the reduction is approximately a factor of 2. A survey of the plants analyzed in the Integrated Pressurized-Thermal-Shock studies[9–11] determined that PTS events with a reheat phase accounted for a small percentage of the total frequency of vessel failure. Therefore, the inclusion of dynamic effects would not likely have a significant impact on the frequency of vessel failure in a Regulatory Guide 1.154 (Ref. 12) PTS analysis.

A presentation entitled *Impact of Dynamic Crack Arrest on Probabilistic Fracture Analyses* was given to NRC personnel on October 19, 1993. This presentation documented the analyses assumptions, results, and conclusions. A letter report is currently being prepared with the same title as the presentation.

5.3.2 Technical Bases for Modifying Regulatory Guide 1.154

A proposed workscope was prepared detailing the computational efforts required to develop and document the technical bases for possible modifications to the current regulatory criteria in Regulatory Guide 1.154. The NRC objective is to publish by mid-1996 a revised Regulatory Guide 1.154 that reflects fracture technology developed in the last decade and lessons learned from the recent analysis of the Yankee Rowe nuclear plant.[13,14] The workscope proposed the following six major phases: (1) baseline analysis, (2) refinement of distribution functions, (3) refinement of fracture mechanics model, (4) reanalysis including refinements, (5) assessment, and (6) documentation. The proposed workscope also included identifying the interfaces and critical paths between various organizations, that is, HSST, Pacific Northwest Laboratory, and Sandia National Laboratory.

References

1. J. A. Keeney and T. L. Dickson, Martin Marietta Energy Systems, Inc., Oak Ridge National Laboratory, "Stress-Intensity-Factor Influence Coefficients for Axially Oriented Semielliptical Inner-Surface Flaws in Clad Reactor Pressure Vessels ($R_i/t = 10$)," ORNL/NRC/LTR-93/33, April 1994.*

2. *ABAQUS User Manual*, Hibbit, Karlsson & Sorenson, Inc., Providence, Rhode Island, 1991.

3. T. L. Dickson, Martin Marietta Energy Systems, Inc., Oak Ridge National Laboratory, "FAVOR—Release 9401, A Fracture Analysis Code for Nuclear Reactor Pressure Vessels," ORNL/NRC/LTR/94/1, February 1994.*

4. U.S. Nuclear Regulatory Commission, Regulatory Guide 1.99, "Radiation Embrittlement of Reactor Vessel Materials," Rev. 2, May 1988.†

5. D. S. Moelling et al., "Probabilistic Fracture Mechanics Application of Dynamic Crack Arrest by Static Analogy," *Pressure Vessel Integrity*, PVP-Vol. 213/MPC-Vol. 32, American Society of Mechanical Engineers, June 1991.‡

6. E. Smith and T. J. Griesbach, "Simulating the Effect of Pressure Plus Thermal Loadings on Crack Arrest During a Hypothetical Pressurized-Thermal-Shock Event," *Pressure Vessel Integrity*, PVP-Vol. 213/MPC-Vol. 32, pp. 41–46, American Society of Mechanical Engineers, 1991. ‡

7. D. J. Ayres et al., Combustion Engineering, Inc., "Tests and Analyses of Crack Arrest in Reactor Vessel Materials," Final Report, NP-5121M on EPRI Research Project 2180-3, April 1987.

8. R. J. Fabi and D. J. Ayres, Combustion Engineering, Inc., "Calculating Dynamic Crack Arrest by Static Analogy," Final Report, NP-6223 on EPRI Research Project 2455-14, March 1989.

9. D. L. Selby et al., Martin Marietta Energy Systems, Inc., Oak Ridge National Laboratory, "Pressurized-Thermal Shock Evaluation of the H. B. Robinson Nuclear Power Plant," USNRC Report NUREG/CR-4183 (ORNL/TM-95657/Vol. 1), September 1985.**

10. D. L. Selby et al., Martin Marietta Energy Systems, Inc., Oak Ridge National Laboratory, "Pressurized-Thermal Shock Evaluation of the Calvert Cliffs Nuclear Power Plant," USNRC Report NUREG/CR-4022 (ORNL/TM-9408), September 1985.**

11. T. J. Burns et al., Martin Marietta Energy Systems, Inc., Oak Ridge National Laboratory, "Preliminary Development of an Integrated Approach to the Evaluation of Pressurized Thermal Shock as Applied to the Oconee 1 Nuclear Power Plant," USNRC Report NUREG/CR-3770 (ORNL/TM-9176), May 1986.**

12. U.S. Nuclear Regulatory Commission, Regulatory Guide 1.154, "Format and Content of Plant-Specific Pressurized Thermal Shock Safety Analysis Reports for Pressurized Water Reactors."†

13. T. L. Dickson and R. D. Cheverton, Martin Marietta Energy Systems, Inc., Oak Ridge National Laboratory, "Review of Reactor Pressure Vessel Evaluation Report for Yankee Rowe Nuclear Power Station (YAEC No. 1735)," Appendix D "ORNL Review of Probabilistic Fracture Mechanics," NUREG/CR-5799 (ORNL/TM-11982), March 1992.**

14. T. L. Dickson et al., Martin Marietta Energy Systems, Inc., Oak Ridge National Laboratory, "Pressurized Thermal Shock Probabilistic Fracture Mechanics Sensitivity Analysis for Yankee Rowe Reactor Pressure Vessel," NUREG/CR-5782 (ORNL/TM-11945), August 1993.**

---

*Available in NRC PDR for inspection and copying for a fee.
†Copies are available from U.S. Government Printing Office, Washington, D.C. 20402. ATTN: Regulatory Guide Account.
‡Available from public technical libraries.
**Available for purchase from the National Technical Information Service, Springfield, VA 22161.

6 Material Property Data and Test Methods

R. K. Nanstad

6.1 J-R Curve Evaluations on A 302 Grade B Steel (D. E. McCabe)

A previous study[1] with one particular heat of A 302 grade B steel that had low upper-shelf energy (USE) in the transverse (T-L) orientation showed decreasing J-R curve with increased specimen thickness. Compact specimens ranged in size from 1/2TC(T) to 6TC(T). The usual pattern for upper-shelf toughness trend with increased specimen thickness shows improved J-R curve.

Originally, the plan was to select four heats of A 302 grade B steel from materials that are in use in reactors; the steel was to be donated by the General Electric Company, San Jose, California. Instead of four heats, seven heats of modified A 302 grade B and one heat of vintage A 533 grade B were selected. The final plan included the development of J-R curves in three orientations, viz., T-L, L-T, and L-S, and three test temperatures, viz., 82, 204, and 288°C (180, 400, and 550°F). Four compact specimen sizes were used (1/2 T, 1T, 2T, and 4T). The total number of compact specimens in the test matrix was 233. Tensile tests and Charpy-V transition curves were also made in three orientations. Another supplementary test that was planned but not covered for all heats was the drop-weight NDT test.

Presently, all compact specimens with the exception of five 4T specimens have been tested. All heats have been tested for chemistries and examined metallographically. Charpy-V transition curves and tensile results at four temperatures have been generated.

A preliminary evaluation of these results indicates that all materials except for one heat of A 302 grade B met the minimum 102-J (75-ft-lb) USE (Table 6.1) required by 10CFR50 (Ref. 2). All 50% shear temperatures were below room temperature. However, the tests at 288°C (550°F) showed that some of these materials were strongly susceptible to strain aging. Also, it was noted that the large compact specimens cleaved at room temperature when opened after the R-curve tests had been completed. Preliminary data on one heat of A 302 grade E material was transmitted to NRC during this reporting period.* Another letter report is in preparation that will present data on all the heats in the experiment.

*D. E. McCabe, Oak Ridge National Laboratory, letter to S. N. M. Malik, U.S. Nuclear Regulatory Commission, "Example Data, Plate 27 of A 302 Grade Beta Development Task, HSST Program," December 1993.

Table 6.1 Preliminary material characterization data

		Charpy-V data (T–L)			Tensile data, transverse (MPa)					
		Temperature (°C)		USE	Room temperature			288°C		
Material code	Heat	41 J	Onset USE	(J)	Yield strength	Ultimate tensile strength	Elongation (%)	Yield strength	Ultimate tensile strength	Elongation (%)
Z1, Z2	B3990–2	–36	50	171	448	586	25.5	414	586	24.5
Z3	C1256–2	–18	60	115	469	620	23.0	427	607	25.0
Z4	C1290–2	–39	100	150	489	615	25.0	420	607	24.0
Z5	P2130–2	–28	65	129	338	538	26.5	372	551	26.5
Z6A	B5013–2	–27	65	153	427	558	28.5	386	558	21.5
Z6B	C1079–1	–12	65	87	448	593	24.5	420	593	21.5
Z7	C2463–1	–29	100	130	469	634	24.5	427	620	23.4
Z8[a]	C2220–2	–3	115	130	427	600	13.0	379	586	8.0

[a]A 533 grade B class 1 steel.

6.2 Effects of Metallurgical Gradients in RPV Steels (R. K. Nanstad)

The literature review of metallurgical gradients in RPV steels continued. A letter report was prepared,[3] and the abstract follows:

> The Heavy-Section Steel Technology (HSST) Program at Oak Ridge National Laboratory includes an ongoing assessment of the margins in reactor pressure vessel (RPV) integrity analyses. Section XI of the ASME Code includes both K_{Ic} and K_{Ia} curves; the K_{Ia} curve is identical to the K_{IR} curve in Section III. Section XI of the ASME Code is referenced in 10CFR50. All three curves are related to a normalized temperature, $T - RT_{NDT}$, where the RT_{NDT} is determined using data from drop-weight and Charpy impact specimens. Because these fracture-toughness curves were constructed as lower bounds to the available data, statistical variations in material behavior were not considered. Furthermore, the data bases used for construction of the reference toughness curves were obtained from material in the central portions of the plates and forgings utilized. For some integrity analyses, consideration of shallow surface flaws is important. In this case, the flaw may reside in a region of the vessel where a substantial gradient in properties exists. As part of the margin assessment task, a review has been undertaken to evaluate the variability in fracture properties of typical RPV steels. This letter report provides a preliminary review of data related to the inhomogeneity of plates, forgings, and welds. The variations shown by plates and welds are quite similar, dependent on orientation effects due to fabrication practice. Variations in fracture toughness appear to be as great as those of Charpy impact toughness. Substantial gradients in properties may exist from near-surface to mid-thickness of base metals but can be quite variable with Charpy-V-notch (CVN) transition temperature differences from 0 to 85°C (0 to 153°F) noted.

6.3 Dynamic Fracture Toughness (R. K. Nanstad and B. R. Bass)

A specification, "Dynamic Fracture Initiation Toughness Testing of a Reactor Pressure Vessel Steel," for conduct of dynamic fracture toughness testing was prepared under Task H.2. Recommendations regarding material characterization testing were prepared for inclusion in that specification. The material characterization testing will include Charpy impact, tensile, drop-weight, and quasi-static fracture toughness testing. The specification will be used as the basis for a dynamic fracture-toughness testing subcontract.

References

1. A. L. Hiser and J. B. Terrel, "Size Effects on J-R Curves for A 302 B Plate," USNRC Report NUREG/CR-5265, November 1988.*

2. "Title 10," U.S. Code of Federal Regulations, Part 50, Appendix G, U.S. Government Printing Office, Washington, D.C., 1993.†

3. R. K. Nanstad, "Preliminary Review of Data Related to Inhomogeneity of Steels for Reactor Pressure Vessels," ORNL/NRC/LTR-93/36, December 30, 1993.‡

*Available for purchase from the National Technical Information Service, Springfield, VA 22161.

†Available from American National Standards Institute, 1430 Broadway, New York, NY 10018, copyrighted.

‡Available in NRC PDR for inspection and copying for a fee.

7 Integration of Results

J. G. Merkle

7.1 Effect of Assumed Yield Function on Calculated Plastic Strains and Displacements in Fracture Test Specimens (J. G. Merkle and J. W. Bryson)

7.1.1 Background

Recent experience has consistently shown that elastic-plastic finite-element analyses based on the actual measured uniaxial tensile stress-strain curve and the von Mises yield function tend to undercalculate the measured plastic strains and displacements near the crack plane in fracture test specimens.[1–3] In addition, in the case of the biaxial beam fracture specimens currently being tested by the HSST Program, the calculated ratio of CMOD to LLD is significantly less than the experimentally measured ratio. An earlier observation of a similar nature was made with respect to the pressure for through-thickness yielding in the cylindrical portions of the HSST Program Intermediate Test Vessels.[4] For these vessels, the average gross yield pressure of the cylinders was about 4% above the value calculated according to the Tresca (maximum shear stress) yield criterion rather than the theoretical 15% above that value predicted according to the von Mises (octahedral shear stress) yield criterion.[4]

Several possible causes of systematic differences between numerically calculated and measured plastic displacements have been examined without success. In the case of the biaxial beam fracture specimens, initial calculations were performed using finite-element models that employed isoparametric 20-node brick elements with reduced integration. These higher-order elements allow for quadratic variations in the element displacement field, and relatively few of them are generally required for accurate stress analysis. Reduced integration increases the flexibility of the element by eliminating "shear locking," which can occur with full integration for bending loading. More refined finite-element meshes utilizing these higher order elements did not improve the agreement between measured and computed plastic displacements. In addition, subsequent analyses employing highly refined models composed of first-order 8-node brick elements gave essentially the same results as those obtained with the 20-node elements.

At present the method being used to prevent undercalculation of CMOD is to lower the postyield portion of the stress-strain curve by about 10%. This percentage corresponds closely to the difference between the theoretical von Mises and experimentally measured ratios of cylinder gross yield pressures to the theoretical Tresca value mentioned above. However, since the unaltered stress-strain curve is known to be correct for uniaxial loading, this adjustment can result in an overcalculation of LLD, which depends mainly on uniaxial behavior, while improving the calculation of CMOD, which depends to a greater degree on multiaxial behavior. Consequently, there is reason to examine the other elements of the elastic-plastic analysis procedures in use to determine the real causes of the observed discrepancies between analysis and experiment.

7.1.2 Examination of Analytical and Experimental Trends

Five biaxial shallow-cracked beams have been tested at two different transverse stress ratios, 0:1 (uniaxial loading) and 0.6:1 (biaxial loading).[2,3] Three of these specimens, BB-2, 4, and 5, provide representative LLD and CMOD data.[3] A detailed study of these data reveals that the analytical and experimental curves of CMOD vs LLD appear to be affected in somewhat opposite ways by the transverse strain ratio.* As shown in Fig. 7.1, the experimental curves of CMOD vs LLD for a transverse stress ratio of 0.6:1 are higher than for a ratio of 0:1. However, the analytical curve for 0.6:1 is lower than the uniaxial curve, while the analytical curve for 1:1 is higher. The analytical curves imply a minimum in the CMOD at a given LLD, as a function of the transverse stress ratio, and the experimental data imply monotonically increasing values of CMOD, at a given LLD, as the transverse stress ratio increases. This discrepancy between analysis and experiment is not likely to be remedied by an adjustment of the uniaxial stress-strain curve because the discrepancy pertains to the effects of multiaxial stress, which are modeled by the yield and hardening criteria rather than by the stress-strain curve. Recalling that the gross yield pressures of the intermediate test vessel cylinders were actually closer to those predicted according to the Tresca yield criterion rather than those from the von Mises yield criterion, it was decided to investigate the differences in plastic strain and displacement ratios predicted according to the two yield criteria. In particular, it was desired to determine whether the strain and displacement ratios predicted according to the Tresca yield criterion might be in better accord with the experimental data. The investigation was pursued in three steps. First,

*D. K. M. Shum, "Interpretation of HSST Cruciform Specimen 3-D Analysis Results," letter to B. R. Bass, Oak Ridge National Laboratory, Oak Ridge, Tennessee, August 24, 1993.

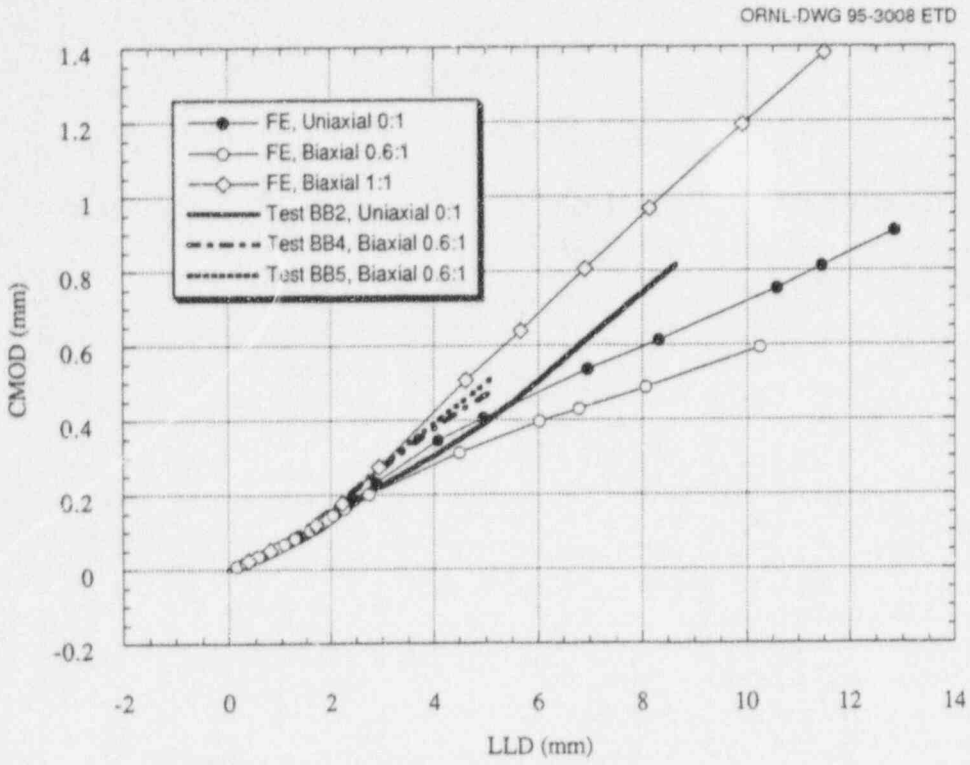

Figure 7.1 Biaxial shallow-flaw beam tests and analyses

published evidence was sought supporting the premise that at least the initial yield behavior of structural metals might be described as well or better by the Tresca yield criterion rather than by the von Mises yield criterion. This search was at least partially successful. Second, simplified analytical calculations were performed to compare the ratio of plastic to elastic strains in the direction of the maximum principal tensile stress, as a function of the biaxial transverse stress ratio, for the two yield criteria. The results of these calculations were interpreted by considering the plastic strain to be analogous to the CMOD and the elastic strain to be analogous to the LLD. Third, preliminary elastic-plastic plane strain calculations were performed for a uniaxially loaded shallow-cracked beam to investigate the P vs LLD, P vs CMOD, and CMOD vs LLD behavior calculated according to the two yield criteria, represented exactly or approximately, for in-plane (uniaxial) bending.

7.1.3 Published Evidence Concerning Yield Criteria

The yield criteria for steel and other metals are discussed by Hill in his book on the theory of plasticity,[5] from which an interesting but slightly ambiguous comparison emerges. The upper (initial) yield point of annealed mild steel is better described by the Tresca criterion than by the von Mises criterion.[5] However, Hill also states, "The yield criterion of von Mises has been shown to be in excellent agreement with experiment for many ductile metals, for example copper, nickel, aluminum, iron, cold-worked mild steel, medium carbon, and alloy steels."[5] The level of plastic strain at which the von Mises criterion was more accurate is not stated, but it seems possible that for steels with an initial yield point elongation, there may be a transition from one yield criterion to the other.

Hill[5] also discusses the elastic-ideally plastic analysis of a pressurized thick-walled hollow cylinder for which there is a closed form solution for the Tresca criterion, but not for the von Mises criterion. It is concluded (see p. 118 of Ref. 5) that a numerically accurate calculation for the von Mises criterion can be made by multiplying the value of the factor σ_Y in the Tresca solution by $2\sqrt{3}$. This result validates the comparison discussed earlier between the measured gross yield pressures for the intermediate test vessels and those calculated according to the Tresca and von Mises yield criteria.

Prager and Hodge[6] summarized the experimental and analytical aspects of yield criteria rather concisely. From the experimental perspective, probably considering the same data as Hill,[5] they stated,

> By and large, Mises' yield condition represents the yield limits of most structural metals at least as well as the condition of maximum shear stress . . . . Mises' yield condition is, therefore, generally adopted in the stress analysis of perfectly plastic

> bodies . . . . Actually, Mises' yield condition derives its importance in the mathematical theory of plasticity not from the fact that the invariant J_2 appearing therein can be interpreted physically in this or that manner, but from the fact that it has the simplest mathematical form compatible with the general postulates that any yield condition must fulfill. The fact that it is also in reasonably good agreement with the empirical evidence regarding the yielding of structural metals must be considered as fortuitous: even if this agreement had been less satisfactory, the mathematically simple yield condition would certainly have attracted the attention of those interested in the development of a general and yet workable theory of plasticity.[6]

The subsequently published book, *Plasticity and Creep of Metals*, by Lubahn and Felgar[7] contains a figure from a paper by Marin et al.,[8] which postdates the data considered in both Refs. 5 and 6, and is reproduced here as Fig. 7.2. This figure shows that the biaxial yield points for aluminum 75S-T6 lie between the Tresca and the von Mises curves, in general lying closer to the Tresca curve. A discussion on the same subject appears in a paper by Orowan,[9] which appraises the situation as follows:

> Experiments indicate that the behavior of metals with no sharp yield point, as a rule, is intermediate between the Tresca and Mises yield conditions, usually somewhat closer to the latter. For mathematical investigations of stress and strain distribution in plastically deformed bodies, the Mises condition is often simpler to handle. For materials with an upper and a lower yield point there is no reliable criterion for the onset of yielding at the upper yield point, since this quantity is extremely sensitive to slight non-uniformities of stress distribution and to the size of the specimen. As mentioned, however, the upper yield point is of little importance to the designer, since the allowable stress must be based on the lower yield point, which is the stress required for the first Lüders' bands to widen. From this it follows at once that the yield condition in this case cannot be the Mises condition. Since the Lüders' bands are sheared layers embedded between still rigid blocks

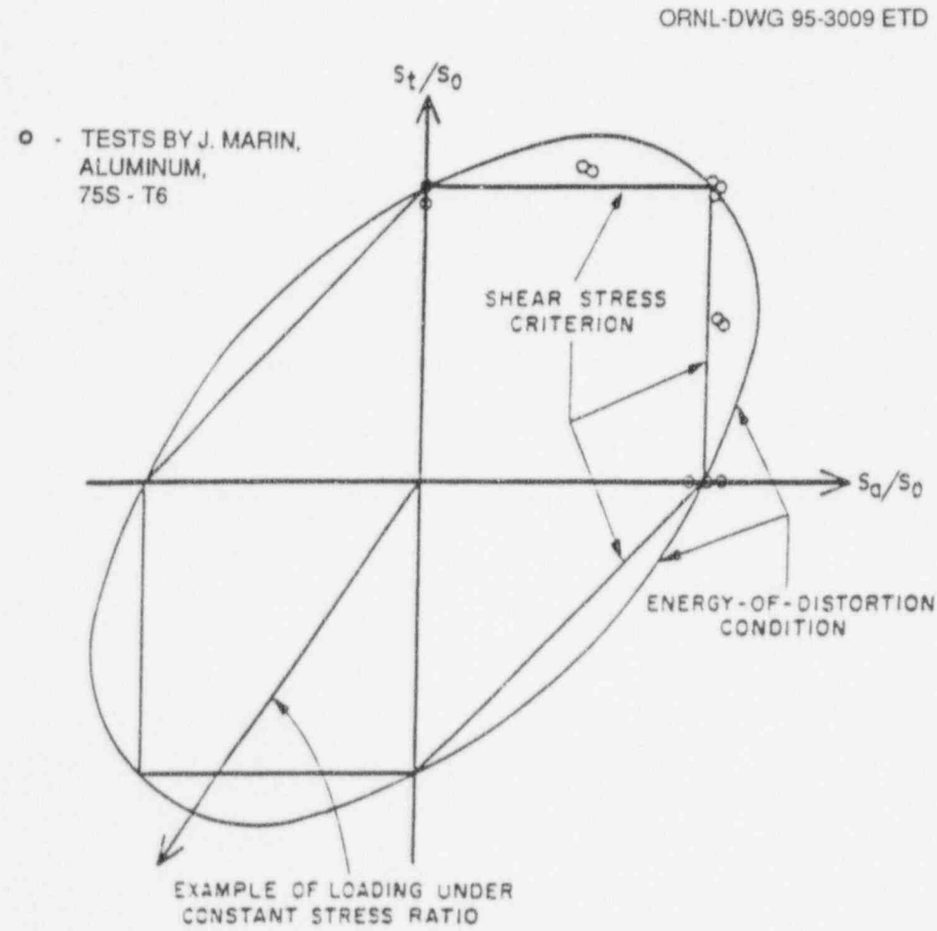

Figure 7.2 Biaxial yield curves for Tresca and von Mises yield criteria and experimental data for 75S-T6 aluminum

of the material, only the shear stress acting in their plane can cause them to become thicker, and the intermediate principal stress which is parallel to the Lüders' layer and perpendicular to the direction of shear in the layer must be ineffective. Consequently, the appropriate yield condition in this case must be closer to the Tresca condition.

It follows from the above discussions that there is ample reason to investigate the possibility that the accuracy of calculated plastic strains and displacements for cracked specimens near limit load might be improved by using a yield criterion equal to or approximating the Tresca yield criterion.

7.1.4 Analytical Calculations

Before performing comparative elastic-plastic finite-element calculations for cracked specimens with different yield criteria, simplified closed form calculations were performed for a unit element subjected to a biaxial state of stress. It was reasoned that only if a simple unit element displays different plastic strain trends for the two different yield criteria is a cracked specimen likely to do so. Plastic strain in the direction of the maximum principal tensile stress was considered analogous to CMOD, and the elastic strain in the same direction was considered analogous to LLD. An elastic-linear strain hardening material was assumed, for which the yield strain was assumed to be 0.2% and the tangent modulus of the effective stress-plastic strain curve was assumed to be five times the uniaxial yield stress. The maximum principal tensile stress was assumed to be 1.2 times the uniaxial yield stress, so that the states of stress for all biaxiality ratios satisfy both yield criteria. The ratio of plastic to elastic strain in the direction of σ_1 was calculated as a function of the biaxiality ratio, σ_2/σ_1, for both the Tresca and the von Mises yield criteria.

For the von Mises yield criterion, the plastic strain in the direction of σ_1 is given by

$$\varepsilon_1^P = \frac{\left(\frac{\sigma_1}{\sigma_Y}\right)}{H}\left[1 - \frac{1}{\left(\frac{\sigma_1}{\sigma_Y}\right)\sqrt{1 - \left(\frac{\sigma_2}{\sigma_1}\right) + \left(\frac{\sigma_2}{\sigma_1}\right)^2}}\right]\left[1 - \frac{1}{2}\left(\frac{\sigma_2}{\sigma_1}\right)\right] . \quad (7.1)$$

For the Tresca yield criterion, the same plastic strain is given by

$$\varepsilon_1^P = \frac{\frac{\sigma_1}{\sigma_Y} - 1}{H} . \quad (7.2)$$

In the latter case, ε_1^P is independent of the biaxiality ratio, σ_1/σ_Y. The elastic strain in the same direction is given by

$$\varepsilon_1^E = \varepsilon_Y\left(\frac{\sigma_1}{\sigma_Y}\right)\left[1 - \nu\left(\frac{\sigma_2}{\sigma_1}\right)\right] , \quad (7.3)$$

regardless of the yield criterion. Figure 7.3 shows that the ratios of plastic to elastic strain under biaxial loading calculated according to Eqs. (7.1–7.3) do follow different trends as the biaxiality ratio increases. The Tresca curve monotonically increases with increasing biaxiality ratio, as does the experimental value of CMOD vs LLD for a shallow-cracked specimen. On the other hand, the von Mises curve passes through a minimum at a biaxiality ratio of 0.5, in a fashion similar to the values of CMOD vs LLD for a shallow-cracked specimen, calculated according to the von Mises yield criterion. These results indicate that a numerical investigation of the effects of the yield criterion on the variation of CMOD and LLD with biaxiality ratio is worthwhile.

7.1.5 Finite-Element Calculations

The elastic-plastic finite-element stress analysis program currently in use by the HSST Program is ABAQUS.[10] The ABAQUS program does not have a Tresca yield criterion option for metal plasticity. However, it does have a smoothed Mohr-Coulomb (SMC) yield surface option for analyzing granular and polymeric materials, and this criterion appears adaptable to metal plasticity analysis by setting the angle of internal friction, β, and a normality angle, ψ, both equal to zero. One other parameter, K, which determines the cross-sectional shape of the yield surface, takes values between 1.0 and 0.8; K = 1 corresponds to the circular von Mises yield surface, and K = 0.8 corresponds to a rounded polygon lying tangent to the von Mises circle at its rounded vertices and otherwise lying within the circle. All the intricacies of the approximate relationship between the SMC yield surface and the Tresca yield surface have not yet been fully explored mathematically. Nevertheless, it has been assumed that because of the most salient feature of the SMC yield surface, namely that it lies tangent to or within the von Mises circle, the SMC yield surface should lead to results indicative of those that would be obtained with a Tresca yield surface if programming for the latter were available.

Two-dimensional, plane strain calculations were performed with the ABAQUS[10] program for an elastic-plastic

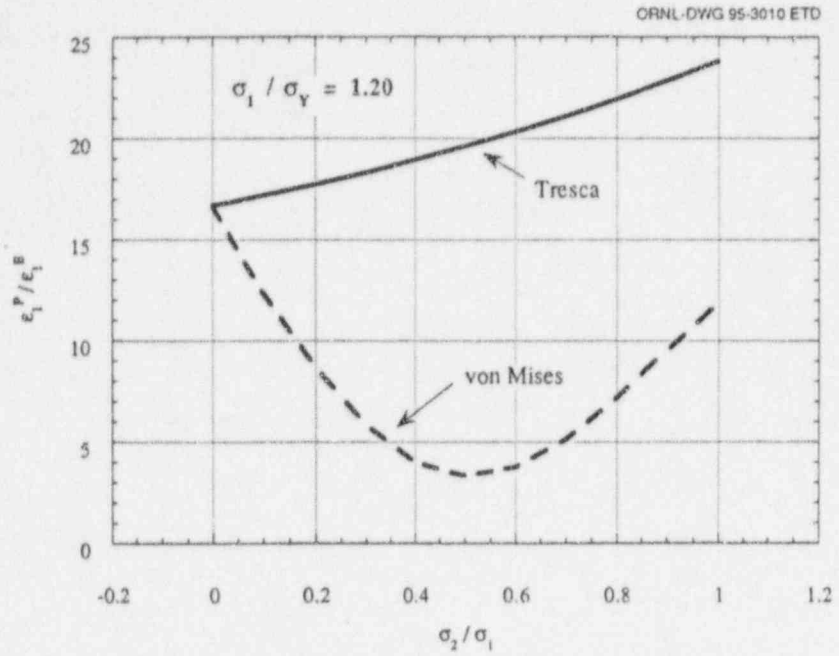

Figure 7.3 Curves showing ratio of plastic to elastic maximum principal tensile strain for Tresca and von Mises yield criteria as functions of stress biaxiality ratio

four-point loaded simply supported shallow-cracked beam of unit thickness. The beam dimensions were height, W = 10.16 cm (4 in.); outer span, S_1 = 60.96 cm (24 in.); and inner span, S_2 = 10.16 cm (4 in.). The crack depth to beam height ratio, a/W, was 0.10. The elastic and plastic uniaxial stress-strain properties in compression were assumed to be the same as the posttest tensile properties for HSST A 533 B plate WP-CE, as given in Fig. 40 of Ref. 2. Results are shown in Figs. 7.4–7.6. As shown in Figs. 7.4 and 7.5, the plastic portions of the LLD and CMOD, at a given load, increase as the yield surface shape deviation parameter K decreases between 1.0 and 0.8. However, as shown in Fig. 7.6, the relationship between CMOD and LLD remains nearly invariant for plane strain. These preliminary results indicate only the effects of the yield surface lying inside the von Mises yield surface at some stress states. The effects of biaxial loading have not been determined here because these are only 2-D plane strain analyses. Further investigations using 3-D analysis are deemed to be worthwhile for examining the effects of interactions between the yield function and biaxial loading.

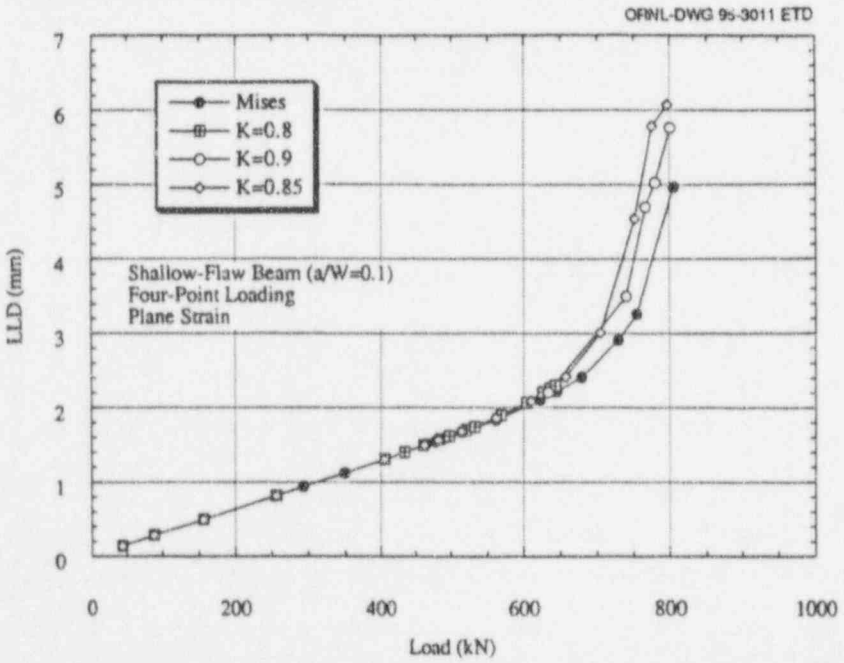

Figure 7.4 LLD response as function of load for different values of yield surface shape deviation parameter K

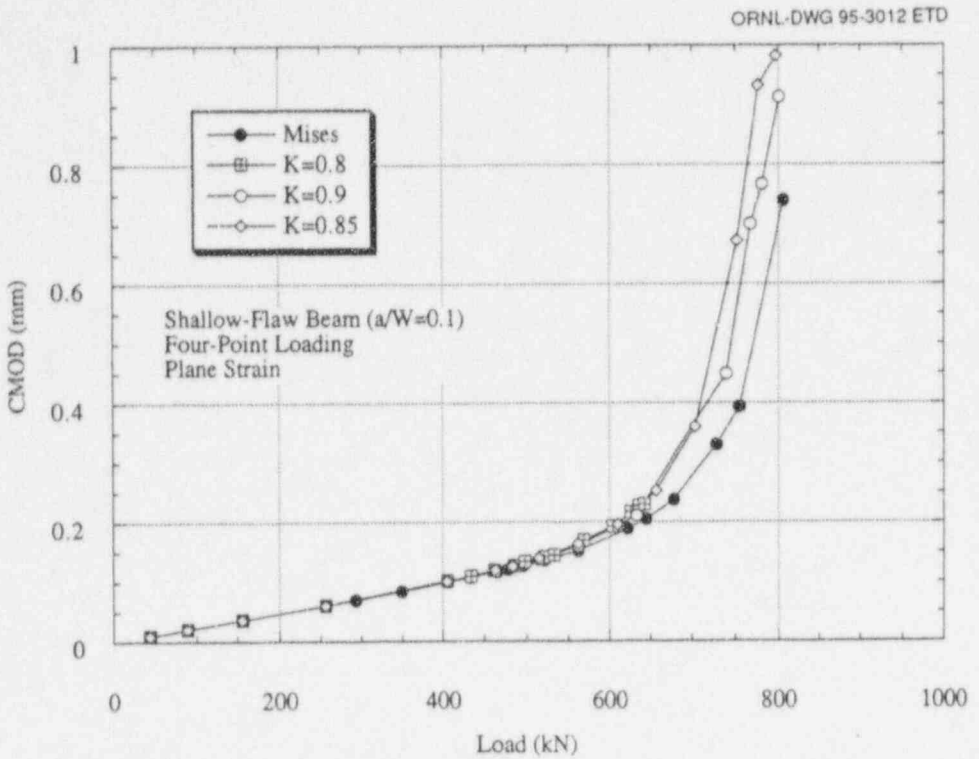

Figure 7.5 CMOD response as function of load for different values of yield surface shape deviation parameter K

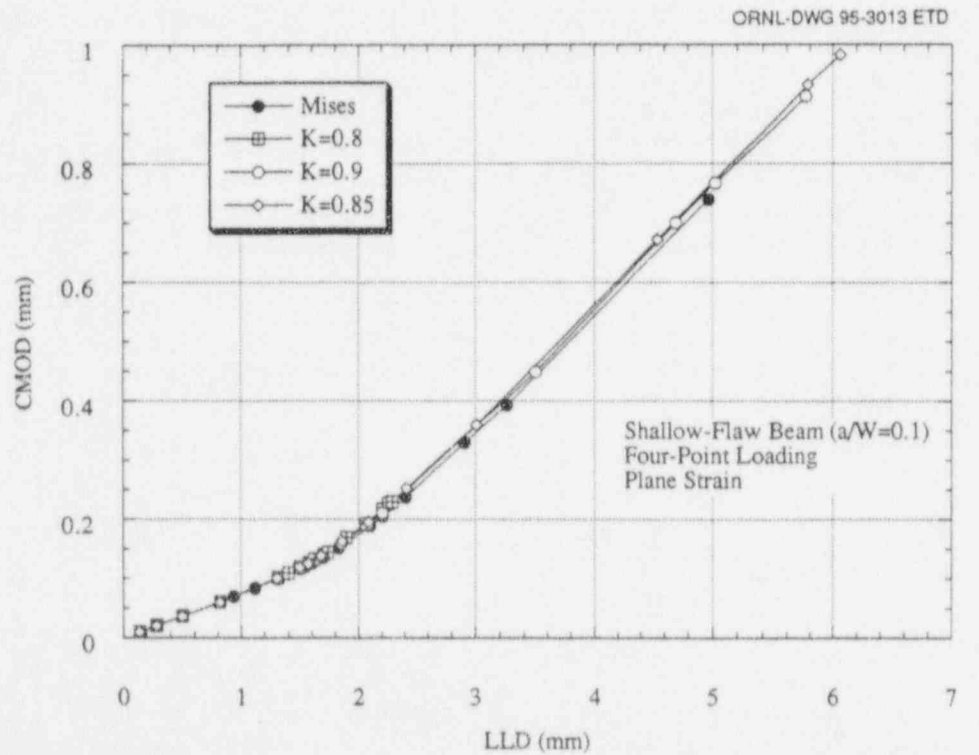

Figure 7.6 Relationship between CMOD and LLD for different values of yield surface shape deviation parameter K that remains nearly invariant

References

1. T. J. Theiss, D. K. M. Shum, and S. T. Rolfe, Martin Marietta Energy Systems, Inc., Oak Ridge National Laboratory, "Experimental and Analytical Investigation of the Shallow-Flaw Effect in Reactor Pressure Vessels," USNRC Report NUREG/CR-5886, July 1992.*

2. T. J. Theiss et al., Martin Marietta Energy Systems, Inc., Oak Ridge National Laboratory, "Initial Results of the Influence of Biaxial Loading on Fracture Toughness," USNRC Report NUREG/CR-6036, June 1993.*

3. B. R. Bass et al., Martin Marietta Energy Systems, Inc., Oak Ridge National Laboratory, "Biaxial Loading and Shallow-Flaw Effects on Crack-Tip Constraint and Fracture Toughness," USNRC Report NUREG/CR-6132, January 1994.*

4. J. G. Merkle, "An Approximate Method of Elastic-Plastic Fracture Analysis for Nozzle Corner Cracks," pp. 674–702 in *ASTM STP 668*, American Society for Testing and Materials, 1979.†

5. R. Hill, *The Mathematical Theory of Plasticity*, Oxford Press, 1950, pp. 22–23.

6. W. Prager and P. G. Hodge, Jr., *Theory of Perfectly Plastic Solids*, Dover Publications, 1968.

7. J. D. Lubahn and R. P. Felgar, *Plasticity and Creep of Metals*, Wiley, New York, 1961.

8. J. Marin, B. H. Ulrich, and W. P. Hughs, "Plastic Stress-Strain Relations for 75S-T6 Aluminum Alloy Subjected to Biaxial Tensile Stress," *NACA T.N. 2425*, August 1951.†

9. E. Orowan, "Strength and Failure of Materials," pp. 478–506 in *Pressure Vessel and Piping Design, Collected Papers 1927–1959*, American Society of Mechanical Engineers, New York, 1960.†

10. *ABAQUS Theory Manual*, Version 5.3, Hibbitt, Karlson and Sorensen, Inc., Providence, Rhode Island, 1993.

*Available from National Technical Information Service, Springfield, VA 22161.

†Available in public technical libraries.

CONVERSION FACTORS[a]

SI unit	English unit	Factor
mm	in.	0.0393701
cm	in.	0.393701
m	ft	3.28084
m/s	ft/s	3.28084
kN	lb_f	224.809
kPa	psi	0.145038
MPa	ksi	0.145038
$MPa \cdot \sqrt{m}$	$ksi \cdot \sqrt{in.}$	0.910048
J	ft•lb	0.737562
K	°F or °R	1.8
kJ/m^2	$in.\text{-}lb/in.^2$	5.71015
$W \cdot m^{-2} \cdot K^{-1}$	$Btu/h \cdot ft^2 \cdot °F$	0.176110
kg	lb	2.20462
kg/m^3	$lb/in.^3$	3.61273×10^{-5}
mm/N	$in./lb_f$	0.175127
$T(°F) = 1.8(°C) + 32$		

[a]Multiply SI quantity by given factor to obtain English quantity.

Prior Heavy-Section Steel Technology Program Publications

The work reported here was performed at Oak Ridge National Laboratory under the Heavy-Section Steel Technology (HSST) Program, W. E. Pennell, Program Manager. The program is sponsored by the Office of Nuclear Regulatory Research of the U.S. Nuclear Regulatory Commission (NRC). The technical monitor for NRC is S. N. M. Malik. Prior and future reports in this series are listed below.

1. S. Yukawa, General Electric Company, Schenectady, N.Y., *Evaluation of Periodic Proof Testing and Warm Prestressing Procedures for Nuclear Reactor Vessels*, HSSTP-TR-1, July 1, 1969.
2. L. W. Loechel, Martin Marietta Corporation, Denver, Colo., *The Effect of Testing Variables on the Transition Temperature in Steel*, MCR-69-189, November 20, 1969.
3. P. N. Randall, TRW Systems Group, Redondo Beach, Calif., *Gross Strain Measure of Fracture Toughness of Steels*, HSSTP-TR-3, November 1, 1969.
4. C. Visser, S. E. Gabrielse, and W. VanBuren, Westinghouse Electric Corporation, PWR Systems Division, Pittsburgh, Pa., *A Two-Dimensional Elastic-Plastic Analysis of Fracture Test Specimens*, WCAP-7368, October 1969.
5. T. R. Mager and F. O. Thomas, Westinghouse Electric Corporation, PWR Systems Division, Pittsburgh, Pa., *Evaluation by Linear Elastic Fracture Mechanics of Radiation Damage to Pressure Vessel Steels*, WCAP-7328 (Rev.), October 1969.
6. W. O. Shabbits, W. H. Pryle, and E. T. Wessel, Westinghouse Electric Corporation, PWR Systems Division, Pittsburgh, Pa., *Heavy-Section Fracture Toughness Properties of A533 Grade B Class 1 Steel Plate and Submerged Arc Weldment*, WCAP-7414, December 1969.
7. F. J. Loss, Naval Research Laboratory, Washington, D.C., *Dynamic Tear Test Investigations of the Fracture Toughness of Thick-Section Steel*, NRL-7056, May 14, 1970.
8. P. B. Crosley and E. J. Ripling, Materials Research Laboratory, Inc., Glenwood, Ill., *Crack Arrest Fracture Toughness of A533 Grade B Class 1 Pressure Vessel Steel*, HSSTP-TR-8, March 1970.
9. T. R. Mager, Westinghouse Electric Corporation, PWR Systems Division, Pittsburgh, Pa., *Post-Irradiation Testing of 2T Compact Tension Specimens*, WCAP-7561, August 1970.
10. T. R. Mager, Westinghouse Electric Corporation, PWR Systems Division, Pittsburgh, Pa., *Fracture Toughness Characterization Study of A533, Grade B, Class 1 Steel*, WCAP-7578, October 1970.
11. T. R. Mager, Westinghouse Electric Corporation, PWR Systems Division, Pittsburgh, Pa., *Notch Preparation in Compact Tension Specimens*, WCAP-7579, November 1970.
12. N. Levy and P. V. Marcal, Brown University, Providence, R.I., *Three-Dimensional Elastic-Plastic Stress and Strain Analysis for Fracture Mechanics, Phase I: Simple Flawed Specimens*, HSSTP-TR-12, December 1970.
13. W. O. Shabbits, Westinghouse Electric Corporation, PWR Systems Division, Pittsburgh, Pa., *Dynamic Fracture Toughness Properties of Heavy Section A533 Grade B Class 1 Steel Plate*, WCAP-7623, December 1970.
14. P. N. Randall, TRW Systems Group, Redondo Beach, Calif., *Gross Strain Crack Tolerance of A 533-B Steel*, HSSTP-TR-14, May 1, 1971.
15. H. T. Corten and R. H. Sailors, University of Illinois, Urbana, Ill., *Relationship Between Material Fracture Toughness Using Fracture Mechanics and Transition Temperature Tests*, T&AM Report 346, August 1, 1971.
16. T. R. Mager and V. J. McLaughlin, Westinghouse Electric Corporation, PWR Systems Division, Pittsburgh, Pa., *The Effect of an Environment of High Temperature Primary Grade Nuclear Reactor Water on the Fatigue Crack Growth Characteristics of A533 Grade B Class 1 Plate and Weldment Material*, WCAP-7776, October 1971.
17. N. Levy and P. V. Marcal, Brown University, Providence, R.I., *Three-Dimensional Elastic-Plastic Stress and Strain Analysis for Fracture Mechanics, Phase II: Improved Modelling*, HSSTP-TR-17, November 1971.
18. S. C. Grigory, Southwest Research Institute, San Antonio, Tex., *Tests of 6-in.-Thick Flawed Tensile Specimens, First Technical Summary Report, Longitudinal Specimens Numbers 1 through 7*, HSSTP-TR-18, June 1972.
19. P. N. Randall, TRW Systems Group, Redondo Beach, Calif., *Effects of Strain Gradients on the Gross Strain Crack Tolerance of A533-B Steel*, HSSTP-TR-19, June 15, 1972.

20. S. C. Grigory, Southwest Research Institute, San Antonio, Tex., *Tests of 6-Inch-Thick Flawed Tensile Specimens, Second Technical Summary Report, Transverse Specimens Numbers 8 through 10, Welded Specimens Numbers 11 through 13*, HSSTP-TR-20, June 1972.

21. L. A. James and J. A. Williams, Hanford Engineering Development Laboratory, Richland, Wash., Heavy Section Steel Technology Program Technical Report No. 21, *The Effect of Temperature and Neutron Irradiation Upon the Fatigue-Crack Propagation Behavior of ASTM A533 Grade B, Class 1 Steel*, HEDL-TME 72-132, September 1972.

22. S. C. Grigory, Southwest Research Institute, San Antonio, Tex., *Tests of 6-Inch-Thick Flawed Tensile Specimens, Third Technical Summary Report, Longitudinal Specimens Numbers 14 through 16, Unflawed Specimen Number 17*, HSSTP-TR-22, October 1972.

23. S. C. Grigory, Southwest Research Institute, San Antonio, Tex., *Tests of 6-Inch-Thick Tensile Specimens, Fourth Technical Summary Report, Tests of 1-Inch-Thick Flawed Tensile Specimens for Size Effect Evaluation*, HSSTP-TR-23, June 1973.

24. S. P. Ying and S. C. Grigory, Southwest Research Institute, San Antonio, Tex., *Tests of 6-Inch-Thick Tensile Specimens, Fifth Technical Summary Report, Acoustic Emission Monitoring of One-Inch and Six-Inch-Thick Tensile Specimens*, HSSTP-TR-24, November 1972.

25. R. W. Derby, J. G. Merkle, G. C. Robinson, G. D. Whitman, and F. J. Witt, Oak Ridge Natl. Lab., Oak Ridge, Tenn., *Test of 6-Inch-Thick Pressure Vessels. Series 1: Intermediate Test Vessels V-1 and V-2*, ORNL-4895, February 1974.

26. W. J. Stelzman and R. G. Berggren, Oak Ridge Natl. Lab., Oak Ridge, Tenn., *Radiation Strengthening and Embrittlement in Heavy Section Steel Plates and Welds*, ORNL-4871, June 1973.

27. P. B. Crosley and E. J. Ripling, Materials Research Laboratory, Inc., Glenwood, Ill., *Crack Arrest in an Increasing K-Field*, HSSTP-TR-27, January 1973.

28. P. V. Marcal, P. M. Stuart, and R. S. Bettes, Brown University, Providence, R.I., *Elastic Plastic Behavior of a Longitudinal Semi-Elliptic Crack in a Thick Pressure Vessel*, HSSTP-TR-28, June 1973.

29. W. J. Stelzman, R. G. Berggren, and T. N. Jones, Oak Ridge Natl. Lab., Oak Ridge, Tenn., *ORNL Characterization of Heavy-Section Steel Technology Program Plates 01, 02 and 03*, USNRC Report NUREG/CR-4092 (ORNL/TM-9491), April 1985.

30. Canceled.

31. J. A. Williams, Hanford Engineering Development Laboratory, Richland, Wash., *The Irradiation and Temperature Dependence of Tensile and Fracture Properties of ASTM A533, Grade B, Class 1 Steel Plate and Weldment*, HEDL-TME 73-75, August 1973.

32. J. M. Steichen and J. A. Williams, Hanford Engineering Development Laboratory, Richland, Wash., *High Strain Rate Tensile Properties of Irradiated ASTM A533 Grade B Class 1 Pressure Vessel Steel*, July 1973.

33. P. C. Riccardella and J. L. Swedlow, Westinghouse Electric Corporation, Pittsburgh, Pa., *A Combined Analytical-Experimental Fracture Study of the Two Leading Theories of Elastic-Plastic Fracture (J-Integral and Equivalent Energy)*, WCAP-8224, October 1973.

34. R. J. Podlasek and R. J. Eiber, Battelle Columbus Laboratories, Columbus, Ohio, *Final Report on Investigation of Mode III Crack Extension in Reactor Piping*, December 14, 1973.

35. T. R. Mager, J. D. Landes, D. M. Moon, and V. J. McLaughlin, Westinghouse Electric Corporation, Pittsburgh, Pa., *Interim Report on the Effect of Low Frequencies on the Fatigue Crack Growth Characteristics of A533 Grade B Class 1 Plate in an Environment of High-Temperature Primary Grade Nuclear Reactor Water*, WCAP-8256, December 1973.

36. J. A. Williams, Hanford Engineering Development Laboratory, Richland, Wash., *The Irradiated Fracture Toughness of ASTM A533, Grade B, Class 1 Steel Measured with a Four-Inch-Thick Compact Tension Specimen*, HEDL-TME 75-10, January 1975.

37. R. H. Bryan, J. G. Merkle, M. N. Raftenberg, G. C. Robinson, and J. E. Smith, Oak Ridge Natl. Lab., Oak Ridge, Tenn., *Test of 6-Inch-Thick Pressure Vessels. Series 2: Intermediate Test Vessels V-3, V-4, and V-6*, ORNL-5059, November 1975.

38. T. R. Mager, S. E. Yanichko, and L. R. Singer, Westinghouse Electric Corporation, Pittsburgh, Pa., *Fracture Toughness Characterization of HSST Intermediate Pressure Vessel Material*, WCAP-8456, December 1974.

39. J. G. Merkle, G. D. Whitman, and R. H. Bryan, Oak Ridge Natl. Lab., Oak Ridge, Tenn., *An Evaluation of the HSST Program Intermediate Pressure Vessel Tests in Terms of Light-Water-Reactor Pressure Vessel Safety*, ORNL/TM-5090, November 1975.

40. J. C. Merkle, G. C. Robinson, P. P. Holz, J. E. Smith, and R. H. Bryan, Oak Ridge Natl. Lab., Oak Ridge, Tenn., *Test of 6-In.-Thick Pressure Vessels. Series 3: Intermediate Test Vessel V-7*, USNRC Report ORNL/NUREG-1, August 1976.

41. J. A. Davidson, L. J. Ceschini, R. P. Shogan, and G. V. Rao, Westinghouse Electric Corporation, Pittsburgh, Pa., *The Irradiated Dynamic Fracture Toughness of ASTM A533, Grade B, Class 1 Steel Plate and Submerged Arc Weldment*, WCAP-8775, October 1976.

42. R. D. Cheverton, Oak Ridge Natl. Lab., Oak Ridge, Tenn., *Pressure Vessel Fracture Studies Pertaining to a PWR LOCA-ECC Thermal Shock: Experiments TSE-1 and TSE-2*, USNRC Report ORNL/NUREG/TM-31, September 1976.

43. J. G. Merkle, G. C. Robinson, P. P. Holz, and J. E. Smith, Oak Ridge Natl. Lab., Oak Ridge, Tenn., *Test of 6-In.-Thick Pressure Vessels. Series 4: Intermediate Test Vessels V-5 and V-9 with Inside Nozzle Corner Cracks*, USNRC Report ORNL/NUREG-7, August 1977.

44. J. A. Williams, Hanford Engineering Development Laboratory, Richland, Wash., *The Ductile Fracture Toughness of Heavy Section Steel Plate*, USNRC Report NUREG/CR-0859, September 1979.

45. R. H. Bryan, T. M. Cate, P. P. Holz, T. A. King, J. G. Merkle, G. C. Robinson, G. C. Smith, J. E. Smith, and G. D. Whitman, Oak Ridge Natl. Lab., Oak Ridge, Tenn., *Test of 6-in.-Thick Pressure Vessels. Series 3: Intermediate Test Vessel V-7A Under Sustained Loading*, USNRC Report ORNL/NUREG-9, February 1978.

46. R. D. Cheverton and S. E. Bolt, Oak Ridge Natl. Lab., Oak Ridge, Tenn., *Pressure Vessel Fracture Studies Pertaining to a PWR LOCA-ECC Thermal Shock: Experiments TSE-3 and TSE-4 and Update of TSE-1 and TSE-2 Analysis*, USNRC Report ORNL/NUREG-22, December 1977.

47. D. A. Canonico, Oak Ridge Natl. Lab., Oak Ridge, Tenn., *Significance of Reheat Cracks to the Integrity of Pressure Vessels for Light-Water Reactors*, USNRC Report ORNL/NUREG-15, July 1977.

48. G. C. Smith and P. P. Holz, Oak Ridge Natl. Lab., Oak Ridge, Tenn., *Repair Weld Induced Residual Stresses in Thick-Walled Steel Pressure Vessels*, USNRC Report NUREG/CR-0093 (ORNL/NUREG/TM-153), June 1978.

49. P. P. Holz and S. W. Wismer, Oak Ridge Natl. Lab., Oak Ridge, Tenn., *Half-Bead (Temper) Repair Welding for HSST Vessels*, USNRC Report NUREG/CR-0113 (ORNL/NUREG/TM-177), June 1978.

50. G. C. Smith, P. P. Holz, and W. J. Stelzman, Oak Ridge Natl. Lab., Oak Ridge, Tenn., *Crack Extension and Arrest Tests of Axially Flawed Steel Model Pressure Vessels*, USNRC Report NUREG/CR-0126 (ORNL/NUREG/TM-196), October 1978.

51. R. H. Bryan, P. P. Holz, J. G. Merkle, G. C. Smith, J. E. Smith, and W. J. Stelzman, Oak Ridge Natl. Lab., Oak Ridge, Tenn., *Test of 6-in.-Thick Pressure Vessels. Series 3: Intermediate Test Vessel V-7B*, USNRC Report NUREG/CR-0309 (ORNL/NUREG-38), October 1978.

52. R. D. Cheverton, S. K. Iskander, and S. E. Bolt, Oak Ridge Natl. Lab., Oak Ridge, Tenn., *Applicability of LEFM to the Analysis of PWR Vessels Under LOCA-ECC Thermal Shock Conditions*, USNRC Report NUREG/CR-0107 (ORNL/NUREG-40), October 1978.

53. R. H. Bryan, D. A. Canonico, P. P. Holz, S. K. Iskander, J. G. Merkle, J. E. Smith, and W. J. Stelzman, Oak Ridge Natl. Lab., Oak Ridge, Tenn., *Test of 6-in.-Thick Pressure Vessels, Series 3: Intermediate Test Vessel V-8*, USNRC Report NUREG/CR-0675 (ORNL/ NUREG-58), December 1979.

54. R. D. Cheverton and S. K. Iskander, Oak Ridge Natl. Lab., Oak Ridge, Tenn., *Application of Static and Dynamic Crack Arrest Theory to TSE-4*, USNRC Report NUREG/CR-0767 (ORNL/NUREG-57), June 1979.

55. J. A. Williams, Hanford Engineering Development Laboratory, Richland, Wash., *Tensile Properties of Irradiated and Unirradiated Welds of A533 Steel Plate and A508 Forgings*, USNRC Report NUREG/CR-1158 (ORNL/Sub/79-50917/2), July 1979.

56. K. W. Carlson and J. A. Williams, Hanford Engineering Development Laboratory, Richland, Wash., *The Effect of Crack Length and Side Grooves on the Ductile Fracture Toughness Properties of ASTM A533 Steel*, USNRC Report NUREG/CR-1171 (ORNL/Sub/79-50917/3), October 1979.

57. P. P. Holz, Oak Ridge Natl. Lab., Oak Ridge, Tenn., *Flaw Preparations for HSST Program Vessel Fracture Mechanics Testing; Mechanical-Cyclic Pumping and Electron-Beam Weld-Hydrogen Charge Cracking Schemes*, USNRC Report NUREG/CR-1274 (ORNL/ NUREG/TM-369), May 1980.

58. S. K. Iskander, Computer Sciences Div., Union Carbide Corp. Nuclear Div., Oak Ridge, Tenn., *Two Finite Element Techniques for Computing Mode I Stress Intensity Factors in Two- or Three-*

Dimensional Problems, USNRC Report NUREG/CR-1499 (ORNL/NUREG/CSD/TM-14), February 1981.

59. P. B. Crosley and E. J. Ripling, Materials Research Laboratory, Glenwood, Ill., *Development of a Standard Test for Measuring K_{Ia} with a Modified Compact Specimen,* USNRC Report NUREG/CR-2294 (ORNL/Sub/81-7755/1), August 1981.

60. S. N. Atluri, B. R. Bass, J. W. Bryson, and K. Kathiresan, Computer Sciences Div., Oak Ridge Gaseous Diffusion Plant, Oak Ridge, Tenn., *NOZ-FLAW: A Finite Element Program for Direct Evaluation of Stress Intensity Factors for Pressure Vessel Nozzle-Corner Flaws,* USNRC Report NUREG/CR-1843 (ORNL/NUREG/CSD/TM-18), March 1981.

61. A. Shukla, W. L. Fourney, and G. R. Irwin, University of Maryland, College Park, Md., *Study of Energy Loss and Its Mechanisms in Homalite 100 During Crack Propagation and Arrest,* USNRC Report NUREG/CR-2150 (ORNL/Sub/79-7778/1), August 1981.

62. S. K. Iskander, R. D. Cheverton, and D. G. Ball, Oak Ridge Natl. Lab., Oak Ridge, Tenn., *OCA-I, A Code for Calculating the Behavior of Flaws on the Inner Surface of a Pressure Vessel Subjected to Temperature and Pressure Transients,* USNRC Report NUREG/CR-2113 (ORNL/NUREG-84), August 1981.

63. R. J. Sanford, R. Chona, W. L. Fourney, and G. R. Irwin, University of Maryland, College Park, Md., *A Photoelastic Study of the Influence of Non-Singular Stresses in Fracture Test Specimens,* USNRC Report NUREG/CR-2179 (ORNL/Sub/79-7778/2), August 1981.

64. B. R. Bass, S. N. Atluri, J. W. Bryson, and K. Kathiresan, Oak Ridge Natl. Lab., Oak Ridge, Tenn., *OR-FLAW: A Finite Element Program for Direct Evaluation of K-Factors for User-Defined Flaws in Plate, Cylinders, and Pressure-Vessel Nozzle Corners,* USNRC Report NUREG/CR-2494 (ORNL/CSD/TM-165), April 1982.

65. B. R. Bass and J. W. Bryson, Oak Ridge Natl. Lab., Oak Ridge Tenn., *ORMGEN-3D: A Finite Element Mesh Generator for 3-Dimensional Crack Geometries,* USNRC Report NUREG/CR-2997, Vol. 1 (ORNL/TM-8527/V1), December 1982.

66. B. R. Bass and J. W. Bryson, Oak Ridge Natl. Lab., Oak Ridge, Tenn., *ORVIRT: A Finite Element Program for Energy Release Rate Calculations for 2-Dimensional and 3-Dimensional Crack Models,* USNRC Report NUREG/CR-2997, Vol. 2 (ORNL/TM-8527/V2), February 1983.

67. R. D. Cheverton, S. K. Iskander, and D. G. Ball, Oak Ridge Natl. Lab., Oak Ridge, Tenn., *PWR Pressure Vessel Integrity During Overcooling Accidents: A Parametric Analysis,* USNRC Report NUREG/CR-2895 (ORNL/TM-7931), February 1983.

68. D. G. Ball, R. D. Cheverton, J. B. Drake, and S. K. Iskander, Oak Ridge Natl. Lab., Oak Ridge, Tenn., *OCA-II, A Code for Calculating Behavior of 2-D and 3-D Surface Flaws in a Pressure Vessel Subjected to Temperature and Pressure Transients,* USNRC Report NUREG/ CR-3491 (ORNL-5934), February 1984.

69. A. Sauter, R. D. Cheverton, and S. K. Iskander, Oak Ridge Natl. Lab., Oak Ridge, Tenn., *Modification of OCA-I for Application to a Reactor Pressure Vessel with Cladding on the Inner Surface,* USNRC Report NUREG/CR-3155 (ORNL/TM-8649), May 1983.

70. R. D. Cheverton and D. G. Ball, Martin Marietta Energy Systems, Inc., Oak Ridge Natl. Lab., Oak Ridge, Tenn., *OCA-P, A Deterministic and Probabilistic Fracture-Mechanics Code for Application to Pressure Vessels,* USNRC Report NUREG/CR-3618 (ORNL-5991), May 1984.

71. J. G. Merkle, Martin Marietta Energy Systems, Inc., Oak Ridge Natl. Lab., Oak Ridge, Tenn., *An Examination of the Size Effects and Data Scatter Observed in Small Specimen Cleavage Fracture Toughness Testing,* USNRC Report NUREG/CR-3672 (ORNL/TM-9088), April 1984.

72. C. E. Pugh et al., Martin Marietta Energy Systems, Inc., Oak Ridge Natl. Lab., Oak Ridge, Tenn., *Heavy-Section Steel Technology Program—Five-Year Plan FY 1983–1987,* USNRC Report NUREG/CR-3595 (ORNL/TM-9008), April 1984.

73. D. G. Ball, B. R. Bass, J. W. Bryson, R. D. Cheverton, and J. B. Drake, Martin Marietta Energy Systems, Inc., Oak Ridge Natl. Lab., Oak Ridge, Tenn., *Stress Intensity Factor Influence Coefficients for Surface Flaws in Pressure Vessels,* USNRC Report NUREG/CR-3723 (ORNL/CSD/TM-216), February 1985.

74. W. R. Corwin, R. G. Berggren, and R. K. Nanstad, Martin Marietta Energy Systems, Inc., Oak Ridge Natl. Lab., Oak Ridge, Tenn., *Charpy Toughness and Tensile Properties of Neutron Irradiated Stainless Steel Submerged-Arc Weld Cladding Overlay,* USNRC Report NUREG/CR-3927 (ORNL/TM-9309), September 1984.

75. C. W. Schwartz, R. Chona, W. L. Fourney, and G. R. Irwin, University of Maryland, College Park, Md., *SAMCR: A Two-Dimensional Dynamic Finite Element Code for the Stress Analysis of Moving CRacks,* USNRC Report NUREG/CR-3891 (ORNL/Sub/79-7778/3), November 1984.

76. W. R. Corwin, G. C. Robinson, R. K. Nanstad, J. G. Merkle, R. G. Berggren, G. M. Goodwin, R. L. Swain, and T. D. Owings, Martin Marietta Energy Systems, Inc., Oak Ridge Natl. Lab., Oak Ridge, Tenn., *Effects of Stainless Steel Weld Overlay Cladding on the Structural Integrity of Flawed Steel Plates in Bending, Series 1,* USNRC Report NUREG/CR-4015 (ORNL/TM-9390), April 1985.

77. R. H. Bryan, B. R. Bass, S. E. Bolt, J. W. Bryson, D. P. Edmonds, R. W. McCulloch, J. G. Merkle, R. K. Nanstad, G. C. Robinson, K. R. Thoms, and G. D. Whitman, Martin Marietta Energy Systems, Inc., Oak Ridge Natl. Lab., Oak Ridge, Tenn., *Pressurized-Thermal-Shock Test of 6-in.-Thick Pressure Vessels. PTSE-1: Investigation of Warm Prestressing and Upper-Shelf Arrest,* USNRC Report NUREG/CR-4106 (ORNL-6135), April 1985.

78. R. D. Cheverton, D. G. Ball, S. E. Bolt, S. K. Iskander, and R. K. Nanstad, Martin Marietta Energy Systems, Inc., Oak Ridge Natl. Lab., Oak Ridge, Tenn., *Pressure Vessel Fracture Studies Pertaining to the PWR Thermal-Shock Issue: Experiments TSE-5, TSE-5A, and TSE-6,* USNRC Report NUREG/CR-4249 (ORNL-6163), June 1985.

79. R. D. Cheverton, D. G. Ball, S. E. Bolt, S. K. Iskander, and R. K. Nanstad, Martin Marietta Energy Systems, Inc., Oak Ridge Natl. Lab., Oak Ridge, Tenn., *Pressure Vessel Fracture Studies Pertaining to the PWR Thermal-Shock Issue: Experiment TSE-7,* USNRC Report NUREG/CR-4304 (ORNL-6177), August 1985.

80. R. H. Bryan, B. R. Bass, S. E. Bolt, J. W. Bryson, J. G. Merkle, R. K. Nanstad, and G. C. Robinson, Martin Marietta Energy Systems, Inc., Oak Ridge Natl. Lab., Oak Ridge, Tenn., *Test of 6-in.-Thick Pressure Vessels. Series 3: Intermediate Test Vessel V-8A—Tearing Behavior of Low Upper-Shelf Material,* USNRC Report NUREG/CR-4760 (ORNL-6187), May 1987.

81. R. D. Cheverton and D. G. Ball, Martin Marietta Energy Systems, Inc., Oak Ridge Natl. Lab., Oak Ridge, Tenn., *A Parametric Study of PWR Pressure Vessel Integrity During Overcooling Accidents, Considering Both 2-D and 3-D Flaws,* USNRC Report NUREG/CR-4325 (ORNL/TM-9682), August 1985.

82. E. C. Rodabaugh, E. C. Rodabaugh Associates, Inc., Hilliard, Ohio, *Comments on the Leak-Before-Break Concept for Nuclear Power Plant Piping Systems,* USNRC Report NUREG/CR-4305 (ORNL/Sub/82-22252/3), August 1985.

83. J. W. Bryson, Martin Marietta Energy Systems, Inc., Oak Ridge Natl. Lab., Oak Ridge, Tenn., *ORVIRT.PC: A 2-D Finite Element Fracture Analysis Program for a Microcomputer,* USNRC Report NUREG/CR-4367 (ORNL-6208), October 1985.

84. D. G. Ball and R. D. Cheverton, Martin Marietta Energy Systems, Inc., Oak Ridge Natl. Lab., Oak Ridge, Tenn., *Adaptation of OCA-P, A Probabilistic Fracture-Mechanics Code, to a Personal Computer,* USNRC Report NUREG/CR-4468 (ORNL/CSD/TM-233), January 1986.

85. J. W. Bryson and B. R. Bass, Martin Marietta Energy Systems, Inc., Oak Ridge Natl. Lab., Oak Ridge, Tenn., *ORMGEN.PC: A Microcomputer Program for Automatic Mesh Generation of 2-D Crack Geometries,* USNRC Report NUREG/CR-4475 (ORNL-6250), March 1986.

86. G. D. Whitman, Martin Marietta Energy Systems, Inc., Oak Ridge Natl. Lab., Oak Ridge, Tenn., *Historical Summary of the Heavy-Section Steel Technology Program and Some Related Activities in Light-Water Reactor Pressure Vessel Safety Research,* USNRC Report NUREG/CR-4489 (ORNL-6259), March 1986.

87. C. Inversini and J. W. Bryson, Martin Marietta Energy Systems, Inc., Oak Ridge Natl. Lab., Oak Ridge, Tenn., *ORPLOT PC: A Graphic Utility for ORMGEN.PC and ORVIRT.PC,* USNRC Report NUREG/CR-4633 (ORNL-6291), June 1986.

88. J. J. McGowan, R. K. Nanstad, and K. R. Thoms, Martin Marietta Energy Systems, Inc., Oak Ridge Natl. Lab., Oak Ridge, Tenn., *Characterization of Irradiated Current-Practice Welds and A533 Grade B Class 1 Plate for Nuclear Pressure Vessel Service,* USNRC Report NUREG/CR-4880 (ORNL/TM-10387), July 1988.

89. K. V. Cook and D. W. McClung, Martin Marietta Energy Systems, Inc., Oak Ridge Natl. Lab., Oak Ridge, Tenn., *Flaw Density Examinations of a Clad Boiling Water Reactor Pressure Vessel Segment,* USNRC Report NUREG/CR-4860 (ORNL/TM-10364), April 1987.

90. D. J. Naus, B. R. Bass, C. E. Pugh, R. K. Nanstad, J. G. Merkle, W. R. Corwin, and G. C. Robinson, Martin Marietta Energy Systems, Inc., Oak Ridge

Natl. Lab., Oak Ridge, Tenn., *Crack-Arrest Behavior in SEN Wide Plates of Quenched and Tempered A 533 Grade B Steel Tested Under Nonisothermal Conditions,* USNRC Report NUREG/CR-4930 (ORNL-6388), August 1987.

91. D. B. Barker, R. Chona, W. L. Fourney, and G. R. Irwin, University of Maryland, College Park, Md., *A Report on the Round Robin Program Conducted to Evaluate the Proposed ASTM Standard Test Method for Determining the Plane Strain Crack Arrest Fracture Toughness, K_{Ia},* of Ferritic Materials, USNRC Report NUREG/CR-4966 (ORNL/Sub/79-7778/4), January 1988.

92. W. H. Bamford, Westinghouse Electric Corporation, Pittsburgh, Pa., *A Summary of Environmentally Assisted Crack-Growth Studies Performed at Westinghouse Electric Corporation Under Funding from the Heavy-Section Steel Technology Program,* USNRC Report NUREG/CR-5020 (ORNL/Sub/82-21598/1), May 1988.

93. R. H. Bryan, B. R. Bass, S. E. Bolt, J. W. Bryson, W. R. Corwin, J. G. Merkle, R. K. Nanstad, and G. C. Robinson, Martin Marietta Energy Systems, Inc., Oak Ridge Natl. Lab., Oak Ridge, Tenn., *Pressurized-Thermal-Shock Test of 6-in.-Thick Pressure Vessels. PTSE-2: Investigation of Low Tearing Resistance and Warm Prestressing,* USNRC Report NUREG/CR-4888 (ORNL-6377), December 1987.

94. J. H. Giovanola and R. W. Klopp, SRI International, Menlo Park, Calif., *Viscoplastic Stress-Strain Characterization of A533B Class 1 Steel,* USNRC Report NUREG/CR-5066 (ORNL/Sub/87-SA193/1), September 1989.

95. L. F. Miller et al., Martin Marietta Energy Systems, Inc., Oak Ridge Natl. Lab., Oak Ridge, Tenn., *Neutron Exposure Parameters for the Metallurgical Test Specimens in the Fifth Heavy-Section Steel Technology Irradiation Series Capsules,* USNRC Report NUREG/ CR-5019 (ORNL/TM-10582), March 1988.

96. Canceled.

97. D. J. Naus, J. Keeney-Walker, and B. R. Bass, Martin Marietta Energy Systems, Inc., Oak Ridge Natl. Lab., Oak Ridge, Tenn., *High-Temperature Crack-Arrest Behavior in 152-mm-Thick SEN Wide Plates of Quenched and Tempered A 533 Grade B Steel,* USNRC Report NUREG/CR-5330 (ORNL/TM-11083), April 1989.

98. K. V. Cook, R. A. Cunningham, Jr., and R. W. McClung, Martin Marietta Energy Systems, Inc., Oak Ridge Natl. Lab., Oak Ridge, Tenn., *Detection and Characterization of Indications in Segments of Reactor Pressure Vessels,* USNRC Report NUREG/ CR-5322 (ORNL/TM-11072), August 1989.

99. R. D. Cheverton, W. E. Pennell, G. C. Robinson, and R. K. Nanstad, Martin Marietta Energy Systems, Inc., Oak Ridge Natl. Lab., Oak Ridge, Tenn., *Impact of Radiation Embrittlement on Integrity of Pressure Vessel Supports for Two PWR Plants,* NUREG/ CR-5320 (ORNL/TM-10966), February 1989.

100. D. J. Naus, J. Keeney-Walker, B. R. Bass, S. K. Iskander, R. J. Fields, R. deWitt, and S. R. Low III, Martin Marietta Energy Systems, Inc., Oak Ridge Natl. Lab., Oak Ridge, Tenn., *SEN Wide-Plate Crack-Arrest Tests* Utilizing *A 533 Grade B Class 1 Material: WP-CE Test Series,* USNRC Report NUREG/CR-5408 (ORNL/TM-11269), November 1989.

101. D. J. Naus, J. Keeney-Walker, B. R. Bass, S. K. Iskander, R. J. Fields, R. deWitt, and S. R. Low III, Martin Marietta Energy Systems, Inc., Oak Ridge Natl. Lab., Oak Ridge, Tenn., *High Temperature Crack-Arrest Tests Using 152-mm-Thick SEN Wide Plates of Low Upper-Shelf Base Material: Tests WP-2.2 and WP-2.6,* USNRC Report NUREG/ CR-5450 (ORNL/TM-11352), February 1990.

102. Canceled.

103. D. J. Naus, J. Keeney-Walker, B. R. Bass, G. C. Robinson, S. K. Iskander, D. J. Alexander, R. J. Fields, R. deWitt, S. R. Low, C. W. Schwartz, and I.-B. Johansson, Martin Marietta Energy Systems, Inc., Oak Ridge Natl. Lab., Oak Ridge, Tenn., *Crack-Arrest Behavior in SEN Wide Plates of Low Upper-Shelf Base Metal Tested Under Non-isothermal Conditions: WP-2 Series,* USNRC Report NUREG/ CR-5451 (ORNL-6584), August 1990.

104. T. L. Dickson, R. D. Cheverton, and D. K. Shum, Martin Marietta Energy Systems, Inc., Oak Ridge Natl. Lab., Oak Ridge, Tenn., *Inclusion of Unstable Ductile Tearing and Extrapolated Crack-Arrest Toughness Data in PWR Vessel Integrity Assessment,* USNRC Report NUREG/CR-5473 (ORNL/ TM-11450), May 1990.

105. T. J. Theiss, Martin Marietta Energy Systems, Inc., Oak Ridge Natl. Lab., Oak Ridge, Tenn., *Recommendations for the Shallow-Crack Fracture Toughness Testing Task Within the HSST Program,* USNRC Report NUREG/CR-5554 (ORNL/TM-11509), September 1990.

106. J. G. Merkle, Martin Marietta Energy Systems, Inc., Oak Ridge Natl. Lab., Oak Ridge, Tenn., *An Overview of the Low Upper Shelf Toughness Safety Margin Issue*, USNRC Report NUREG/CR-5552 (ORNL/TM-11314), August 6, 1990.

107. D. K. M. Shum, J. G. Merkle, J. Keeney-Walker, and B. R. Bass, Martin Marietta Energy Systems, Inc., Oak Ridge Natl. Lab., Oak Ridge, Tenn., *Analytical Studies of Transverse Strain Effects on Fracture Toughness for Circumferentially Oriented Cracks*, USNRC Report NUREG/CR-5592 (ORNL/TM-11581), April 1991.

108. J. D. Landes, The University of Tennessee for Martin Marietta Energy Systems, Inc., Oak Ridge natl. Lab., Oak Ridge, Tenn., *Extrapolation of the J-R Curve for Predicting Reactor Vessel Integrity*, USNRC Report NUREG/CR-5650 (ORNL/Sub/89-99732/1), January 1992.

109. J. Keeney-Walker, B. R. Bass, and J. D. Landes, (The University of Tennessee), Martin Marietta Energy Systems, Inc., Oak Ridge Natl. Lab., Oak Ridge, Tenn., *An Investigation of Crack-Tip Stress-Field Criteria for Predicting Cleavage-Crack Initiation*, USNRC Report NUREG/ CR-5651 (ORNL/TM-11692), September 1991.

110. G. R. Irwin, University of Maryland, for Martin Marietta Energy Systems, Inc., Oak Ridge Natl. Lab., Oak Ridge, Tenn., *Use of Thickness Reduction to Estimate Values of K*, USNRC Report NUREG/ CR-5697 (ORNL/Sub/79-7778/5), November 1991.

111. P. Albrecht and X. Chen, University of Maryland for Martin Marietta Energy Systems, Inc., Oak Ridge Natl. Lab., Oak Ridge, Tenn., *Limit Pressure Analysis of PTSE-2 Vessel*, USNRC Report NUREG/CR-5698 (ORNL/Sub/79-7778/6) (to be published).

112. J. W. Dally, W. L. Fourney, and G. R. Irwin, University of Maryland for Martin Marietta Energy Systems, Inc., Oak Ridge Natl. Lab., Oak Ridge, Tenn., *Lower-Bound Initiation Toughness with a Modified-Charpy Specimen*, USNRC Report NUREG/CR-5703 (ORNL/Sub/79-7778/7), November 1991.

113. S. K. Iskander, G. C. Robinson, W. R. Corwin, B. C. Oland, D. J. Alexander, and K. V. Cook, Martin Marietta Energy Systems, Inc., Oak Ridge Natl. Lab., Oak Ridge, Tenn., *Experimental Results of Tests to Investigate Flaw Behavior of Mechanically Loaded Stainless Steel Clad Plates*, USNRC Report NUREG/ CR-5785 (ORNL/TM-11950), April 1992.

114. S. T. Rolfe, University of Kansas for Martin Marietta Energy Systems, Inc., Oak Ridge Natl. Lab., Oak Ridge, Tenn., *Interpretive Report on the Application of Shallow-Flaw CTOD Test Data to the Structural Margin Assessment of Reactor Pressure Vessels with Flaws*, USNRC Report NUREG/ CR-5767 (ORNL/Sub/90-SH640/1), November 1991.

115. D. E. McCabe, Martin Marietta Energy Systems, Inc., Oak Ridge Natl. Lab., Oak Ridge, Tenn., *Comparison of Weibull and β_{1c} Analysis of Transition Range Fracture Toughness Data*, USNRC Report NUREG/CR-5788 (ORNL/ TM-11959), January 1992.

116. R. D. Cheverton, T. L. Dickson, J. G. Merkle, and R. K. Nanstad, Martin Marietta Energy Systems, Inc., Oak Ridge Natl. Lab., Oak Ridge, Tenn., *Review of Reactor Pressure Vessel Evaluation Report for Yankee Rowe Nuclear Power Station (YAEC No. 1735)*, USNRC Report NUREG/ CR-5799 (ORNL/ TM-11982), March 1992

117. T. L. Dickson, R. D. Cheverton, and J. W. Bryson, Martin Marietta Energy Systems, Inc., Oak Ridge Natl. Lab., Oak Ridge, Tenn., *Pressurized-Thermal-Shock Probabilistic Fracture Mechanics Sensitivity Analyses for Yankee Rowe Reactor Pressure Vessel*, USNRC Report NUREG/CR-5782 (ORNL/ TM-11945) (to be published).

118. Canceled

119. J. W. Dally, G. R. Irwin, X-J. Zhang, and R. J. Bonenberger, University of Maryland for Martin Marietta Energy Systems, Inc., Oak Ridge Natl. Lab., Oak Ridge, Tenn., *The Influence of Precompression on the Lower-Bound Initiation Toughness of A 533 B Reactor Grade Steel*, USNRC Report NUREG/CR-5847 (ORNL/Sub/79-7778/8), May 1992.

120. Canceled

121. C. W. Schwartz, University of Maryland for Martin Marietta Energy Systems, Inc., Oak Ridge Natl. Lab., Oak Ridge, Tenn., *Crack Speed Relations Inferred from Large SEN Specimens of A 533 B Steel*, USNRC Report NUREG/CR-5861 (ORNL/Sub/79-7778/9) (to be published).

122. A. R. Rosenfield and C. W. Marschall, Battelle Columbus Division for Martin Marietta Energy Systems, Inc., Oak Ridge Natl. Lab., Oak Ridge, Tenn., *Fracture-Mechanics-Based Failure Analysis*, USNRC Report NUREG/CR-5860 (ORNL/Sub/ 82-17651/1), June 1992.

123. G. R. Irwin and X-J. Zhang, University of Maryland for Martin Marietta Energy Systems, Inc., Oak Ridge Natl. Lab., Oak Ridge, Tenn., *Gradient Study of a Large Weld Joining Two Forged A 508 Shells of the Midland Reactor Vessel*, USNRC Report NUREG/CR-5867 (ORNL/Sub/79-7778/10), June 1992.

124. J. Keeney-Walker and B. R. Bass, Martin Marietta Energy Systems, Inc., Oak Ridge Natl. Lab., Oak Ridge, Tenn., *ORNOZL: A Finite-Element Mesh Generator for Nozzle-Cylinder Intersections Containing Inner-Corner Cracks*, USNRC Report NUREG/CR-5872 (ORNL/TM-11049), September 1992.

125. J. Keeney-Walker and B. R. Bass, Martin Marietta Energy Systems, Inc., Oak Ridge Natl. Lab., Oak Ridge, Tenn., *A Comparison of Analysis Methodologies for Predicting Cleavage Arrest of a Deep Crack in a Reactor Pressure Vessel Subjected to Pressurized-Thermal-Shock Loading Conditions*, USNRC Report NUREG/CR-5793 (ORNL/TM-11969), September 1992.

126. T. J. Theiss, D. K. M. Shum, and S. T. Rolfe (University of Kansas), Martin Marietta Energy Systems, Inc., Oak Ridge Natl. Lab., Oak Ridge, Tenn., *Experimental and Analytical Investigation of the Shallow-Flaw Effect in Reactor Pressure Vessels*, USNRC Report NUREG/CR-5886 (ORNL/TM-12115), July 1992.

127. B. R. Bass, D. K. M. Shum, and J. Keeney-Walker, Martin Marietta Energy Systems, Inc., Oak Ridge Natl. Lab., Oak Ridge, Tenn., *Constraint Effects on Fracture Toughness for Circumferentially Oriented Cracks in Reactor Pressure Vessels*, USNRC Report NUREG/CR-6008, (ORNL/TM-12131), August 1992.

128. R. E. Stoller, Martin Marietta Energy Systems, Inc., Oak Ridge Natl. Lab., Oak Ridge, Tenn., *Modeling the Influence of Irradiation Temperature and Displacement Rate on Radiation-Induced Hardening in Ferritic Steels*, USNRC Report NUREG/CR-5859 (ORNL/TM-12073), July 1992.

129. J. Keeney-Walker, J. G. Merkle, S. K. Iskander, and T. L. Dickson, Martin Marietta Energy Systems, Inc., Oak Ridge Natl. Lab., Oak Ridge, Tenn., *Recommendations for Thermal-Shock Testing of Clad Cylinders with Shallow Surface Cracks*, USNRC Report NUREG/CR-5915 (ORNL/TM-12166), November 1992.

130. W. E. Pennell, B. R. Bass, R. K. Nanstad, J. G. Merkle, T. L. Dickson, T. J. Theiss, J. Keeney-Walker, and D. K. Shum, *Heavy-Section Steel Technology Program Semiannual Progress Report for October 1991 through March 1992*, NUREG/CR-4219 (ORNL/TM-9593/V9&N1) June 30, 1992.

131. W. E. Pennell, Martin Marietta Energy Systems, Inc., Oak Ridge Natl. Lab., "Heavy-Section Steel Technology Program: Recent Developments in Crack Initiation and Arrest Research," *Nineteenth Water Reactor Safety Information Meeting*, NUREG/CP-0119, Vol. 1, pp. 29–51, October 1992.

132. W. E. Pennell, Martin Marietta Energy Systems, Inc., Oak Ridge Natl. Lab., "Aging Impact on the Safety and Operability of Nuclear Reactor Pressure Vessels," *Proceedings of the Aging Research Information Conference*, USNRC Conference Proceeding NUREG/CP-0122, Vol. 1, pp. 431–453, March 1992.

133. T. L. Dickson and F. A. Simonen, Martin Marietta Energy Systems, Inc., Oak Ridge Natl. Lab., "The Application of Probabilistic Fracture Analysis to Residual Life Evaluation of Embrittled Reactor Vessels," *Proceedings of the Aging Research Information Conference*, USNRC Conference Proceeding NUREG/CP-0122, Vol. 1, pp. 454-467, March 1992.

134. R. K. Nanstad, F. M. Haggag, D. E. McCabe, S. K. Iskander, K. O. Bowman, and B. H. Menke, Martin Marietta Energy Systems, Inc., Oak Ridge Natl. Lab., *Irradiation Effects on Fracture Toughness of Two High-Copper Submerged-Arc Welds, HSSI Series 5*, USNRC Report NUREG/CR-5913, Vol. 1 (ORNL/TM-12156/V1) October 1992.

135. D. E. McCabe, Martin Marietta Energy Systems, Inc., Oak Ridge Natl. Lab., *Evaluation of Crack Pop-ins and the Determination of Their Relevance to Design Consideration*, USNRC Report NUREG/CR-5952 (ORNL/TM-12247), February 1993.

136. Canceled

137. R. K. Nanstad, D. E. McCabe, R. L. Swain, and M. K. Miller, Martin Marietta Energy Systems, Inc., Oak Ridge Natl. Lab., *Chemical Composition and RT_{NDT} Determinations for Midland Weld WF-70*, USNRC Report NUREG/CR-5914 (ORNL-6740) December 1992.

138. T. J. Theiss, B. R. Bass, J. W. Bryson, W. J. McAfee, R. K. Nanstad, W. E. Pennell, and M. C. Rao, Martin Marietta Energy Systems, Inc., Oak Ridge Natl. Lab., *Initial Results of the Influence of Biaxial Loading on Fracture Toughness*, USNRC Report NUREG/CR-6036 (ORNL/TM-12349), June 1993.

139. D. K. Shum, J. W. Bryson, and J. G. Merkle, Martin Marietta Energy Systems, Inc., Oak Ridge Natl. Lab., *Potential Change in Flaw Geometry of an Initially Shallow Finite-Length Surface Flaw During a Pressurized Thermal Shock Transient*, NUREG/CR-5968 (ORNL/TM-12279), September 1993.

140. T. L. Dickson, Martin Marietta Energy Systems, Inc., Oak Ridge Natl. Lab., *Generic Analyses for Evaluation of Low Charpy Upper-Shelf Energy Effects on Safety Margins Against Fracture of Reactor Pressure Vessel Materials*, USNRC Report NUREG/CR-6023 (ORNL/TM-12340), July 1993.

141. C. W. Schwartz, Department of Civil Engineering, University of Maryland, *Crack-Speed Relations Inferred from Large Single-Edge-Notched Specimens of A 533 B Steel*, NUREG/CR-5861 (ORNL/Sub/79-7778/9) (to be published).

142. W. E. Pennell, B. R. Bass, J. W. Bryson, W. J. McAfee, T. J. Theiss, and M. C. Rao, Martin Marietta Energy Systems, Inc., Oak Ridge Natl. Lab., *Biaxial Loading and Shallow-Flaw Effects on Crack-Tip Constraint and Fracture Toughness*, NUREG/CR-6132 (ORNL/TM-12498), January 1994.

143. J. A. Keeney, B. R. Bass, W. J. McAfee, S. K. Iskander, Martin Marietta Energy Systems, Inc., Oak Ridge Natl. Lab., *Preliminary Assessment of the Fracture Behavior of Weld Material in Full-Thickness Clad Beams*, NUREG/CR-6228 (ORNL/TM-12735) (to be published).

144. Canceled.

145. Canceled.

NUREG/CR-4219
ORNL/TM-9593/V11&N1
Vol. 11, No. 1
Dist. Category RF

Internal Distribution

1. D. J. Alexander
2. B. R. Bass
3. J. W. Bryson
4. J. M. Corum
5. W. R. Corwin
6. T. L. Dickson
7. R. G. Gilliland
8. J. J. Henry
9. F. M. Haggag
10. W. F. Jackson
11. S. K. Iskander
12. J. A. Keeney
13. W. J. McAfee
14. D. E. McCabe
15. J. G. Merkle
16. R. K. Nanstad
17. D. J. Naus
18. C. B. Oland
19–22. W. E. Pennell
23. C. E. Pugh
24. C. C. Southmayd
25. R. L. Swain
26. ORNL Patent Section
27. Central Research Library
28. Document of Reference
29–30. Laboratory Records
31. Laboratory Records (RC)

External Distribution

32. R. D. Thompson, Office of Administration, Division of Contracts and Properties, U.S. Nuclear Regulatory Commission, Mailstop T17/G-21, Mailstop T17/G21, Washington, DC, 20555-0001
33. J. Strosnider, Division of Engineering, NRR, U.S. Nuclear Regulatory Commission, Mailstop O7-D4, Washington, DC 20555-0001
34. E. M. Hackett, Materials and Chemical Engineering Branch, Mailstop O7-D4, U.S. Nuclear Regulatory Commission, Washington, DC 20555-0001
35–37. S. N. M. Malik, EMMEB/DET/RES, U.S. Nuclear Regulatory Commission, Washington, DC 20555-001
38. M. E. Mayfield, EMMEB/DET/RES, U.S. Nuclear Regulatory Commission, Washington, DC 20555-0001
39. G. C. Millman, Division of Engineering, U.S. Nuclear Regulatory Commission, Washington, DC 20555-0001
40. M. Vassilaros, EMMEB/DET/RES, Mailstop T10-E10, U.S. Nuclear Regulatory Commission, Washington, DC 20555-0001
41. J. W. Dally, Department of Mechanical Engineering, University of Maryland, College Park, Maryland 20742
42. G. R. Irwin, Department of Mechanical Engineering, University of Maryland, College Park, Maryland 20742
43. L. James, Westinghouse Bettis Lab., P.O. Box 79, ZAP 13A, 814 Pittsburgh McKeesport Blvd., West Mifflin, Pennsylvania 15122
44. C. F. Shih, Box D, Division of Engineering, Brown University, Providence, Rhode Island, 02912
45. R. Dodds, 3140 Newmark Laboratory, 205 North Matthews, Urbana, Illinois 61801
46. R. Fields, National Institute of Standards and Technology, Bldg. 223, B144, Gaithersburg, Maryland 20899
47. W. L. Fourney, Department of Mechanical Engineering, University of Maryland, College Park, Maryland 20742
48. J. D. Landes, The University of Tennessee, Knoxville, Tennessee 37996-2030
49. S. T. Rolfe, The University of Kansas, Lawrence, Kansas 66045-2235
50. A. R. Rosenfield, Battelle Columbus Division, Columbus, Ohio 43201
51. C. W. Schwartz, Department of Civil Engineering, University of Maryland, College Park, Maryland 20742
52. E. T. Wessel, 312 Wolverine, Haines City, Florida 33844
53. Office of Assistant Manager for Energy Research and Development, DOE–ORO, Oak Ridge, Tennessee 37831
54–55. Office of Scientific and Technical Information, P.O. Box 62, Oak Ridge, Tennessee 37831

NRC FORM 335 (2-89) NRCM 1102, 3201, 3202

U.S. NUCLEAR REGULATORY COMMISSION

BIBLIOGRAPHIC DATA SHEET

(See instructions on the reverse)

1. REPORT NUMBER (Assigned by NRC, Add Vol., Supp., Rev., and Addendum Numbers, if any.)
NUREG/CR-4219
ORNL/TM-9593/V11&N1
Vol. 11, No. 1

2. TITLE AND SUBTITLE
Heavy-Section Steel Technology Program
Semiannual Progress Report for October 1993 - March 1994

3. DATE REPORT PUBLISHED
MONTH: November
YEAR: 1995

4. FIN OR GRANT NUMBER
B0119

5. AUTHOR(S)
W.E. Pennell

6. TYPE OF REPORT
technical

7. PERIOD COVERED (Inclusive Dates)
10/93 - 3/94

8. PERFORMING ORGANIZATION – NAME AND ADDRESS (If NRC, provide Division, Office or Region, U.S. Nuclear Regulatory Commission, and mailing address; if contractor, provide name and mailing address.)
Oak Ridge National Laboratory
Oak Ridge, TN 37831-6285

9. SPONSORING ORGANIZATION – NAME AND ADDRESS (If NRC, type "Same as above"; if contractor, provide NRC Division, Office or Region, U.S. Nuclear Regulatory Commission, and mailing address.)
Division of Engineering Technology
Office of Nuclear Regulatory Research
U.S. Nuclear Regulatory Commission
Washington, DC 20555-0001

10. SUPPLEMENTARY NOTES
S.N.M. Malik, NRC Project Manager

11. ABSTRACT (200 words or less)
The Heavy-Section Steel Technology (HSST) Program is conducted for the U.S. Nuclear Regulatory Commission (NRC) by Oak Ridge National Laboratory (ORNL). The program focus is on the development and validation of technology for the assessment of fracture-prevention margins in commercial nuclear reactor pressure vessels. The HSST Program is organized in seven tasks: (1) progam management, (2) constraint effects analytical development and validation, (3) evaluation of cladding effects, (4) ductile to cleavage fracture mode conversion, (5) fracture analysis methods development and applications, (6) material property data and test methods, and (7) integration of results into a state-of-the-art methodology. The program tasks have been structured to place emphasis on the resolution fracture issues with near-term licensing significance. Resources to execute the research tasks are drawn from ORNL with subcontract support from universities and other research laboratories. Close contact is maintained with the sister Heavy-Section Steel Irradiation Program at ORNL with related research programs both in the United States and abroad. This report provides an overview of principal developments in each of the seven program tasks from October 1993 - March 1994.

12. KEY WORDS/DESCRIPTORS (List words or phrases that will assist researchers in locating the report.)
Heavy-Section Steel Technology (HSST), assessment, fracture prevention, semiannual progress report

13. AVAILABILITY STATEMENT
unlimited

14. SECURITY CLASSIFICATION
(This Page)
unclassified
(This Report)
unclassified

15. NUMBER OF PAGES

16. PRICE

Federal Recycling Program

UNITED STATES
NUCLEAR REGULATORY COMMISSION
WASHINGTON, DC 20555-0001

OFFICIAL BUSINESS
PENALTY FOR PRIVATE USE, $300

SPECIAL FOURTH-CLASS MAIL
POSTAGE AND FEES PAID
USNRC
PERMIT NO. G-67

120555139531 1 1AN1R5
US NRC-OADM
DIV FOIA & PUBLICATIONS SVCS
TPS-PDR-NUREG
2WFN-6E7
WASHINGTON DC 20555